Bulgarian Academy of Sciences **ISSN 1311-753X**

Bulgarian Geophysical Journal

2018, Vol. 41

Contents

DETERMINISTIC SEISMIC SCENARIOS BASED ON MACROSEISMIC INTENSITY GENERATED BY REAL STRONG EARTHQUAKES OF THE PAST

I. Aleksandrova, S. Simeonova, D. Solakov and P. Raykova

National Institute of Geophysics, Geodesy and Geography-BAS,
Acad. G .Bonchev str., bl. 3, BG-1113 Sofia, Bulgaria
e-mail: i.alex@abv.bg, stelas@geophys.bas.bg, dimos@geophys.bas.bg,
plamena.raikova@gmail.com

Abstract: The territory of Bulgaria represents a typical example of high seismic risk area. In the present study deterministic scenarios in intensity for two Bulgarian cities (Ruse and Plovdiv) are presented. By deterministic scenario it is mean a representation of the severity of ground shaking over an urban area, using one or more hazard descriptors. Such representation can be obtained: - either from the assumption of a "reference earthquake" specified by a magnitude or an epicentral intensity, associated to a particular earthquake source - or, directly, showing values of local macroseimic intensity generated by a damaging, real earthquakes of the past. In the study we chose for the second method using the values of macroseimic intensity caused by damaging historical earthquakes (the 1928 quakes in southern Bulgaria; and the 1940 and the 1977 Vrancea intermediate earthquakes).

Key words: earthquake, seismic impact, macroseismic intensity, deterministic scenarios, seismogenic area.

Introduction

Earthquakes are the most deadly of the natural disasters affecting the human environment; indeed catastrophic earthquakes have marked the whole human history. Global seismic hazard and vulnerability to earthquakes are increasing steadily as urbanization and development occupy more areas that are prone to effects of strong earthquakes. Additionally, the uncontrolled growth of mega cities in highly seismic areas around the world is often associated with the construction of seismically unsafe buildings and infrastructures, and undertaken with an insufficient knowledge of the regional seismicity peculiarities and seismic hazard. The assessment of seismic hazard

and generation of earthquake scenarios is the first link in the prevention chain and the first step in the evaluation of the seismic risk.

Bulgaria situated in the Balkan Peninsula (that is a part of the Alpo-Himalayan seismic belt, which is characterized by high seismicity) is exposed to a high seismic risk. Bulgaria contains important industrial areas that face considerable earthquake risk. Over the centuries, Bulgaria has experienced strong earthquakes. Some of the Europe¢s strongest earthquakes in 20-th century occurred on the territory of Bulgaria. Impressive seismic activity developed in the SW Bulgaria during 1904-1906. The seismic sequence started on 4 of April 1904 with two catastrophic earthquakes within 23 minutes (the first quake with MS=7.1 considered as a foreshock and the second, the main shock, with MS=7.8 and I0=X). Along the Maritza valley (central part of Bulgaria), a sequence of three destructive earthquakes occurred in 1928. However, no such large earthquakes occurred in Bulgaria since 1928, which may induce non-professionals to underestimate the earthquake risk. Moreover, the seismicity of the neighboring countries, like Greece, Turkey, former Yugoslavia and Romania (especially Vrancea-Romania intermediate earthquakes), influences the seismic hazard for Bulgaria.

In the present study deterministic scenarios (expressed in seismic intensity) for the cities of Plovdiv and Rouse are presented. Both deterministic scenarios were generated using the values of macroseimic intensity cased by damaging, real earthquakes of the past. The methodology applied is described among others in Solakov et al., 2009 and Solakov et al., 2011. The work on scenarios was guided by the perception that usable and realistic (also in the sense of being compatible with seismic histories of cities that are several centuries long) ground motion maps had to be produced for urban areas.

Earthquake senario for the city of Plovdiv

The city of Plovdiv

Now

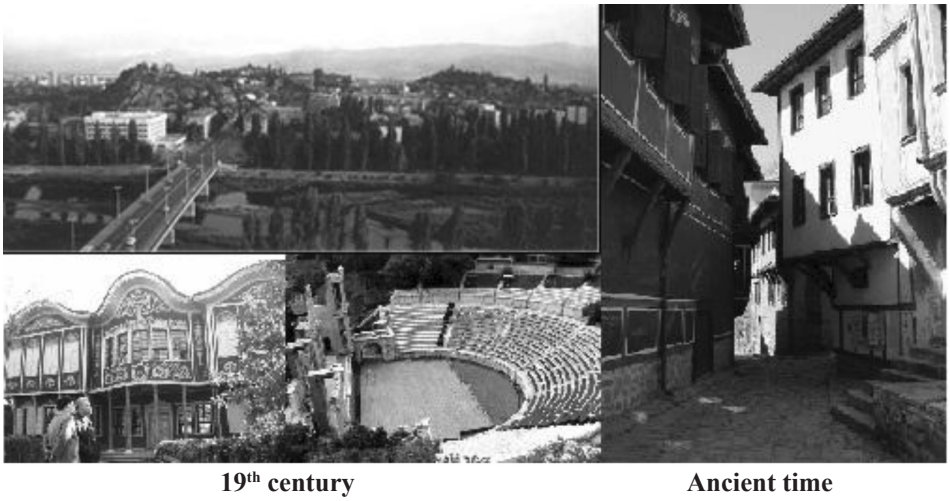

19th century **Ancient time**

The Bulgarian city of Plovdiv is located in the South-Central Bulgaria on the two banks of the Maritsa River. Being the second largest city in the country, it has a population of about 350 000. The city has historically developed on seven syenite hills, some of which are 250 m high. Because of these seven hills, Plovdiv is often referred to in Bulgaria as "The City of the Seven Hills". History of the city of Plovdiv spans some 6,000 years, with traces of a Neolithic settlement dating to roughly 4000 BC. In the beginning of the 20th century Plovdiv grew as a significant industrial and commercial center. At present Plovdiv is one of the most populated cultural region of Bulgaria that faces considerable earthquake risk.

Over the past century, the city of Plovdiv has experienced several strong earthquakes. The earthquakes that mainly influence the hazard of Plovdiv originate near the city. The contemporary tectonic activity of the area is associated with Maritsa fault system with WNW-ESE direction. The Maritsa fault with its satellites belongs to structures with a longlasting development, which continues in the neotectonic period. The oblique Maritsa Fault striking N 116º, and the dipping towards N is of length of about 36 km. It is known with the surface rupturing during the MW = 7.0 earthquake of 18 of April 1928 (Yankov, 1945). The strongest known earthquakes occurred on the fault system are those in 1928 (the Chirpan earthquake of April 14, 1928 with MW=6.8 and the Plovdiv earthquake of April 18, 1928 with MW=7.0, I= 9-10 MSK). The 1928 earthquakes completely destroyed 74000 buildings in the towns of Plovdiv, Chirpan and Parvomay (Kirov, 1945).

The 1928 M_W7.0 earthquake impact on the city of Plovdiv

The 1928 earthquake ruined 3600 and partially destroyed 6000 buildings in the city of Plovdiv (DIPOZE, 1931). Some of the damages in the city of Plovdiv are illustrated in Fig. 1.

Fig. 1. Damages in the city of Plovdiv caused by the 1928 (M_W=7.0) earthquake

In the present study the earthquake damages are assessed on the base of descriptions and analyses presented in DIPOZE ,1931. Additionally, available documents and materials that were collected in the territorial Directorate "State Archive" and the National Library "Ivan Vazov", Plovdiv were used.

The most of the destructions have been observed north of the Maritsa River due to very bad soil conditions and not well constructed buildings. The maximum observed intensity there reaches 9-10th degree MSK.

One of the worst hit districts is, located in the southeast part of the city. The district is built on drought and loose sleeve of the Maritsa River. 95% of the houses there were destroyed. The intensity of the impact in this region is higher than 9th degree MSK.

Major damages have been identified in the southern marginal part of the city (the size of the city of Plovdiv in 1928 is considerably smaller than the current size of the city) where the buildings are small, ramshackle homes built without any supporting structures. The impact is assessed by intensity 9th degree MSK.

Overall the city center and houses around the hills have suffered slight damage. South of Maritza River damage on buildings are considerably smaller. The public and private buildings are well built and the soil conditions are stable - compacted sediments. The maximum observed intensity in that part of the city is 7–8 th degree MSK. Least affected are buildings situated on and around the hills. The houses are solid with thick stone walls situates on syenite hills. The maximum seismic intensity in this area is 7th degree MSK.

Observed damage can be regarded as a combined effect of seismic impact, geological conditions and the type of construction.

Distribution of macroseismic effects (in intensity) along the city of Plovdiv is presented in Fig. 2.

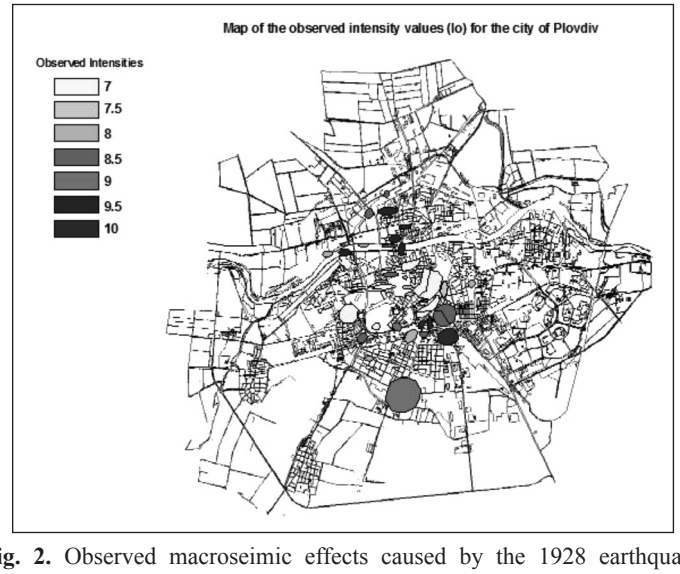

Fig. 2. Observed macroseimic effects caused by the 1928 earthquake (M_W =7.0) on the city of Plovdiv (in intensity MSK);colore represent the intensities in MSK scale;**(**Map of Plovdiv from the beginning 20th century**)**

The intensity scenario map is presented in Fig. 3. Base of seismic history of the city of Plovdiv the 1928 earthquake (M_W =7.0) is considered as responsible of the macroseismic intensity scenario. The generation of intensity scenario use directly the intensity assessment of the 1928 quake with M_W=7.0. The scenario map illustrates the distribution of the maximum values of macroseismic intensity (MSK) along the central part of the city of Plovdiv. The soil properties of the urban area were incorporated in the senario generation by using the very simplified geotechnical map for the city of Plovdiv.

Fig. 3. Earthquake scenario for the city of Plovdiv (in intensity MSK) based on macroseimic effects generated by a damaging, real earthquake of the past; colors represent the intensities in MSK scale. (Map of Plovdiv from the beginning 20th century)

Earthquake scenario for the city of Ruse

The city of Ruse

The city of Ruse that is located in the north-eastern part of the country is the fifth largest city in Bulgaria. Its population is about 162000 people. The city of Ruse is situated on the right bank of the Danube River, in the mouth of Rusenski Lom River. It is the most significant Bulgarian river port, serving an important part of the international trade of the country.

The city emerged as a Neolithic settlement from the 3rd to 2nd millennium BCE, when pottery, fishing, agriculture, and hunting developed. During the reign of Vespasian (69-70 CE) it developed into a Roman military and naval centre as part of the fortification system along the northern boundary of Moesia. Its name, Sexaginta Prista, suggests a meaning of "the port town of the sixty ships. After it became part of modern Bulgaria on 20 February 1878, Ruse was one of the key cultural and economic centres of the country. Intensive building during the end of the 19th and the beginning of the 20th century changed the city's architectural appearance to a typical Central European one. The city is famous for its 19th- and 20th-century Neo-Baroque and Neo-Rococo architecture, which attracts many tourists. It is often called the Little Vienna.

Now

Bank "Girdap" - built in1881

National theatre - built 1898-1902

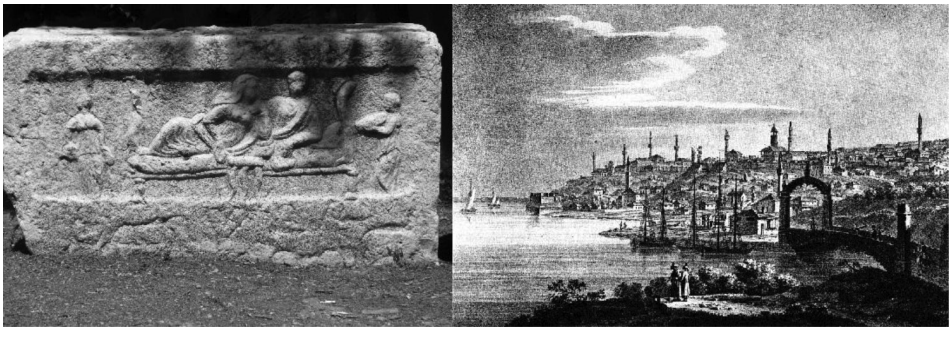

Ancient "Sexaginta Prista"

Ruse in 1824

The Vrancea seismogenic zone of Romania is a very peculiar seismic source, often described as unique in the world, and it represents a major concern for most of the northern part of Bulgaria. The events generated in this seismogenic zone are characterized by relatively deep hypocenters and wide area of marcoseismic impact. In this area strong intermediate-focused earthquakes are being realized with depth 90-230 km. The strongest known events, occurred in the Vrancea seismogenic zone are the following earthquakes: the 1802 quake with magnitude M_W=7.9 (Watzof, 1902), the 1940 M_W=7.7 (Kirov, 1941) and the 1977 quake, M_W=7.4 (the Mw estimates are according to ROMPLUS, 2007). Situated at distances larger than 200 km from the Vrancea zone, several cities in the northern Bulgaria suffered many damages due to high energy Vrancea intermediate-depth earthquakes. The March 4, 1977 event (Mw 7.4) caused partial or total damages in 8470 buildings (as illustrated in Fig. 4), and 125 casualties on the territory of Bulgaria.

Fig. 4. Damages in Northern Bulgaria caused by the 1977 (M=7.2) Vrancea earthquake

Impact of Vrancea earthquakes on the city of Ruse

The strongest documented seismic impacts on the city of Ruse until nowadays are from earthquakes generated in Vrancea seismogenic zone. In the present study two intermediate-focused Vrancea earthquakes are considered: the 1940 (M_W=7.7) and the 1977 (M_W=7.4).

For both earthquakes distribution of macroseismic effects along the city is estimated on the base of documents available in Regional administration of "State Archive" and Regional Library "L.Karavelov", Ruse.

The intensity map illustrating the impact of the 1940 M_W7.7 earthquake on the city of Ruse is presented in Fig.5. The figure shows that the intensity values range between 6 and 7 MSK. The most affected are the central and the coastal areas of city of Ruse.

Distribution of macroseismic effects (in intensity) of the 1977 M_W7.4 earthquake along the city of Ruse is presented in Fig.6. The highest intensities (7-8MSK) are observed in the west-southwest, central and coastal part of the city where the intensity reaches the 9^{th} MSK.

The observed distribution of intensity function along the city of Ruse in both cases is identical (though a scant information about the earthquake of 1940). Impacts of the both earthquakes are with the highest intensity in coastal parts of the city. Strong effects are observed in the western and central parts of the city of Ruse. In the central and western parts of the city buildings and facilities were built on subsiding loess soils. The water content of these soils is increased by the proximity of the river Rousse Lom River and aquifers formed the basis of loess, leading amending strength-deformation characteristics.

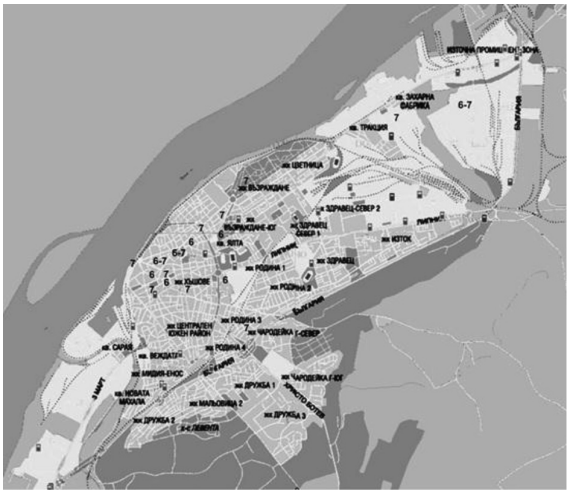

Fig. 5. Impact of the 1940 Vrancea earthquake (M_W=7.7) on the city of Ruse; the numbers represent the intensities in MSK scale.

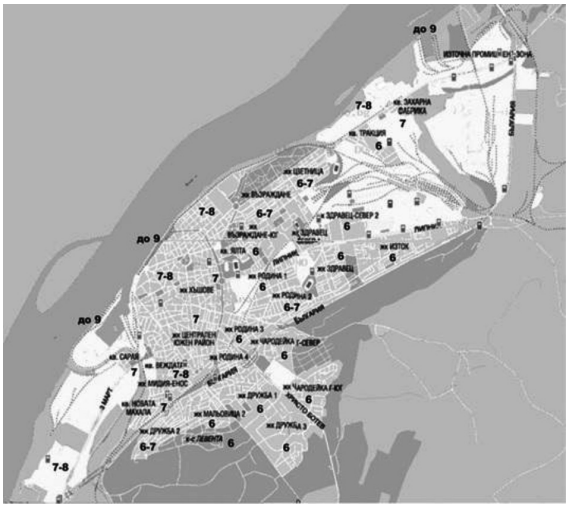

Fig. 6. Impact of the 1977 Vrancea earthquake (M_W=7.4) on the city of Rus; numbers represent the intensities in MSK scale

The earthquake scenario (in intensity) for the city of Ruse is presented in Fig.7. The generation of intensity scenario used directly assessed impacts of the strongest past intermediate-focused earthquakes-the 1940 quake with M_W=7.7 and the 1977 quake with $M_{W=}$ 7.4, both generated in Vrancea, Romania. A good spatial coincidence between the value of the impacts assessed and configuration of the Danube and Ruse Lom Rivers terraces was found. The seismic scenario for the city of Ruse (presented in Figure 7) is generated by matching the observed distribution of intensity function along the city with the configuration of river terraces. The scenario map illustrates the distribution of the maximum values of macroseismic intensity (in MSK) along the city of Ruse.

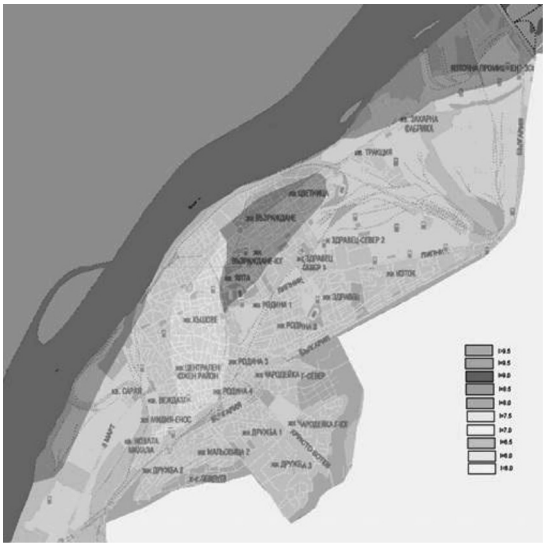

Fig. 7. Earthquake scenario for the city of Ruse (in intensity MSK) based on macroseimic effects generated by damaging, real earthquakes of the past; colors represents the intensities in MSK scale.

Conclusions

Such scenarios are intended as a basic input for developing detailed earthquake damayge scenarios for the cities. They can be used also to improve urban development and for risk mapping and management

The scenarios may be efficiently used for the purpose of microzonation, urban planning, retrofitting or insurance of the built environment and infrastructure planning, etc.

The damages caused by these earthquakes have outlined the need of in-depth analysis in what concerns the seismic hazard specific for the regions, as well as the need to suggest solutions to reduce the possible negative effects.

The implementation of the earthquake scenarios into the policies for seismic risk reduction will allow focusing on the prevention of earthquake effects rather than on intervention following the disasters.

It is hoped that the themes inherent in the analysis of seismic hazard and risk, aimed at the conservation of the historical architectural heritage and the detailed knowledge of a territory, may inspire a new "historic" awareness of environmental risk.

All these concerns may enter into the world of schools and be propagated by the mass media, in the forms best suited to arouse the interest of the young generation and to stimulate in them the need for a culture of safety and prevention as a new form of habitation civilization.

References

DIPOZE, 1931. Report for post earthquake activities that were undertaken in the time interval April 1928 - November 1931. State Press, Sofia, pp. 421 (in Bulgarian).

Kirov, K., 1945. Tremblements de terre en Bulgarie 29-32. Liste des tremblements de terre ressentis pendant les annees 1928-1930. Inst. Meteorol. Sentr. De Bulgarie, S. pp. 140. (in Bulgarian and abstract in French)

ROMPLUS, 2007 - Romanian Earthquake Catalogue (computer file), first published as: Oncescu, M. C., Marza, V. I, Rizescu, M., Popa, M. (1999), The Romanian Earthquake Catalogue between 984-1997, in Vrancea Earthquakes: Tectonics, Hazard and Risk Mitigation, F. Wenzel, D. Lungu (eds.) & O. Novak (co-ed), pp. 43-47, Kluwer Academic Publishers, Dordrecht, Netherlands.

Solakov D., S. Simeonova, I. Aleksandrova, I. Popova, G. Georgieva, 2009. Earthquake Scenarios: cases study for the cities of Rousse and Vratsa. 5th Congress of Balkan Geophysical Society — Belgrade, Serbia10 – 16 May 2009, 6497, computer file on CD

Solakov D., S. Simeonova, I. Alexandrova, P. Trifonova, M. Metodiev, 2011. Verification of seismic scenario using historical data-case study for the city of Plovdiv. In Proceedings V. 2 (Edts. Grützner C., R. Perez-Lopez, T. Steeger, I. Papanikolaou, K. Reicherter, P. Silva and A.Vött) of 2nd INQUA-IGCP-567 International Workshop on Active Tectonics, Earthquake Geology, Archaeology and Engineering, Corinth, Greece, 39-41

Watzof S., 1902. Earthquakes in Bulgaria during XIX century, Central Meteorological Station, Imprimerie de I¢Etat, Sofia, pp. 93. (in Bulgarian and French)

Yankov K. (1945) Changes in ground level produced by the earthquakes of April, 14 and April, 18 1928 in southern Bulgaria. In: Tremblements de Terre en Bulgarie, No 29-31, pp. 131-136, National Metheo Ins., Sofia, (in Bulgarian).

Archive materials from:

Territorial Directorate "State Archive" – Plovdiv,
National Library "Ivan Vazov", Plovdiv
Central Management of the archives in Council of Ministers, Territorial Directorate
"State archive", Ruse
Regional library "L. Karavelov", Ruse.

Детерминистични сеизмични сценарии, базирани на макросеизмични интензивности, генерирани от силни земетресения реализирани в миналото

И. Александрова, С. Симеонова, Д. Долаков, Пл. Райкова

Резюме. България представлява типичен пример за територия с висока степен на сеизмична опасност. В настоящото изследване са представени детерминистични сценарии в макросеизмична интензивност за два големи българси града (Русе и Пловдив). Детерминистичният сценарий е една оценкаа на най-силните възможни сеизмични въздействия върху урбанизираната територия. Такъв сценарий се генерира: – или чрез използване на „референтно земетресение“ с определен магнитуд (или епицентралната интензивност), свързано с конкретен сеизмичен източник – или директно, чрез изпозуване на наблюдавани въздействия, причинени от разрушителни земетресения, реализирани в миналото. В иастоящото изследване е избран вторият подход като са приложени наблюдаваните макросеизмични въздействия, причинени от силни исторически земетресения – събитията, генерирани в южна България през 1928 г., и земетресенията от 1940 г. и 1977 г., реализирани в междинофокусно огнище Вранча.

Bulgarian Geophysical Journal, 2018, Vol. 41
National Institute of Geophysics, Geodesy and Geography, Bulgarian Academy of Sciences

IONOSPHERIC ANOMALIES OVER BULGARIA DURING TWO GEOMAGNETIC STORMS

R. Bojilova

[1]Geophysical Institute, ul. Acad.G. Bonchev, bl. 3, Sofia 1113, Bulgaria
e-mail: bojilova@geophys.bas.bg

Abstract. This paper considers ionospheric anomalies over the territory of Bulgaria during geomagnetic storms - the storm on 5 April 2010 and the event on 9 March 2012. The response of the ionosphere over Bulgaria is represented by data, collected by the ionospheric station in Sofia at NIGGG- BAS. The values of the Total Electron Content (TEC) have been provided by the Center for Orbit Determination of Europe (CODE). The data for variations on Earth magnetic field are received from INTERMAGNET. It was used the station Panagyurishte (PAG) located on the territory of Bulgaria. The impact of ionospheric anomalies on radio communication on frequencies in shortwave and satellite navigation is also analyzed.

Key words: Geomagnetic storm, TEC, Critical frequency, Ionospheric anomalies.

Introduction

Geomagnetic storms is the common name of the physical processes in the Earth's atmosphere and ionosphere, caused by large increases in plasma streams discharged into interplanetary space during Coronal mass ejections from the sun. Historically, they were first seen as anomalies in the values of Earth's magnetic field, which is one of the visible manifestations, with the help of ground-based measuring devices (magnetometers), of processes that accompany the entering of flows of charged particles (electrons and ions) discharged from solar corona into Earth's atmosphere. Because of the constant Earth magnetic field, the flows of particles penetrate deep into the Earth's atmosphere only in polar regions where the geomagnetic field lines are highly inclined (near vertical). Abnormal changes in the readings of magnetometers are due to the electric currents (generated by streams of charged particles) whose magnetic field is summed with the constant Earth magnetic field. The values of the variations in the magnetic field near

the Earth's surface are used to create geomagnetic indices that characterize the intensity of storms. One of the most commonly used is the index Kp, which is obtained by summarizing the variation of a sufficient number of geomagnetic stations. Values of the Kp index vary between 0 and 9. Kp <4 is reported calm state, 4 <= Kp <5 – active state and when Kp>= 5 - geomagnetic storm. The intensity of magnetic storms is denoted by numbers (Scale) from G1 (Kp=5) to G5 (Kp=9). Storms with number G5 are considered extreme (NOAA Space Weather Scales).

Anomalous variations of the Earth's magnetic field are not the only result of the penetration of solar plasma flows into the Earth's atmosphere. Geomagnetic storms are accompanied by the so-called ionospheric storms, which are anomalous variations of the electronic concentration in the ionosphere (increase or decrease). Entering the atmosphere in the polar regions, the flows of charged particles cause further ionization, as well as an increase in the temperature of the neutral air, which changes the general atmospheric circulation at heights above 100 km. A change occurs in the ratio of oxygen to nitrogen and as a consequence the coefficients of recombination in the ionosphere change, which in turn causes anomalies in the electron concentration (Mukhtarov et al., 2013).These anomalies propagate from the polar regions to the equator through the processes of atmospheric dynamic (presence of neutral wind) (Kutiev & Mukhtarov, 2003).

The ability of the ionosphere (the area of the atmosphere, in which free electrons are present in addition to neutral gas molecules) is used to carry out the distant radio connection that are based on the ability of the ionized air to reflect radio waves with a certain frequency transmitted from terrestrial stations. Single and multiple reflection of radio waves from the ionosphere makes possible, under certain conditions, the implementation of communications between widely separated points on Earth with minimal energy consumption.

The ability of the ionosphere to reflect radio waves is directly related to the maximum of electron concentration, formed at altitudes between approximately 200 and 400 kilometers. The height and the value of this maximum vary depending on diurnal and seasonal variations. This two parameters depending also of 11-year solar cycle.

Two variables are used to characterize the possibility of radio communication, their values being derived from the data, gathered by ground- based ionosondes - critical frequency vertical distribution foF2 and maximum applicable frequency in 3000 km distance MUF3000. The critical frequency is actually the maximum applicable frequency for ionospheric radio communication at distances below 100 km.

Total electron content (TEC) is the total amount of free electrons in a vertical column with height limits of the ionosphere (about 1000 km). This ionosphere characteristic is important for determining the so-called ionosphere correction using GNSS (Global Navigation Satellite Systems). Radio waves, used for satellite navigation have a very high frequency and are not reflected by the ionosphere, but as they pass through it, they receive additional delay, which introduces errors in determining the coordinates of the receiver. Knowing the values of TEC allows for correction of the readings (Hansen et al., 1997).

Data

This study uses values of the planetary index of geomagnetic activity Kp, published in NOAA- https://www.ngdc.noaa.gov. Data from the vertical probing of the ionosphere with radio waves (foF2 and MUF3000) are provided by the Ionospheric station at NIGGG-BAS. Data for the variations of the Earth's magnetic field are provided by INTERMAGNET- http://www.intermagnet.org/. To present the magnetic field course, data from the Panagyurishte (PAG) station with coordinates 42.5 ° N, 24.2 E° was taken. The TEC values were obtained by the Center for Orbit Determination of Europe (CODE) - ftp://ftp.unibe.ch/aiub/CODE/. Because the data are in grid with a 2.5° step in latitude and 5° in longitude, the point nearest to Sofia was selected, namely 42.5°N, 25°E.

Experimental results

This work examines two geomagnetic storms - the storm on 5 April 2010 and the other storm on 9 March 2012. Both of them are Severe (G4, Kp =8), according to NOAA Space Weather Scales. The first storm to be explored on April 5, 2010 is a typical storm with a sudden start. The sharp increase of Kp to value (~ 8) occurs at noon (local time) on 5 April of practically calm or slightly disturbed conditions. The subsequent response of Kp is a gradual decrease in value, on 6 April - the index ranges around 5, which is considered a (Minor) disturbed state. Normalization of the geomagnetic activity occurs at 7 April - when the value of Kp is about 4.

The path of the X component of the magnetic field on the graphic (Figure 1), measured at Panagyurishte station, is typical for geomagnetic stations at middle latitudes. During the storm an overall decrease in the value of the X component around 80nT (about 0.34%) is observed. In geomagnetic storms middle latitude stations show effects such as an increase of the equatorial circular current (Dst- variations) and the currents, that are induced in the polar regions (chaotic variations). Anomalies in the ionosphere (ionospheric storm) obviously come with some delay. It is noted that at 5 April the values of foF2 and MUF3000 do not differ significantly from those in the calm state. A significant negative anomaly occurs on 6 April, with a half-day delay from the onset of the storm. This phenomenon is due to the inertia of the ionosphere. The decrease in MUF300 is about 10-12 MHz, which is the narrowing of the range of frequencies at which radio communication is possible at a distance of 3000 km.

TEC anomalies are fundamentally different from the anomalies in the critical frequencies. The sharp rise in TEC values at around 5 TECU at noon by around 15 TECU indicates that the response is entirely positive and the delay to the storm is minimal. The presence of positive and negative phases in TEC response is due to different mechanisms of change of the electron concentration in the areas of the ionosphere (Pancheva et al, 2016).

The other storm, this paper considers, occurred on 9 March 2012. Unlike the first storm examined this one doesn`t have a sudden onset, and its manifestation affects

reviewed charts on the previous date as early as 7 March. There is a disturbance at midday (Moderate; G2, Kp = 6), which may indicate an upcoming geomagnetic activity. In the coming days, Kp switches, with a maximum loan amount of 9 March. Then the index becomes 8, which is classified as a severely disturbed state (Severe; G4, Kp = 8). Normalization of geomagnetic activity occurs the next day -10 of March.

For magnetic storm tracking, the same station (PAG) from Mid-Range Geomagnetic Observatories was again selected for this storm. Storm variations in the X-component of the magnetic field are about 140 nT (about 0.6%). The ionospheric storm is expressed by anomalies in foF2 and MUF3000. It can be seen from the graph that the values of the two values for the period 9-10 March 2012 have a very low negative anomaly. Again, the delay in the response is minimal [Kutiev, Mukhtarov, 2001]. The MUF3000 is about 5 MHz. The increase in critical frequencies does not affect radio links. The sudden rise above the TEC by 15 TECU at the end of 7 March shows both the positive response of this magnitude, the first phase of the storm, and the absence of any apparent delay. The second (major phase) of the storm does not produce a visible positive response in the TEC, but in the late hours of 9 and 10 there is a pronounced negative response.

The behavior of the ionosphere over Bulgaria during the geomagnetic storm on 5 April 2010 and 9 March 2012 is shown on Fig. 1 and Fig. 2.

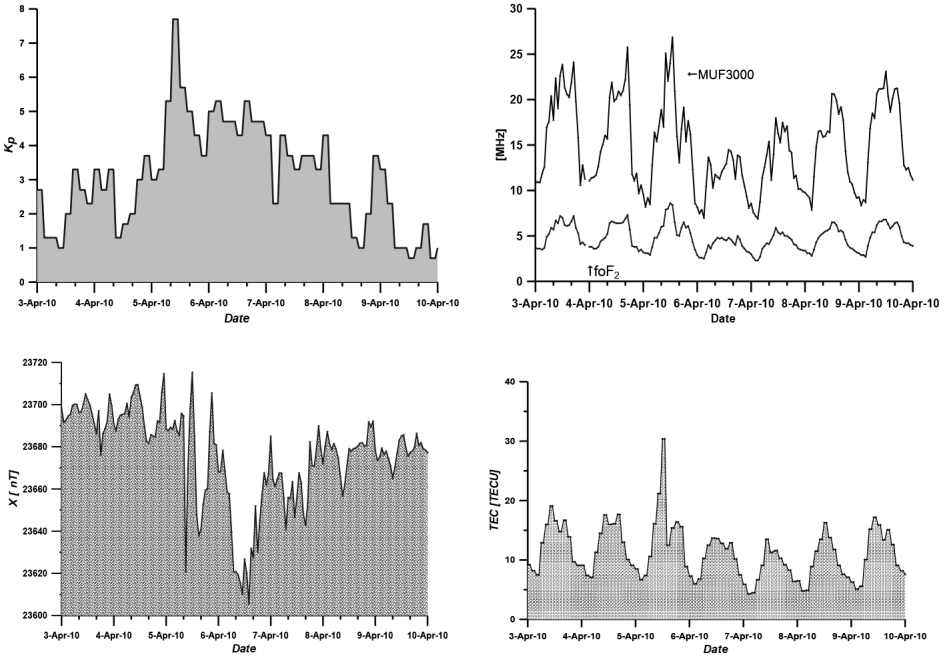

Fig. 1. Variations of Kp-index (upper left plot), the horizontal geomagnetic field (bottom left plot), critical frequencies (upper right plot) and TEC (bottom right plot) during the geomagnetic storm 5 April 2010.

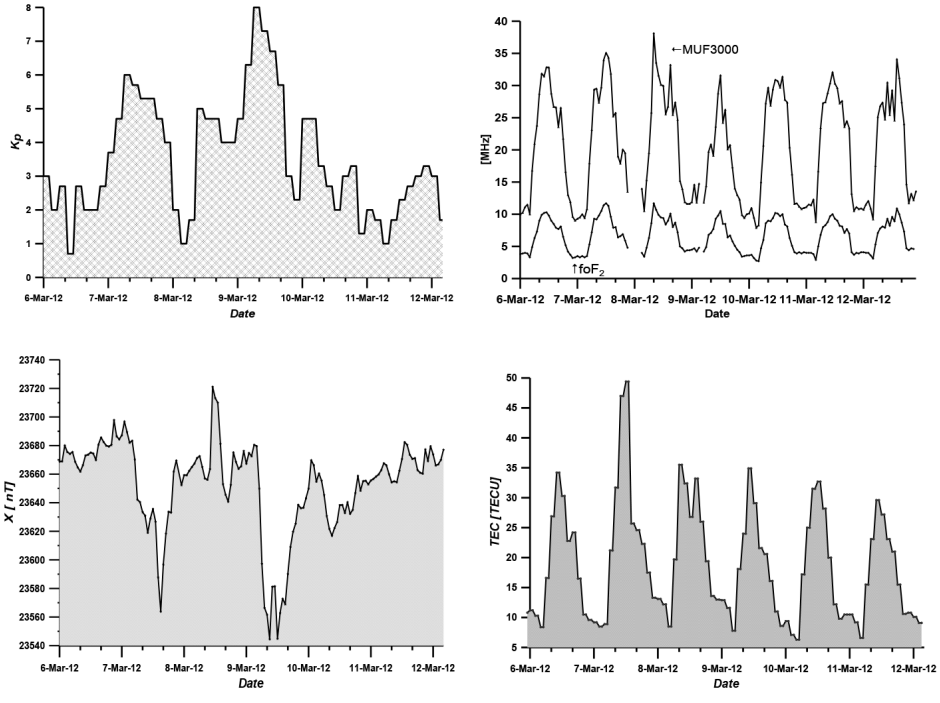

Fig. 2. Variations of Kp-index (upper left plot), the horizontal geomagnetic field (bottom left plot), critical frequencies (upper right plot) and TEC (bottom right plot) during the geomagnetic storm 9 March 2012.

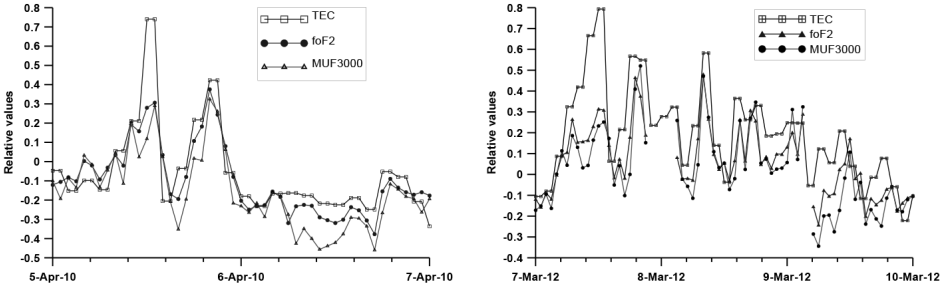

Fig. 3. Relative values of ionospheric quantities during two geomagnetic storms. Upper panel - shows the status of the ionosphere during the storm of April 5, 2010. Bottom panel - shows the status of the ionosphere during the storm of March 9, 2012.

The idea of presenting the relative values (Kutiev & Muhtarov, 2003, Pancheva et al., 2016) of the variables shown in this study is to eliminate the 24-hour diurnal course in each component and to eliminate the impact of different measurement units. As shown in Fig. 3 the relative shift path shows that in TEC the positive response is much stronger than

in foF2 and MUF3000. Due to the fact that foF2 and MUF3000 characterize the area of the ionosphere around its maximum, and the TEC is also formed from the upper F-region, this means that the increase in electronic concentration in the initial phase of the storms occurs predominantly at heights above the maximum.

Comments and conclusions

The geomagnetic and ionospheric anomalies during two geomagnetic storms, discussed in this article illustrate their impact on communications and navigation. Changes in the geomagnetic field itself are insignificant. The analysis shows that the horizontal component of the magnetic field varies only around 0.34% - 0.6% and can`t be expected to have a noticeable effect on the navigation compass.

Geomagnetic storms impact is strongest on shortwave radio communications. During extreme events the range of frequencies at which radio communication is possible at a certain distance may be reduced nearly twice. This may lead to disintegration of many of the existing radio communications which are based on ionospheric reflection.

The impact of changes of the electron concentration in the ionosphere during the storm on GNSS navigation has a range of several meters, which is significant for precise positioning.

The correct determination of the ionosphere correction on GNSS receivers is essential to improvement the accuracy of satellite navigation. The determination of this ionospheric correction depends on the precision of the estimated value of TEC, which makes the TEC prediction (especially in the case of geomagnetic anomalies) particularly relevant. Forecasting of TEC in case of geomagnetic anomalies requires the determination on the general patterns of ionosphere response during geomagnetic storms.

The present paper analyzes the ionospheric anomalies over Bulgaria during two geomagnetic storms. This article is part of the empirical analysis that is needed to create a prognostic model for the ionospheric characteristics during anomalies of geomagnetic origin. This method can be used by users work with short wave radio communications and GNSS navigations.

References

Hansen, A. J., T. Walter, and P. Enge. “Ionospheric correction using tomography.” Proceedings of Institute of Navigation ION GPS-97, Kansas City (1997): 249-260.

Kutiev, I., P. Mukhtarov. Empirical modeling of global ionospheric fo F2 response to geomagnetic activity, JOURNAL OF GEOPHYSICAL RESEARCH, VOL. 108, NO. A1, 1021, doi: 10.1029/2001JA009134, 2003

Mukhtarov, P., N. Penov, D. Pancheva. N(h) PROFILES DERIVED FROM IONOGRAMS AND THEIR APPLICATION FOR STUDYING MID-LATITUDE IONOSPHERIC RESPONSE TO GEOMAGNETIC STORMS, Comptes rendus de l’Acad´emie bulgare des Sciences, Tome 66, No 9, 2013

NOAA Space Weather Scales, http://www.swpc.noaa.gov/noaa-scales-explanation
Pancheva, D., P. Mukhtarov, B. Andonov. Global structure of ionospheric TEC anomalies driven by geomagnetic storms, Journal of Atmospheric and Solar-Terrestrial Physics 145 (2016) 170–182, www.elsevier.com/locate/jastp

Йоносферни аномалии над България по време на две геомагнитни бури

Р. Божилова

Резюме: В настоящата работа се разглеждат йоносферните аномалии над територията на България по време на геомагнитни бури от слънчев произход – бурята от 5 април 2010 г. и тази от 9 март 2012 г. Реакцията на йоносферата над България е представена чрез данните на Йоносферна станция София при НИГГГ – БАН. Стойностите на Total Electron Content (TEC) са получени от Center for Orbit Determination of Europe (CODE). Данните за вариациите на земното магнитно поле са получени от INTERMAGNET. Разглежда се станция Panagyurishte (PAG), намираща се на територията на България. Анализирано е влиянието на йоносферните аномалии върху радиовръзките на честоти от късовълновия диапазон и спътниковата навигация.

RELATIONS BETWEEN MP AND ML MAGNITUDE SCALES

M. Popova

National Institute of Geophysics, Geodesy and Geography, BAS, Akad G.Bonchev street, bl.3, Sofia, Bulgaria

Abstract. The work focuses on comparison of the magnitude estimations for near earthquakes determined by the Bulgarian Seismic Center (SOF) with the assessments of the national centers in the neighboring Balkan countries (Romania - BUC, Serbia - BEO, Macedonia - SKO, Greece - THE and NOA and Turkey - KAN) and the European Mediterranean Seismic Center (EMSC). 372 earthquakes located in a spatial window of 40.0º - 44.5º N; 21.0º - 29.0º E, occurred in 2007 - 2011, with ML magnitudes ranging from 3.0 up to 5.4 (the lower magnitude threshold M = 3.0 is determined by SOF) were used in the study.

Key words: earthquake, magnitude, magnitude estimates, seismic centers

Introduction

The size of the magnitude is a conditional, scalar, dimensionless indicator of seismic energy released in the seismic focus. Since the first work of Richter (1935) when the local magnitude scale, ML, (commonly called Richter magnitude) was initially defined the earthquake magnitude became the most common measure of the size of an earthquake. This magnitude is known in seismology as local magnitude ML or Richter's magnitude.

The introduction of magnitude makes it possible to compare the size of earthquakes in an instrumental way across the world. Magnitude is used to scale up a number of physical characteristics of earthquakes: emitted seismic energy (eg Gutenberg, Richter, 1936. Gutenberg, Richter, 1956); geometric characteristics of the seismic outbreak (eg Riznichenko 1976, Bonilla et al., 1984; Ambraseys, 1988; Wells, Coppersmith, 1994); shifting of the fault (e.g., Bonilla et al., 1984); (Eg, Ambraseys et al., 1996; Ambraseys et al., 2005, et al., 1996), and attenuation of seismic effects (macroseismic intensity, maximum acceleration, velocity and displacement, etc.); size of the aftershock region (e.g., Utsu, Seki, 1954, Konstantinou et al, 2005).

Magnitude scales are used for systemic classification of earthquakes. The classification is relative: the magnitude of an earthquake is determined by comparison and in relation to the normative, reference earthquake. The comparison is absolute in the

sense of the definitional formalization, and the zero of the scale depends on the definition of the reference earthquake. Richter sets the foundations of the magnitude scale with his publications dating back to 1935. The scale is based on the following equation:

$$M_L = LogA(D)\text{-}LogA_0(D), \text{ where } M_L = 0\ A(100) = 0.001 \text{ mm}) \quad (1)$$

The magnitude is defined as the decimal logarithm of the maximum amplitude $logA_0$ (A_0 measured in mm) from a seismogram of the Wood-Anderson torrent seismograph at an epicentre distance of 100 km. The amplitude A(D) measured at distances D is reduced to a standard distance of 100 km using an empirical calibration function $logA_0$ (D) (tabulated for 25<D<600 km, logA0(100)= -3).

At present different magnitude scales are applied in seizmological practice. Most of these scales are mainly based on empirical dependencies containing several constants (or empirically derived functions). These constants are determined in such a way that the magnitudes on the new scale are in agreement (at least in a certain magnitude interval) with an already existing scale. The introduction of many magnitude scales exacerbates the problem of assessing the magnitude of earthquakes. Unfortunately, attempts to introduce a standard magnitude scale into the world have so far failed.

The target of the present work is to compare the M_L magnitude estimates applied in the routine practice of NOTSSI (the Mp magnitude, defined in Christoskov et al., 2012) and local magnitude M_L (defined by Richter) which has been used in many of the Balkan Centers and the European Seismological Center (EMSC / CSEM). The task was sought by comparing the magnitude estimates for 372 near earthquakes (distant from the territory of the country at distances up to 150 km) determined by the Bulgarian Seismic Center (SOF) with the local magnitude (M_L) estimates of the national centers in the neighboring Balkan countries (Romania - BUC, Greece - THE and NOA, Turkey - KAN, FYROM - SKO and Serbia - BEO) and tne European Mediterranean Seismic Center (EMSC).

Input data and method applied

To perform this study it was necessary to create an earthquake catalog with information on all earthquakes, for which magnitudes expressed in the M_L scale estimated by several agencies, were available, and which occurred during the last few decades.

The sample of data used in the study includes: 372 earthquakes located in a spatial window of 40.0º - 44.5º N; 21.0º - 29.0º E with a ML (marked here M_{sof}) in the interval $3.0 \leq M_L \leq 5.4$ (the lower magnitude threshold M = 3.0 is determined by the NOTSSI); 315 earthquakes determined by the EMSC (marked here M_{emsc}); 88 earthquakes determined by BUC, Romania; 299 earthquakes defined by THE, Greece; 105 earthquakes determined by KAN, Turkey; 115 earthquakes determined by SKO, FYROM; 115 earthquakes set by BEO, Serbia; and 189 earthquakes identified by NOA, Greece.

In the study, a regression analysis was used to minimize mean square deviation using the least squares method (LSQ), which assumes that the independent variable is accurately defined without error.

The study was performed in two stages:

First Stage - It is assumed that the EMSC's magnitude estimates are the most credible because they are based on a large sample of seismological data from the same type of seismometers. To verify this assumption we have plotted M_L given by EMSC versus M_L reported by national centers (SOF, BUC, THE, KAN, SKO, BEO and NOA).

Second Stage - the SOF magnitude estimates are compared with M_L reported by the other national centers (BUC, THE, KAN, SKO, BEO and NOA).

Results

First stage

The results obtained in the first stage of the present study are presented in Figure 1-7. The diagrams illustrate the consistency of M_{emsc} with M_L estimates reported by the national centers.

Figure 1 shows the relation between M_L magnitudes given by EMSC and SOF. 315 events occurred in and around Bulgaria were used. The diagram of Figure1 shows the variation of M_L EMSC versus M_L SOF (least-squares'fit). The relation is:

$$M_{emsc} = 0.98\ M_{sof} + 0.02 \pm 0.33. \quad (2)$$

M_{emsc} / M_{sof} relation is linear for the considered range of magnitudes ($3.0 \leq M_L \leq 4.6$). The relation (2) indicates that the M_L magnitudes given by EMSC and SOF are very close (M EMSC = 0.98 M SOF + 0.02) although the uncertainties are rather high ($\sigma = 0.33$). The data dispersion decreases for magnitudes above 3.5, reaching a value less than 0.3, which is the accuracy of the magnitude determinations.

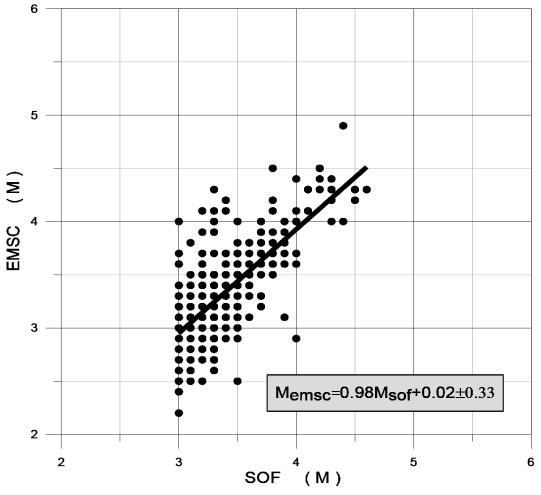

Figure 1. Correlation between M_L from EMSC and M_L from SOF for 315 shallow earthquakes. The straight line is the best fit.

Figure 2 shows the relation between M_L magnitudes given by EMSC and KAN (Turkey). 105 events occurred in a spatial window of 40.0º - 44.5º N; 21.0º - 29.0º E were used. The diagram of Figure2 shows the variation of M_L EMSC versus M_L KAN. The relation that expresses the best-fit line in the least squares'sense is:

$$M_{EMSC} = 0.94\, M_{KAN} + 0.22 \pm 0.18. \quad (3)$$

M_{emsc} / M_{kan} relation is linear for the considered range of magnitudes ($2.6 \leq M_L \leq 4.6$).

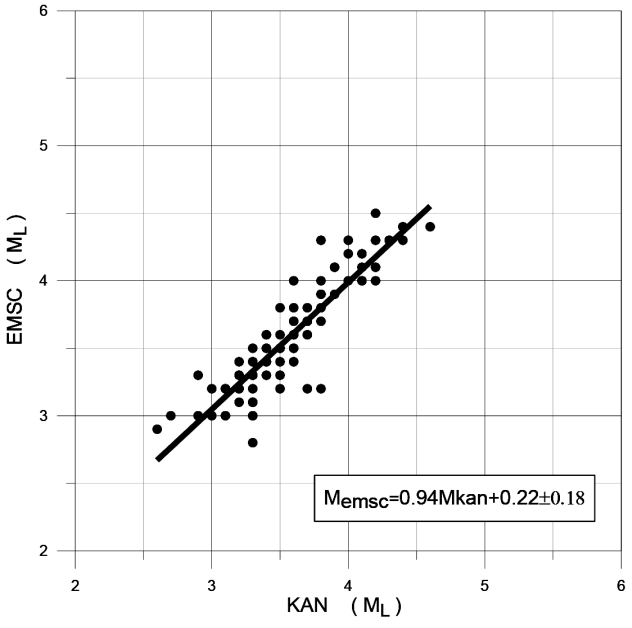

Figure 2. Correlation between ML from EMSC and ML from KAN (Turkey) for 105 shallow earthquakes. The straight line is the best fit.

The relation (3) indicates that the M_L magnitudes given by EMSC and KAN are almost equivalent ($M_{EMSC} = 0.94\, M_{KAN} + 0.22$). Overall, M_L KAN are very slightly higher than the EMSC estimates. The slight bias between M_L EMSC and M_L KAN is observed ($\sigma = 0.18$).

Figure 3 shows the relation between M_L magnitudes given by EMSC and BUC (Romania) 88 events occurred in a spatial window of 40.0º - 44.5º N; 21.0º - 29.0º E were used. The diagram of Figure 3 shows the variation of M_L EMSC versus M_L BUC (least-squares fit). The relation is:

$$M_{EMSC} = 0.68\ M_{BUC} + 1.09 \pm 0.26. \quad (4)$$

M_{emsc} / M_{kan} relation is linear of the considered range of magnitudes ($2.3 \leq M_L \leq 4.8$).

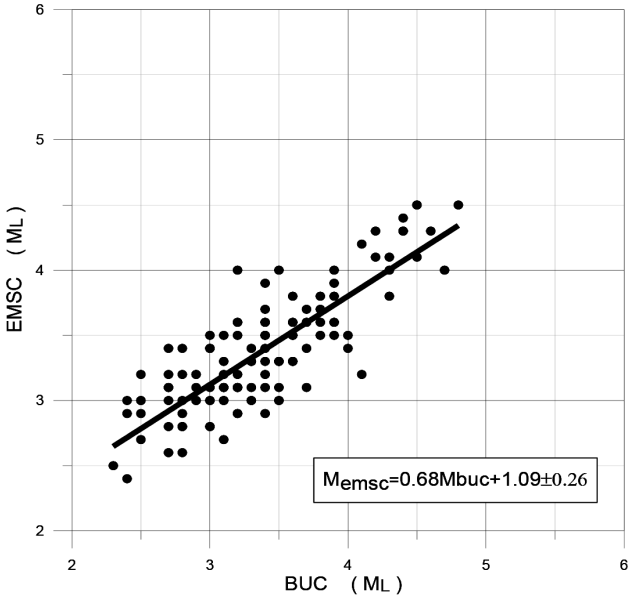

Figure 3. Correlation between ML from EMSC and ML from BUC (Romania) for 88 shallow earthquakes. The straight line is the best fit.

The relation (4) indicates that the M_L magnitudes given by EMSC and BUC canot be considered as equivalent ($M_{EMSC} = 0.68\ M_{BUC} + 1.09$) and the uncertainties are rather high ($\sigma = 0.26$).

Figure 4 shows the relation between M_L magnitudes given by EMSC and THE (Greece). 299 events occurred in a spatial window of 40.0º - 44.5º N; 21.0º - 29.0º E were used. The diagram of Figure4 shows the variation of M_L EMSC versus M_L THE. The relation that expresses the best-fit line in the least squares'sense is:

$$M_{EMSC} = 0.83\ M_{THE} + 0.53 \pm 0.2. \quad (5)$$

M_{emsc} / M_{the} relation is linear of the considered range of magnitudes ($2.5 \leq M_L \leq 5.5$). The relation (5) indicates that the M_L magnitudes given by EMSC and THE are close ($M_{EMSC} = 0.83$ M the + 0.53) although the uncertainties are high ($\sigma = 0.20$). Overall, THE's estimates are slightly lower than the EMSC estimates.

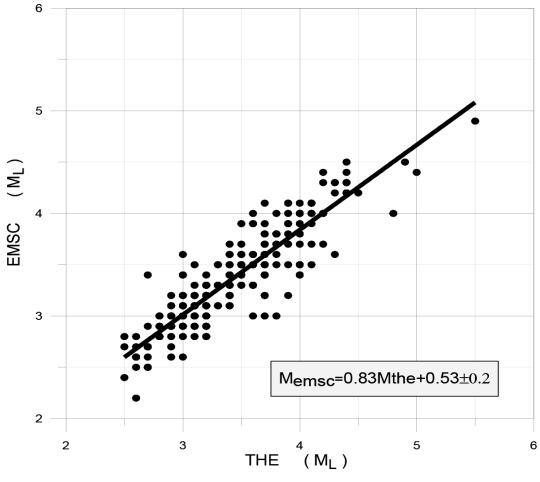

Figure 4. Correlation between ML from EMSC and ML from THE (Greece) for 299 shallow earthquakes. The straight line is the best fit.

Figure 5 shows the relation between M_L magnitudes given by EMSC and SKO (FYROM). 115 events occurred in a spatial window of 40.0º - 44.5º N; 21.0º - 29.0º E were used. The diagram of Figure5 shows the variation of M_L EMSC versus M_L SKO. The relation that expresses the best-fit line in the least squares'sense is:

$$M_{EMSC} = 0.78\ M_{SKO} + 0.832 \pm 0.22. \quad (6)$$

M_{emsc} / M_{sko} relation is linear of the considered range of magnitudes ($2.0 \leq M_L \leq 4.8$).

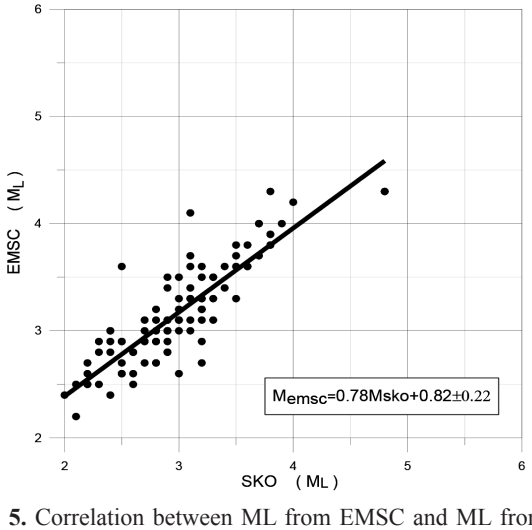

Figure 5. Correlation between ML from EMSC and ML from SKO (FYROM) for 115 shallow earthquakes. The straight line is the best fit.

The relation (6) indicates that the M_L magnitudes given by EMSC and SKO cannot be considered as equivalent ($M_{EMSC} = 0.78\ M_{sko} + 0.82$) and the uncertainties are high ($\sigma = 0.22$).

Figure 6 shows the relation between M_L magnitudes given by EMSC and BEO (Serbia). 115 events occurred in a spatial window of 40.0º - 44.5º N; 21.0º - 29.0º E were used. The diagram of Figure 6 shows the variation of M_L EMSC versus M_L BEO. The relation that expresses the best-fit line in the least squares'sense is:

$$M_{EMSC} = 0.73\ M_{BEO} + 0.97 \pm 0.27. \quad (7)$$

M_{emsc} / M_{sko} relation is linear of the considered range of magnitudes ($2.0 \leq M_L \leq 4.4$).

The relation (7) indicates that the M_L magnitudes given by EMSC and BEO cannot be considered as equivalent ($M_{EMSC} = 0.73 M_{BEO} + 0.97$) and the uncertainties are rather high ($\sigma = 0.27$).

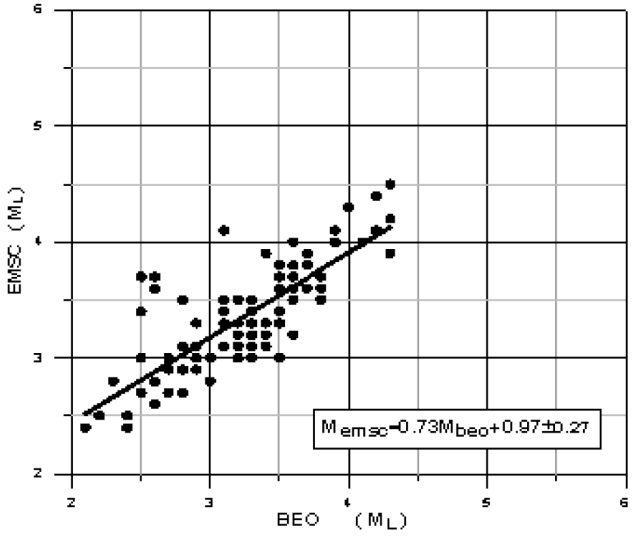

Figure 6. Correlation between ML from EMSC and ML from BEO (Serbia) for 115 shallow earthquakes. The straight line is the best fit.

Figure 7 shows the relation between M_L magnitudes given by EMSC and NOA (Greece). 189 events occurred in a spatial window of 40.0º - 44.5º N; 21.0º - 29.0º E were used. The diagram of Figure 7 shows the variation of M_L EMSC versus M_L NOA. The relation that expresses the best-fit line in the least squares'sense is:

$$M_{EMSC} = 0.75\ M_{NOA} + 0.92 \pm 0.24. \quad (8)$$

M_{emsc} / M_{sko} relation is linear of the considered range of magnitudes ($2.2 \leq M_L \leq 4.5$).

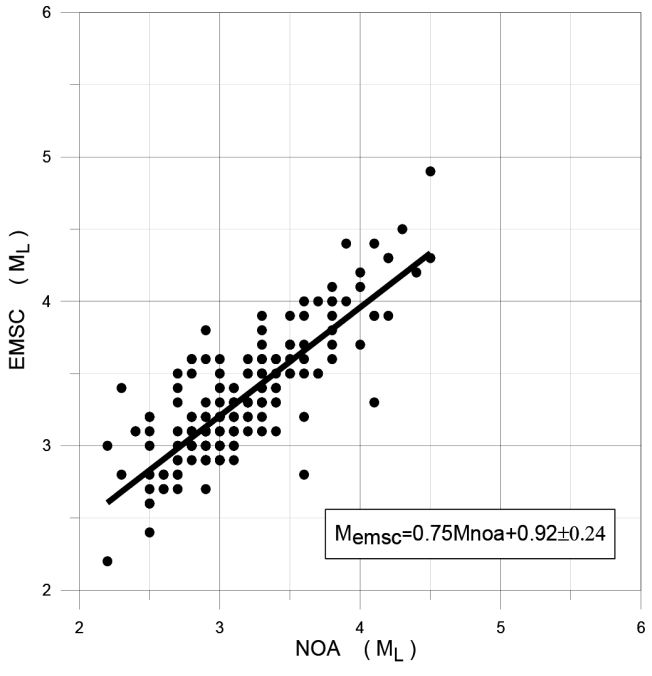

Figure 7. Correlation between ML from EMSC and ML from NOA (Greece) for 189 shallow earthquakes. The straight line is the best fit.

The relation (8) indicates that the M_L magnitudes given by EMSC and NOA cannot be considered as equivalent ($M_{EMSC} = 0.77\ M_{NOA} + 0.92$) and the uncertainties are high ($\sigma = 0.22$).

Second Stage

SOF (Bulgaria) magnitude estimates are compared with M_L reported by the other national centers: BUC (Romania), THE (Greece), KAN (Turkey), SKO (FYROM), BEO (Serbia) and NOA (Greece). The results are presented in Figure 8-13. The magnitude diferences between SOF - BUC, SOF - THE, SOF - KAN, SOF - SKO, SOF - BEO and SOF – NOA versus M_L SOF are presented in the figures.

The diagram of Figure 8 shows the variation of SOF - BUC, versus M_L SOF. The relation that expresses the best-fit line in the least squares'sense is:

$$M_{SOF} - M_{BUC} = 0.1\ M_{SOF} + 0.40 \pm 0.45. \quad (9)$$

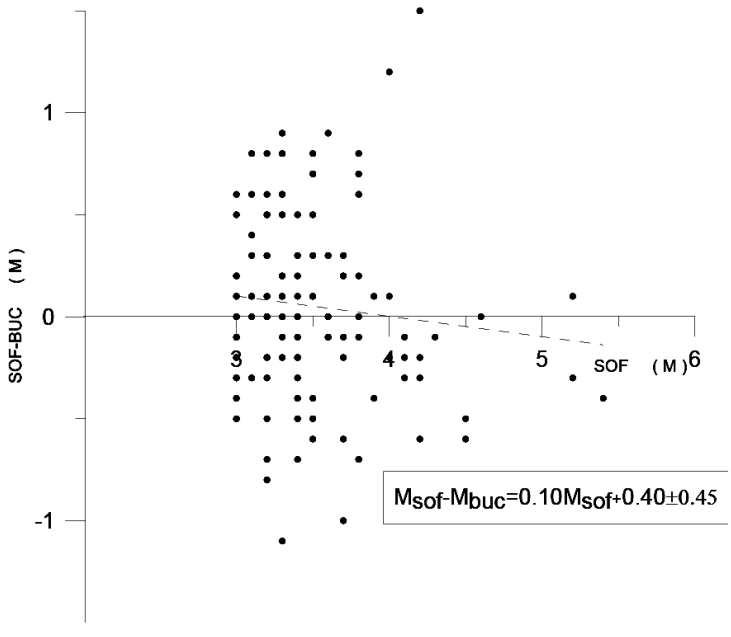

Figure 8. Correlation between magnitude diference SOF – BUC and ML from SOF for 88 shalow earthquakes in the magnitude interval interval 3.0≤ ML ≤ 5.4

As can be seen from the figure, the differences vary predominantly between -1 and +1. In the magnitude interval of 3.0 ≤M≤4.0 the differences are highly dispersed with almost equal number of positive and negative values. For magnitudes above 4.0, negative differences prevail, ie SOF magnitude estimates are lower than those of BUC. Overall, BUC (Romania) estimates are higher than the SOF estimates in the magnitude range considered (3.0≤ M_L ≤ 5.4). The relation (9) indicates that the M_L magnitudes given by SOF and BUC cannot be considered as equivalent and the uncertainties are high ($\sigma = 0.45$).

The diagram of Figure 9 shows the variation of variation of SOF - THE, versus M_L SOF. The relation that expresses the best-fit line in the least squares'sense is:

$$M_{SOF} - M_{THE} = 0.03\ M_{SOF} + 0.08 \pm 0.36. \quad (10)$$

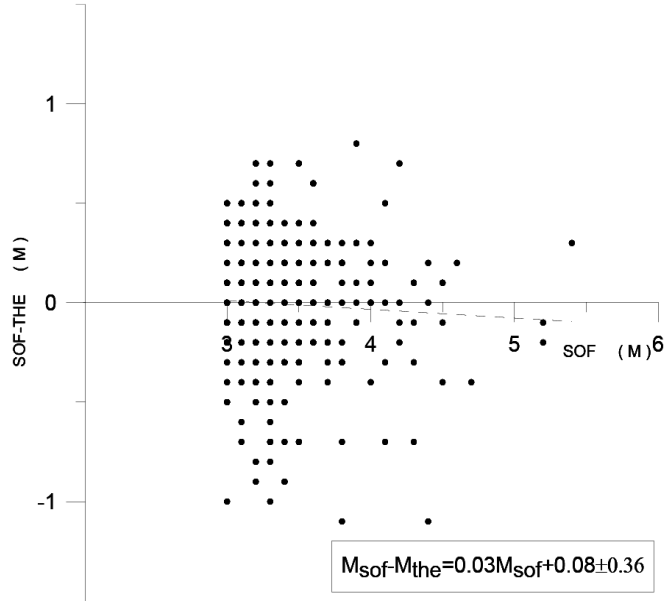

Figure 9. Correlation between magnitude difference SOF – THE and ML from SOF for 299 shalow earthquakes in the magnitude interval 3.0≤ ML ≤ 5.4

As can be seen from the figure, the differences vary predominantly between -1 and +1. In the magnitude interval 3.0 £M≤4.0 the differences are dispersed with almost equal number of positive and negative values. For magnitudes above 4.0, negative differences prevail, ie SOF magnitude estimates are lower than those of THE. The data dispersion decreases for magnitudes above 4.0, reaching a value of about 0.5.

The relation (10) indicates that the M_L magnitudes given by SOF and THE cannot be considered as equivalent and the uncertainties are high ($\sigma = 0.36$).

The diagram of Figure 10 shows the variation of SOF - KAN, versus M_L SOF. The relation that expresses the best-fit line in the least squares'sense is:

$$M_{SOF} - M_{KAN} = 0.18\, M_{SOF} - 0.71 \pm 0.31. \quad (11)$$

As can be seen from the figure, the differences vary mainly between -0.7 and +0.7. Overall, KAN (Turkey) estimates are higher than the SOF estimates in the magnitude range considered ($3.0 \leq M_L \leq 5.4$).

The relation (11) indicates that the M_L magnitudes given by SOF and KAN cannot be considered as equivalent and the uncertainties are high ($\sigma = 0.31$).

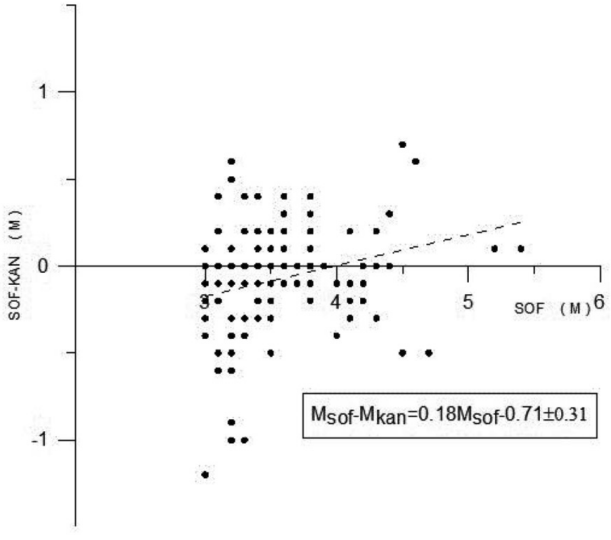

Figure 10. Correlation between magnitude difference SOF – KAN and ML from SOF for 105 shalow earthquakes in the magnitude interval interval 3.0≤ ML ≤ 5.4

The diagram of Figure 11 shows the variation of SOF - SKO versus M_L SOF. The relation that expresses the best-fit line in the least squares'sense is:

$$M_{SOF} - M_{SKO} = 0.06\, M_{SOF} + 0.31 \pm 0.22. \quad (12)$$

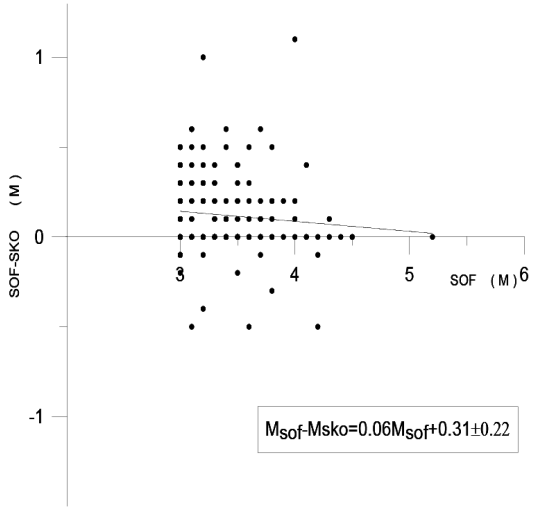

Figure 11. Correlation between magnitude difference SOF – SKO and ML from SOF for 115 shalow earthquakes in the magnitude interval interval 3.0≤ ML ≤ 5.4

As can be seen from the figure, the differences vary mainly between -0.7 and +1.0. For the considered magnitude interval 3.0 £M £5.4, the positive differences prevail, ie SOF magnitude scores are higher than those of the SKO.

The relation (12) indicates that the M_L magnitudes given by SOF and SKO cannot be considered as equivalent and the uncertainties are high ($\sigma = 0.31$).

The diagram of Figure 12 shows the variation of SOF - BEO, versus M_L SOF. The relation that expresses the best-fit line in the least squares'sense is:

$$M_{SOF} - M_{BEO} = 0.21 \pm 0.39. \quad (13)$$

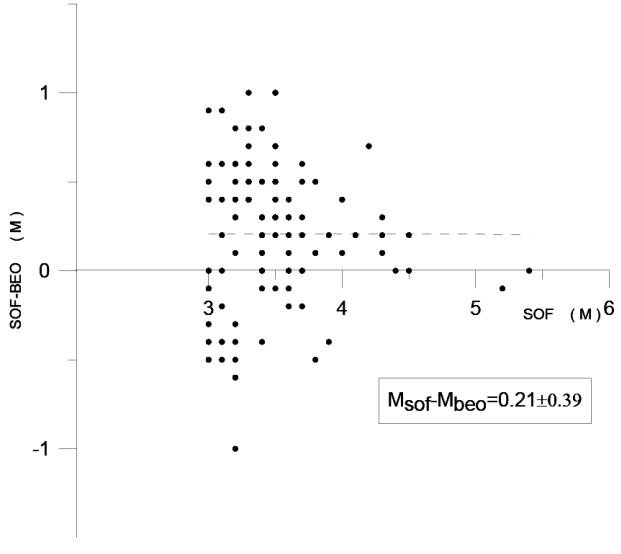

Figure 12. Correlation between magnitude difference SOF – BEO and ML from SOF for 115 shalow earthquakes in the magnitude interval interval 3.0≤ ML ≤ 5.4

As can be seen from the figure, the differences vary mainly between -1.0 and +1.0. The data dispersion decreases for magnitudes above 4.0. For the considered magnitude interval 3.0 £M £5.4, the positive differences prevail, ie SOF magnitude scores are higher than those of the BEO.

The relation (13) indicates that the M_L magnitudes given by SOF exceeded those of BEO by an average of 0.21 - a good match although the uncertainties are rather high ($\sigma = 0.39$).

The diagram of Figure 13 shows the variation of variation of SOF - NOA versus M_L SOF. The relation that expresses the best-fit line in the least squares'sense is:

$$M_{SOF} - M_{NOA} = 0.18 \pm 0.36. \quad (14)$$

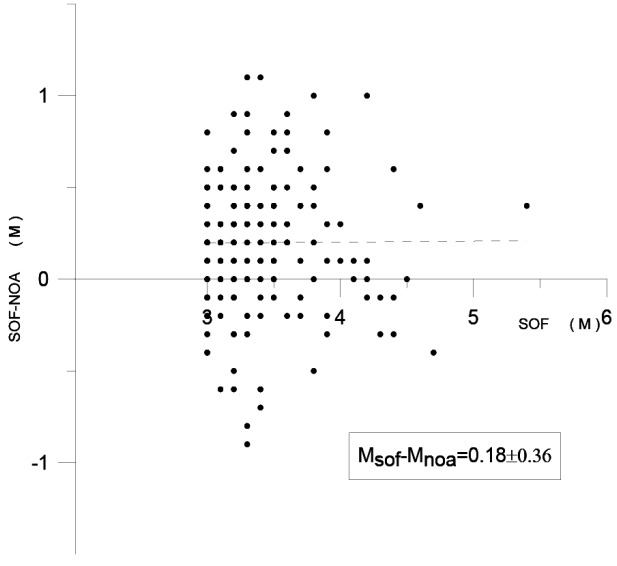

Figure 13. Correlation between magnitude difference SOF – NOA and ML from SOF for 189 shalow earthquakes in the magnitude interval 3.0≤ ML ≤ 5.4

As can be seen from the figure, the differences vary between -1 and +1. For the considered magnitude interval, 3.0 ≤M ≤5.0 the positive differences prevail, ie the SOF magnitude estimates are higher than those of NOA.

The relation (14) indicates that the M_L magnitudes given by SOF exceeded those of NOA by an average of 0.18 - a good match although the uncertainties are rather high ($\sigma = 0.36$).

Conclusion

The results of the study can be summarized in the following conclusions:

The closest to the M_L magnitudes given by EMSC are the M_L magnitudes reported by KAN (Turkish National Center) and SOF (Bulgarian National Center) although the uncertainties between M_L EMSC and M_L SOF are rather high ($\sigma = 0.33$);

The largest deviations from the M_L magnitudes reported by EMSC are observed for M_L magnitudes given by BUC (Romania) and BEO (Serbia);

M_L magnitudes given by NOA (Greece) and SOF are very close although the uncertainties are rather high ($\sigma = 0.36$). M_L magnitudes reported by SOF are slightly higher than those of SKO (FYROM) and BEO (Serbia) while the M_L magnitudes reported by BUC (Romania) and THE (Greece) exceed the M_L SOF (Bulgaria) in the considered magnitude range (3.0≤M≤5.4).

Acknowledgment. The work is supported by the program for career development of young scientists, BAS, Project DFNP-10 (2016–2017).

References:

Ambraseys N., 1988. Magnitude – fault length relationships for earthquakes in the Middle East, In: Historical Seismograms and Earthquakes of the World, Lee, W.H., Meyers, H. & Shimazaki, K. eds, Acad. Press Inc., 309-310.

Ambraseys, N., K. Simpson, J. Bommer, 1996. Prediction of horizontal response spectra in Europe, Earthquake Eng. and Struc. Dyn., 25(4), 371-400.

Ambraseys,. N., J. Douglas, S. K. Sarma,. and P. M. Smit, 2005.Equations for the Estimation of Strong Ground Motions from Shallow Crustal Earthquakes Using Data from Europe and the Middle East: Horizontal Peak Ground Acceleration and Spectral Acceleration. Bulletin of Earthquake Engineering, 3, 1–53.

Bonilla M., R. Mark J. Lienkaemper, 1984. Statistical relations among earthquake magnitude, surface rupture length, and surface fault displacement. Bull. Seism. Soc. Am., 74, p. 2379-2411.

Christoskov L., L. Dimitrova, D. Solakov, 2012. Magnitude determinations of P wave by digital broadband seismometers of NOTSSI network for local and regional events. Comptes Rendus de L'Academie Bulgare des Sciences, 65 (5).

Department of Geophysics, Univ. of Thessaloniki, Greece, http://geophysics.geo.auth.gr/

EMSC, http://www.emsc-csem.org/Earthquake/

Gutenberg, B., C. Richter, 1936. Magnitude and energy of earthquakes, Science, 83, 183-185.

Gutenberg, B. C. Richter, 1956. Earthquake magnitude, intensity, energy and acceleration, Bull. Seismol. Soc. Am., 46, 105-145.

KOERI, Istanbul,Turkey,http://sismo.deprem.gov.tr/

Seismological Survey of Serbia Belgrad, Serbia

Seismological Observatory Skopje, FYR of Macedonia

Konstantinou, I.; G. Papadopoulos, A. Fokaefs, K. Orphanogiannaki, 2005. Empirical relationships between aftershock area dimensions and magnitude for earthquakes in the Mediterranean Sea region Tectonophysics, Volume 403, Issue 1-4, p. 95-115.

NIEPh, Bucarest, Romania, http://infp.ro/

NOTSSI, BAS, Sofia, Bulgaria, http://ndc.niggg.bas.bg/

Richter, C., 1935. An instrumental earthquake scale: Seismological Society of America Bulletin, 25, 1, p. 1-32.

Utsu T., Seki A. 1954. A relation between the area of aftershock region and the energy of mainshock. J. Seism. Soc. Japan, 7, 233-240.

Ризниченко Ю., 1976. Размеры очага корового землетрясения и сейсмический момент, Исследования по физике землетрясений, с. 9-27, Наука, Москва.

Връзки между MP и ML магнитудни скали

М. Попова

Резюме. Настоящата работата е фокусирана върху сравнение на магнитудните оценки за близки земетресения, определени от Българския сеизмичен център (SOF), с оценките на националните центрове в съседните балкански страни (Румъния – BUC, Сърбия – BEO, Македония – SKO, Гърция – THE и NOA и Турция – KAN) и Европейският средиземноморски сеизмичен център (EMSC). В проучването са използвани 372 земетресения, генерирани в пространствен прозорец: 40.0º – 44.5º N; 21.0º - 29.0º E, реализирани между 2007г. и 2011 г., в магнитуден интервал 3,0≤ ML ≤5,4 (долният праг на магнитудната оценка - M = 3,0 е определен в SOF).

THREE GEOMAGNETIC STORMS IN JANUARY 2005 AND THEIR IMPACT ON TOTAL ELECTRON CONTENT

R. Bojilova

[1]National Institute of Geophysics, Geodesy and Geography -BAS, str. Acad. G. Bonchev, bl3, Sofia1113, Bulgaria,
e-mail: rbojilova@geophys.bas.bg

Abstract. This study presents the global and mid-latitude ionospheric response to three geomagnetic storms occurred in January 2005: the first one on 7-8 January, the second one on 17-19 January, and the last one on 21-22 January. This period has been selected, because no major sudden stratospheric warming (SSW) occurred during this month and according to many scientists this winter is represented as an example of a background reference case corresponding to a 'normal' year. Therefore, the observed ionospheric response to the considered geomagnetic storms could be attributed mainly to the external forcing. The reaction is explored by considering N(h) profiles registered by manually scaled ionosonde measurements at station Sofia (42.5°N, 25°E), which are used for calculating the total electron content (TEC) up to the F2-layer maximum (bottom-TEC). The full-TEC data are provided by the Center for Orbit Determination of Europe (CODE)-Bern, for the nearest point to Sofia. The main aim of this work is to compare in details the temporal variability of the full-TEC with bought that below (bottom-TEC) and up (top-TEC) the F2-layer maximum for each of the considered geomagnetic storms. It is found that for all investigated geomagnetic storms in January 2005 the bottom-TEC is considerably different from bought top-TEC and full-TEC. An explanation of the main mechanisms responsible for the observed difference has been proposed.

Key words: geomagnetic activity, TEC, ionospheric anomalies.

Introduction

Geomagnetic storms are associated with high-speed plasma injected into the solar wind from coronal mass ejections or coronal holes that impinges upon Earth's geomagnetic field. If the interplanetary magnetic field (IMF) Bz has southward direction then the solar wind energy enters the magnetosphere-ionosphere-thermosphere system

by establishing an interconnection between the southward IMF and the Earth's magnetic field lines. As a result the geomagnetic space environment becomes strongly disturbed and a global ionospheric storm occurs (Kamide and Kusano, 2015; Mukhtarov and Bojilova, 2017). The ionospheric structure and variability are related to changes in solar radiation and geomagnetic activity, together with the subsequent response of the thermosphere-ionosphere system (Roble, 1995). The ionosphere also varies in response to neutral winds (Schunk et al., 2009), electrodynamic coupling with the overlying plasmasphere and magnetosphere (Huba et al., 2005), and dynamical coupling with the underlying atmosphere particularly effective during low solar activity conditions (Mendillo et al., 2002; Rishbeth, 2006). It is well known that during geomagnetic storms the dynamics, electrodynamics and chemistry of the atmosphere-ionosphere system are modified on a global scale and cause positive and/or negative phases of ionospheric response (Gadzhev et al., 2013). The latitude and longitude, season, as well as the both storm onset time and maximum are the main factors which define the positive/negative response (Andonov et al., 2011; Mukhtarov et al., 2013a; Mukhtarov and Bojilova, 2017).

Three main reasons have been proposed to explain the observed storm phases: thermospheric composition changes, neutral wind perturbations and the electric fields of magnetospheric origin (Mendillo, 2006). The total electron content (TEC) is one of the particularly important physical quantities of the ionosphere. The main reason for the TEC importance is that the trans-ionospheric radio signals, used by the Global Navigation Satellite Systems (GNSS), may reach quite large range errors and these errors are proportional to the integral of the electron density along the ray path, i.e. proportional to slant TEC. It is measured by TEC Unit (TECU) as one TECU is equal to 1016 electrons/m^2. Therefore the ionospheric effect has become the largest error source in GNSS positioning, timing and navigation. Wang et al., (2010) has presented clear evidence that the negative storm response observed in the TEC maps at high- and mid-latitudes is directly related to the changes in the $[O]/[N_2]$ ratio. The geomagnetic storms significantly change the ionosphere especially the electron density and its vertical distribution, as well as the total electron content (TEC). The serious problems in the ground-based HF radio communications during negative ionospheric storm are caused because the electron density and TEC decrease much below their "quiet-time" levels. The positive ionospheric storms in which electron density and TEC increase much above their "quiet-time" levels can cause serious problems in satellite communication and navigation. Because the GPS signals are used by wide range of applications, any geomagnetic storm event which makes GPS signal unreliable could have significant impact on the society. That is why a detailed study of the ionospheric response to forcing from above and below is among the important mission of the ionosphere studies.

The purpose of this study is to compare in detail the temporal variability of the full-TEC with bought that below (bottom-TEC) and up (top-TEC) the F2- layer maximum for each of the considered geomagnetic storms in January 2005. It is found that for all cases examined in this study the bottom-TEC is considerably different from bought the top-TEC and the full-TEC. An explanation of the main mechanisms responsible for the observed difference has been proposed.

Data

The geomagnetic activity is described by the planetary Kp-index and the equatorial Dst-index that are received from: https://omniweb.gsfc.nasa.gov/. The TEC values for the nearest point to Sofia are obtained by the Center for Orbit Determination of Europe (CODE) at Astronomical and Physical Institutes of the University of Bern: ftp://ftp.unibe.ch/aiub/CODE/. The reason for using the closest to Sofia point with coordinates (42.5°N, 25°E) is that the TEC data have a grid spacing of 5◦ x 2.5◦ in longitude and latitude. The N(h) profiles up to the F2-layer maximum are derived from the manually scaled ionograms (Mukhtarov et. al, 2013b) of the ionosonde station Sofia- SQ143 (42.4°N, 23.2°E). The considered quantity bottom-TEC in this paper is defined as an integral of the electron density profile while the top-TEC is the difference between the full-TEC and the bottom-TEC. The TEC response to the geomagnetic storms is described by relative deviations of the considered all three quantities (the top-TEC, bottom-TEC and full-TEC) from their stationary diurnal course and are calculated by the formula:

$$rTEC(t) = \frac{TEC(t) - TECm(UT)}{TECm(UT)}$$

where t is the current time in hours that is counted from the beginning of the period considered, while UT is the universal hour corresponding to the moment t. The value TECm (UT) is the median, calculated on the base of the whole month considered.

Experimental results

Three clear storms, with maximum Kp~8 occurred in January 2005. Fig. 1 shows the planetary Kp-index giving information for the global variations of the geomagnetic field. The first storm begins on 7 January and the Kp-index reaches maximum of ~7.5-8 between 21-23 UT. This storm has duration of only ~18 hours, i.e. it is a short-time one. The second storm, begins on 17 January and has a duration of a few days because the Kp-index has values larger than 5 for more than 2 days. The maximum Kp-index is observed on January 18 having a value close to 8. The recovery phase of the storm begins in the next day but is interrupted because of the appearance of a new geomagnetic disturbance on January 21. The last geomagnetic storm is a short-time one, with duration less than a day. The sharp rise of the Kp-index to values above 8 is in the evening hours on 21 January. It is worth noting that the last storm starts under not very calm conditions due to the disturbances which occurred in the previous days.

The first geomagnetic storm occurs on 7-8 January 2005 and the TEC response is presented in Fig. 2. In order to have a general idea of what the global response to this storm is Fig. 2a presents the latitude-time cross-section of the relative TEC at a longitude of 25°E for the period of 7-10 January. This storm begins in the late hours on 7 January

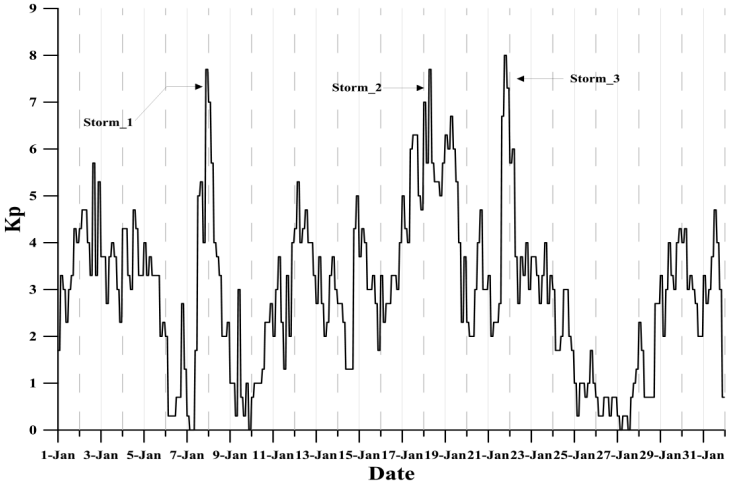

Fig. 1. Variations of the Kp-index in January 2005

and slightly after the midnight on 8 January the Kp-index reaches to ~ 7.5-8 (see Fig. 2c). Then a clear positive response is seen for all latitudes as the relative TEC is the largest at around 60°N. The summer Southern Hemisphere (SH) reacts predominantly negatively after the midnight on 8 January Fig. 2a. Such negative TEC response is typical for geomagnetic storms in summer (Pancheva et. al., 2016). The TEC response in the Northern Hemisphere (NH) is more complex (Fig. 2a). After the positive response seen at all latitudes in the late hours on 7 January it follows a negative response which can be traced only between 15°N and 50°N. At the same time a positive response is formed that is seen first at equatorial latitudes and later with some time delay it appears at mid-latitudes during the day-time on 8 January when the Kp-index is below 5 (sees Fig. 2c). While the positive response at high-mid latitudes during the late hours on 07 January is apparently associated with the direct ionization under the action of the charged particle precipitations into the night-side of the Earth's atmosphere the positive response during the day-time conditions is probably connected with electrodynamic effects. After the decay of the positive response during the afternoon hours on 8 January a long duration negative TEC reaction has been established (Fig. 2a); the latter is related to the change of the [O] / [N_2] ratio. Fig. 2b shows the relative values of the full-TEC (upper plot), top-TEC (middle plot) and bottom-TEC (bottom plot) for the period of 7-10 January. The bottom plot of Fig. 2c displays the Kp-index for the considered period. Considering the variability of the relative TEC (Fig. 2b) it is seen that all three quantities have first a positive response that is followed by a negative and then again a positive response. The largest changes of the relative values are as follow: (i) from -0.6 to +0.6 for the full-TEC; (ii) from -0.5 to +0.5 for the top-TEC, and (iii) from -0.8 to +1 for the bottom-TEC. These results clearly reveal that the bottom-TEC ionospheric changes are larger than those of both the top-TEC and the full-TEC.

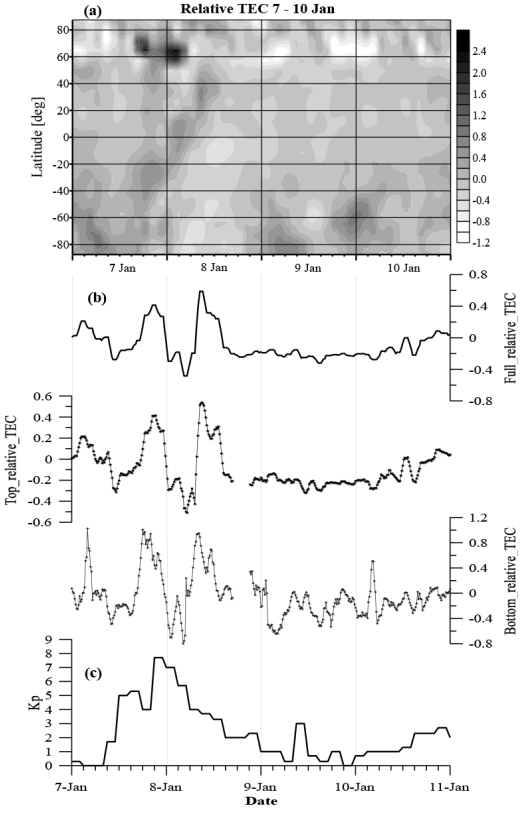

Fig. 2. (a) Global latitude-time cross section of the relative TEC; (b) temporal variability of the relative values of: the full-TEC (upper plot), top-TEC (middle plot), and bottom-TEC (bottom plot), and (c) Kp-index during the period of 7-10 January.

Fig. 3 is the same as Fig. 2 but presents the TEC response to the second geomagnetic storm; the period of 17-20 January is considered. This storm is different from the first one; it is without a sudden commencement and is significantly longer, more than 2 days. Fig. 3a shows the positive responses at latitude of 60°N during the early morning hours on 17 January when the geomagnetic activity, described by the Kp-index, is still lower than 5. Positive anomalies are seen also during the night-time hours of 17/18 and 18/19 January when the Kp-index varies between 6 and 7. It is worth noting that the large values of the night-time relative TEC at high latitudes are a result of the increase of the very low night-time TEC values in conditions close to a polar night. The relative TEC in the SH during the second half of 17 January reveals a positive response however after the midnight a negative response is observed that propagates from the polar latitudes to the equator; this is typical feature for the TEC response to the summer geomagnetic storms. The TEC

response in the tropical and middle latitudes of the NH on 17 and 18 January, presented in Fig. 3a, is predominantly positive one. Two impulses of the negative response are seen during the first half of January 19, however while the first one ranges between 15°N and 50°N the second one is only between 40°N and 50°N. The stable negative response appears during the night hours of 19/20 January observing at tropical and mid-latitudes. The long duration of this storm accompanied by a significant amount of energy draw in the Earth's atmosphere together with the increased inertia (Mukhtarov et al., 2013a; Mukhtarov et al., 2018) defines a considerable time of the ionosphere recovery. The relative values of the three characteristics: full-, top- and bottom-TEC, shown in Fig. 3b, demonstrates positive anomalies on January 18 as the response is the strongest for the bottom-TEC, ~2.2 above the median one. Further, while the full- and top-TEC show two positive peaks the bottom-TEC reveals three peaks. Similarly to the first storm here also, the temporal variability of the relative bottom-TEC is quite different from those of the full- and top-TEC.

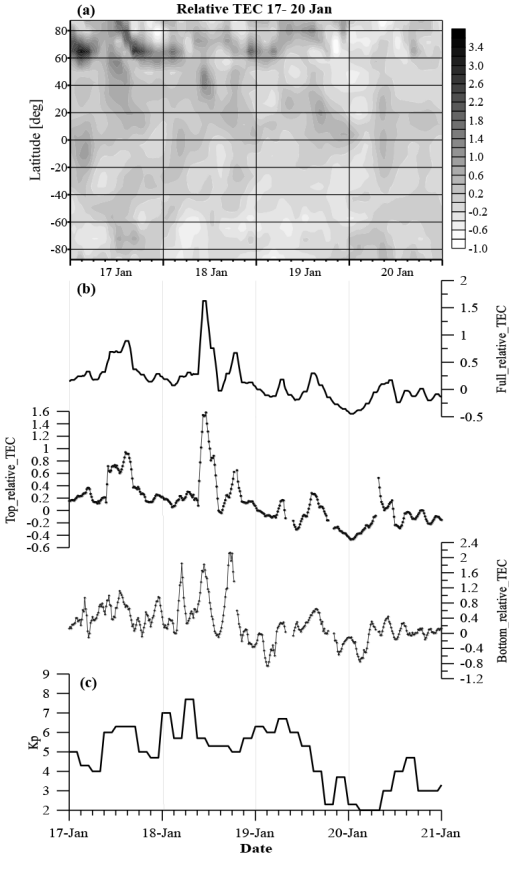

Fig. 3. The same as Fig. 2 but for the period of 17-20 January 2005

Fig. 4 presents the ionospheric response to the third geomagnetic storm that occurs on 21-22 January. This storm has approximately the same intensity as the previous two storms but has a short duration similarly to the first storm, 7-8 January. A short positive response at 60°N (Fig. 4a), coinciding with the onset of the storm, is analogous to the same phenomenon in other storms and is caused by the particle precipitations in the polar oval, i.e. direct ionization. In the SH after the evening hours on January 21 a homogeneous negative response is established. In the NH (Fig. 4a) however the TEC response strongly depends on the latitude. An initial positive response is observed at latitudes lower than 40°N while at high-mid latitudes the response is negative. After midnight all latitudes between the equator and 50°N demonstrate a negative response; only a short-term positive reaction occurs around noon. The observed complex response, particularly of the mid-latitude ionosphere, is probably related to the incomplete recovery of the previous storm leading to the overlapping of the positive and negative reactions due to different mechanisms acting simultaneously. As a result, this winter-time TEC response appears to be different from the winter-time response of the previous two storms considered in

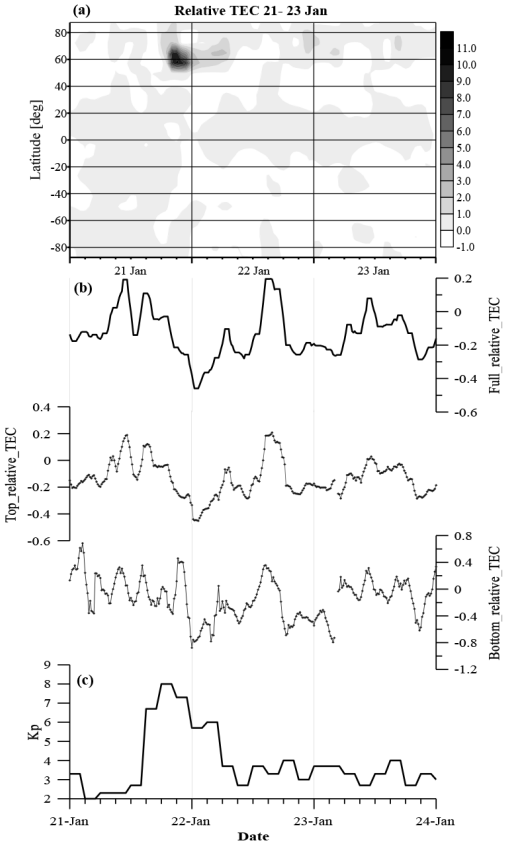

Fig. 4. The same as Fig. 2 but for the period of 21-23 January

this study, revealing strongly expressed latitudinal dependence of the reaction sign. The relative values of the full-, top- and bottom-TEC for the period of 21-23 January is shown in Fig. 4b. Similarly to the previous two storms here again the bottom-TEC reveals the largest changes (from -0.8 to 0.6) compared to the full- (from -0.5 to 0.2) and top-TEC (from -0.4 to 0.3).

Comments and conclusions

In this paper we have presented the global and mid-latitude ionospheric TEC response to three, moderate to intensive, geomagnetic storms occurred in January 2005. The following common pattern of the TEC anomalies is found: (i) there is a positive reaction in the winter during the initial phase of the storm that is most pronounced in day-time; (ii) during the storm with a longer duration (as that in 17-19 January) the positive anomaly continues over two days; (iii) the negative TEC response in the winter is observed during the recovery phase of the storms and after their completion; (iv) the response of the summer TEC is predominantly negative to the considered storms, and (v) the global distribution of the relative TEC during the tree storms considered in this work, show the greatest positive response around 60°N.

The comparison between the top- and bottom-TEC over Sofia has been presented also. It has been found that the bottom-TEC response is significantly bigger than that of the top-TEC for all three geomagnetic storms. This result raises the question: why in the winter and at mid-latitudes mostly the ionosphere below the F2-maximum reacts to the geomagnetic storms. The answer follows from the main drivers of the ionospheric response connected with the changes in the thermospheric wind system, neutral composition and temperature. The auroral heating during the geomagnetic storms can alter the mean global circulation of the thermosphere. Whereas for quiet conditions there is a general upwelling in the summer hemisphere flow toward the winter one at higher levels, and downwelling in the winter hemisphere, the storm-time heating adds a polar upwelling and equatorward flow in both hemispheres. During the winter the disturbed flow usually reverses the poleward one coming from the summer hemisphere and producing in this way two circulation cells which are situated below the F2-maximum. This process seriously affects mainly the vertical and meridional wind velocities which disturbed mainly the ionosphere below the F2-maximum. The increased downwelling at mid-latitudes moves the air into regions of increased pressure, and produces compressional heating, i.e. the neutral temperature at mid-latitudes changes and affects loss and production rates. During winter downwelling of the poleward wind from the summer hemisphere air with low concentrations of molecular species, i.e. reach of atomic oxygen, is carried downward. This leads to a decrease of the loss rate and an increase of production rate. The temperature and composition effects determine the large positive TEC response seen on 7-8, 17-18 and 22 January 2005. It is worth noting also that usually the molecular-rich air at high latitudes carried by the equatorward circulation cannot reach latitudes lower than 50°N as it has been found by (Mukhtarov and Pancheva, 2012). This is another reason explaining why the ionospheric response over Sofia in the winter is predominantly positive one.

Acknowledgments. This work was supported by the Bulgarian Ministry of Education and Science under the National Research Programme "Young scientists and postdoctoral students" approved by DCM №577 / 17.08.2018 and by Contract No D01-161/28.08.2018 (Project "National Geoinformation Center (NGIC)" financed by the National Roadmap for Scientific Infrastructure 2017-2023.

References

Andonov, B., Mukhtarov P., and Pancheva D., 2011. Empirical model of the TEC response to the geomagnetic activity over the North American region, Adv. Space Res., **48.6**, 1041-1048.

Gadzhev, G., Ganev, K., Miloshev, N., Syrakov, D., & Prodanova, M., 2013. Some basic facts about the atmospheric composition in Bulgaria–grid computing simulations. In International Conference on Large-Scale Scientific Computing (pp. 484-490). Springer, Berlin, Heidelberg.

Huba, J. D., Joyce, G., Sazykin, S., Wolf, R., & Spiro, R., 2005. Simulation study of penetration electric field effects on the low-to mid-latitude ionosphere, Geophysical Research Letters, **32**.

Kamide, Y., Kusano, K., 2015. No major solarflares but the largest geomagnetic storm in the present solar cycle, Space weather **13**, 365–367.

Mendillo, M., 2006. Storms in the ionosphere: Patterns and processes for total electron content, Rev. Geophys., **44**, RG4001.

Mendillo, M., Rishbeth, H., Roble, R. G., & Wroten, J., 2002. Modelling F2-layer seasonal trends and day-to-day variability driven by coupling with the lower atmosphere, J. Atmos. Sol.-Terr. Phys., **64(18)**, 1911-1931.

Mukhtarov, P., Andonov, B., Pancheva, D., 2018. Empirical model of TEC response to geomagnetic and solar forcing over Balkan Peninsula, J. Atmos. Sol.-Terr. Phys., **167**, 80–95.

Mukhtarov, P., Andonov B., and Pancheva D., 2013a. Global empirical model of TEC response to geomagnetic activity, J. Geophys. Res. - Space Physics **118.10**, 6666-6685.

Mukhtarov, P., Penov N., Pancheva D., 2013b. N(h) profiles derived from ionograms and their application for studying mid-latitude ionospheric response to geomagnetic storms, Comp. rend. Acad. bulg. Sci. **66 (9)**, 1315-1322.

Mukhtarov, P., Bojilova R., 2017. Influence of Solar and Geomagnetic Activity on the Ionosphere over Bulgaria, C.R. Acad. Bulg. Sci., **70 (9)**, 1289-1296.

Mukhtarov, P. and Pancheva D., 2012. Thermosphere-ionosphere coupling in response to recurrent geomagnetic activity, J. Atmos. Sol.-Terr. Phys., **90-91**, 132-145

Pancheva D., Mukhtarov P., Andonov B., 2016. Global structure of ionospheric TEC anomalies driven by geomagnetic storms. J. Atmos. Sol.-Terr. Phys., **145**, 10.1016/j.jastp.2016.04.015

Rishbeth, H., 2006. F-region links with the lower atmosphere? J. Atmos. Sol.-Terr. Phys, **68(3-5)**, 469-478.

Roble, R. G., 1995. Major greenhouse cooling (yes, cooling): The upper atmosphere response to increased CO2, Reviews of Geophysics, **33**, 539-546.

Schunk, R., & Nagy, A., 2009. Ionospheres: physics, plasma physics, and chemistry, Cambridge university press.

Три геомагнитни бури през януари 2005 и тяхното влияние върху общо съдържание на електрони в йоносферата

Р. Божилова

Резюме: Настоящето изследване представя глобалната и средноширинна йоносферна реакция на три геомагнитни бури случили се през януари 2005: първата буря 7-8 януари, втората на 17-19 януари и последната от 21-22 януари. Този период е избран, тъй като през избрания месец няма мажорно стратосферно затопляне (SSW) и според много учени тази зима представялва пример за т.нар. "нормална" година. По тази причина получената реакция на йоносферата от разглежданите бури може да бъде приписана главно на външно въздействие. Реакцията е изследвана чрез разглеждане на N(h) профилите, регистрирани от йоносферна станция София (42.5°N, 25°E), които се използват за пресмятане на общото електронно съдържание (TEC) до максимума на F2-слоя и са обозначени с (bottom-TEC). Стойностите на пълния TEC (full-TEC) са получени от Center for Orbit Determination of Europe (CODE)-Bern, за най-близката точка до София. Основната задача на настоящата работа е да се направи детайлно сравнение между измененията на пълния TEC (full-TEC) с другите два подмаксимумния TEC (bottom-TEC) и надмаксимумния (top-TEC) за всяка една от разгледаните бури. Установено бе, че за всички разгледани бури през януари 2005 подмаксимумния TEC (bottom-TEC) е доста различен в сравнение с другите два top-TEC and full-TEC. Предложено е обяснение на основните механизми, отговорни за наблюдаваните различия.

Bulgarian Geophysical Journal, 2018, Vol. 41
National Institute of Geophysics, Geodesy and Geography, Bulgarian Academy of Sciences

RECURRENCE OF AIR QUALITY FOR THE CITY OF SOFIA FOR 2013 AND 2014

G. Gadzhev

[1]*National Institute of Geophysics, Geodesy and Geography - BAS, str. Acad. G. Bonchev, bl. 3, Sofia1113, Bulgaria,*
e-mail: ggadjev@geophys.bas.bg

Abstract. The air is the living environment of human beings and obviously the atmospheric composition has a great importance for the quality of life and human health. Air Quality (AQ) is a key element for the well-being and quality of life of European citizens. The objectives of the present work is performing reliable, comprehensive and detailed studies of the impact of lower atmosphere composition on the quality of life and health risks for the population in Sofia city. Lately, together with the numerical weather forecast, in many European countries Systems for Chemical Weather Forecast operate, Chemical Weather being understood as concentration distribution of key pollutants in a particular area and its changes during some forecast period. In Bulgaria, a prototype of such a system was built in the frame of a project with the National Science Fund. It covers a relatively small domain including Bulgaria that requires using chemical boundary conditions from similar foreign systems. As far as this data is prepared abroad and transferred by Internet, many failures took place during the operation of the system. To avoid this problem, a new version of the system was built on the base of the nesting approach. This version is realized on five domains: Europe, Balkan Peninsula, Bulgaria, Sofia Municipality and Sofia City with increasing space resolution - from 81 km (Europe) to 1 km (Sofia City). For the Mother domain (Europe) climatic boundary conditions are applied. All other domains take their boundary conditions from the senior one. Computations start automatically at 00 UTC every day and the forecast period is 3 days. The System is based on the well-known models WRF (Meso-meteorological Model) and US EPA dispersion model CMAQ (Chemical Transport Model). As emission input the TNO data is used for the two biggest domains. For the 3 Bulgarian domains the current emission inventory prepared by Bulgarian environmental authorities is exploited.

Key words: Air Quality Indices, air quality, quality of life, health risks.

Introduction

The Air Quality is a key element for the well-being and quality of life of European citizens. According to the World Health Organization, air pollution severely affects the health of European citizens. There is increasing evidence for adverse effects of air pollution on the respiratory and the cardiovascular system as a result of both acute and chronic exposure. In particular, a significant reduction of life expectancy by a year or more is assumed to be linked to long-term exposure to high air concentrations of particulate matter (PM). There is considerable concern about impaired and detrimental air quality conditions over many areas in Europe, especially in urbanized areas, in spite of about 30 years of legislation and emission reduction. Current legislation, e.g. the Ozone daughter directive 2002/3/EC (European Parliament, 2002), requires informing the public on AQ, assessing air pollutant concentrations throughout the whole territory of Member States and indicating exceedances of limit and target values, forecasting potential exceedances and assessing possible emergency measures to abate exceedances. For the purpose, modeling tools must be used in parallel with air pollution measurements. The goals of reliable air quality forecasts are the efficient control and protection of population exposure as well as possible emission abatement measures. In last years the concept of "chemical weather" arises and in many countries respective forecast systems are being developed along with the usual meteorological weather forecasts (see, for instance, Sofiev at al., 2006, Poupkou et al., 2008, Monteiro et al., 2005, San Jose et al., 2006, and others).

Air pollution easily crosses national borders. It would be cost-effective and beneficial for citizens, society and decision-makers that national chemical weather forecast and information systems were networked across Europe. For the purpose several projects in the European Framework Programs (GEMS, PROMOTE, MEGAPOLI, MACC, PASODOBLE etc.) as well as the COST Action ES0602 "Towards a European Network on Chemical Weather Forecasting and Information Systems") were launched aiming at providing a forum for harmonizing, standardizing and benchmarking approaches and practices in data exchange and multi-model capabilities for air quality forecast and (near) real-time information systems in Europe. It is supposed to examine existing, and work out new solutions for integrating the development efforts at national and international levels. One can find several CW systems' (performance and descriptions) in the Action's web-portal (http://www.chemicalweather.eu/Domains).

Modeling tools

BgCWFIS is designed in a way to fit the real-time constraints and to deliver forecasts for the next days on an hourly basis. US EPA Models-3 air quality modeling system is used, consisting of:

• CMAQ v.4.6 - Community Multi-scale Air Quality model, http://www.cmaq-model.org/, Denis et al. (1996), Byun and Ching (1999), Byun and Schere (2006), the Chemical Transport Model (CTM);

• WRF v.3.2.1 - Weather Research and Forecasting Model, http://www.wrf-model.org/, Skamarock et al. (2007), the meteorological pre-processor to CMAQ. The Weather Research and Forecasting (WRF) Model is a next generation meso-scale numerical weather prediction system designed to serve both operational forecasting and atmospheric research needs. It is an evolutionary successor to the MM5 model. The creation and further development of WRF is due to the collaborative efforts of several US institutions like NCAR, NOAA, NCEP and others. The WRF is a fully compressible and non-hydrostatic model with terrain-following hydrostatic pressure coordinate. The grid staggering is the Arakawa-C type. One can find more info on http://www.wrf-model.org/index.php;

• SMOKE v.2.4 - Sparse Matrix Operator Kernel Emissions Modelling System, http://www.smoke-model.org/, Coats and Houyoux (1996), Houyoux and Vukovich (1999), CEP (2003), the emission pre-processor to CMAQ. CMAQ demands its emission input in specific format reflecting the time evolution of all pollutants accounted for by the chemical mechanism used (CB-IV in this case). Emission inventories are used as row data for anthropogenic emission processing. The inventories are made on annual basis for big territories; many pollutants are estimated as groups (VOC and PM2.5 for instance). Preparation of emission input to a Chemical Transport Model requires emission processing. Such emission processing component in EPA Models-3 system is SMOKE but it is partly used, here, because it's quite strong relation to US emission sources specifics. In BgCWFIS, SMOKE is used only for calculating BgS emissions and for merging AS-, LPS- and BgS-files into a CMAQ emission input file. The area source emissions and the large point source emissions are prepared by the interface programs AEmis and PEmis.

In the System, WRF is driven by the NCEP GFS (Global Forecast System) data that can be accessed freely from http://www.ftp.ncep.noaa.gov/data/nccf/com/gfs/prod/. This data is global weather forecast in GRIB-2 format with space resolution of 1°×1° and 6-hour time resolution. The downloading of this data is invoked automatically every day at 00:00Z. 84-hour runs starting at 12:00Z of the previous day are used; the first 12 hours of the period being spinning-up followed by a 3-day weather forecast. The chemical weather forecast duration is from 00:00Z of the current day to 00:00Z of the fourth day after (3-day forecast).

TNO inventory for 2005 (Denier van der Gon et al., 2010) is exploited partly for Bulgaria domain, TNO being the Netherlands's Organization for Applied Scientific Research. For Bulgaria itself and for the other Bulgarian domains, the National inventory for 2010 as provided by Bulgarian Executive Environmental Agency is used. That means TNO inventory is used only for the territories outside Bulgaria in the mother CMAQ's domain.

The TNO produced several sets of inventories for different years. The anthropogenic sources in this inventories are distributed over 10 SNAPs (Selected Nomenclature for Air Pollution) classifying them according to the processes leading to harmful material release into the atmosphere (EMEP/CORINAIR, 2002). The 2010 TNO inventory has resolution of 0.125°×0.0625° (about 7×8 km). It is distributed as a comma- or tab-delimited text-file. Each line of the file contains data for a single box, namely the center of mesh coordinates, the country, the type of source (A/P), the SNAP, and the yearly emissions of

8 pollutants. The SNAP 7 (road transport) is presented as 5 sub-SNAPs. The pollutants are: methane (CH4), carbon oxide (CO), nitric oxides (NOx), sulfur oxides (SOx), non-methane volatile organic compounds (NMVOC), ammonia (NH3), Particulate Matter with d<10μm (PM10) and Particulate Matter with d<2.5μm (PM2.5).

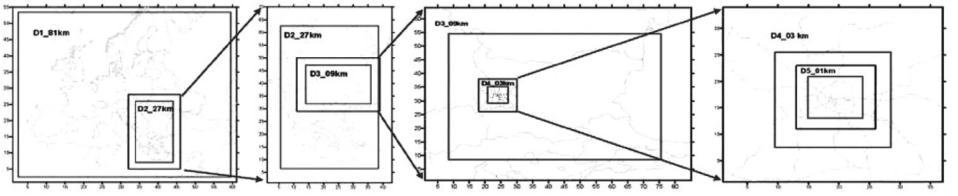

Fig. 1. Five computational domains of BgCWFIS, (CMAQ domain nested in WRF one)

The nesting capabilities of WRF and CMAQ are used to downscale the forecasts from European region to Sofia city area. The resolution of the mother domain (Europe) is 81 km, big enough as to correspond to the GFS met-data space resolution. Four other domains are nested in it and in each other – Balkan Peninsula (27km resolution), Bulgaria (9 km), Sofia municipality (3 km) and Sofia city (1 km) as shown in Fig. 1.

In BgCWFIS, climatic data is used for chemical boundary conditions following the presumption that the errors introduced by this assumption will decrease quickly to the center of the domain due to the continuous acting of the pollution sources. All other domains receive their boundary conditions from the previous domain in the hierarchy.

Operational Performance of BgCWFIS

Fourteen σ-levels with varying thickness determine the vertical structure of CMAQ model. The Planetary Boundary Layer (PBL) is presented by the lowest 8 of these levels.

The CMAQ v.4.6 input consists of various files containing concentration, deposition, visibility and other variables. The concentration output is a NetCDF file with 3-D hourly data for 78 pollutants - gases and aerosols.

The post-processing program XtrCON extracts part of the pollutants for archiving and further handling. Only surface values of the most important pollutants are saved - 8 gases and 11 aerosols (including PM10 and PM2.5). Part of these pollutants is more or less monitored and they are referred in the European legislation with the respective thresholds.

For the moment it presents 4 main pollutants - Ozone, NO_2, SO_2 and PM10 which are used to calculate the Air Quality Indices (AQI).

Calculation of the Air Quality (AQ) impact on human health and quality of life in Sofia city is the objective of the present study. The impact is calculated in the terms of the so called AQI – an integral characteristic directly measuring the effects of AQ on human health. The calculations are made on the basis of long term AQ simulations, which make it possible to reveal the climate of AQI spatial/temporal distribution and behavior.

The AQI is defined as a measure of air pollution seen in the context of its impact on human health. It provides an integrated assessment of the impact of the whole range of pollutants on human health and is calculated based on the concentration of various pollutants obtained from measurements or numerical modeling. The index is defined in several segments (EPA, 2009), each of which is a linear function of the concentration of each considered pollutant:

$$I = ((I_{high} - I_{low}) / (C_{high} - C_{low}))(C - C_{low}) \quad (1)$$

where:

I = the AQI,

C = the pollutant concentration,

C low - the concentration breakpoint that is ≤ C,

C high - the concentration breakpoint that is ≥ C,

I low - the index breakpoint corresponding to C low ,

I high - the index breakpoint corresponding to C high.

In that calculation the index falls in one of the ranges of the dimensionless scale. In each range index values are associated with an intuitive color code, a linguistic description and a health description.

Pretty often in order to evaluate the air quality situation in European cities, all detailed measurements are transformed into a single relative figure: the Common Air Quality Index (CAQI) and this index have 5 levels using a scale from 0 (very low) to > 100 (very high). The index is based on 3 pollutants of major concern in Europe: PM10, NO_2, O_3 and will be able to take into account to 3 additional pollutants (CO, PM2.5 and SO_2).

One of the most commonly used air quality index is the UK Daily Air Quality Index (Leeuw, F. de, Mol, W., 2005), also used in Bulgaria (Etropolska et al. 2010), (Syrakov et al, 2012, 2013, 2014a, 2014b, 2015), (Georgieva, I., 2014), (Georgieva et al. 2015), (Georgieva, I. and Ivanov, V., 2017, 2018) and (Ivanov, V. and Georgieva, I., 2017).

Compute the AQI

To calculate the AQI requires several steps:

- Air pollutant concentrations (from measurements or model)
- Convert this air pollutant concentration to a AQI. The index is defined for each pollutant in a different way converting the concentrations into a dimensionless scale, associated with an intuitive color code (green to purple) and a linguistic description (Low to Very High).
- AQI values are divided into ranges, and each range is assigned a color code and health descriptor.

- An overall air AQI is constructed to describe the ambient pollutant mix – It's set to the highest value of each of the pollutant considered.

The breakpoints between index values are defined for each pollutant separately and the overall index is defined as the maximum value of the index. Different averaging periods are used for different pollutants. Each of the bands comes with advice for at-risk groups and the general population (Table 1).

Table 1 Boundaries Between Index Points for Each Pollutant

Index	O_3 Running 8 hourly mean ($\mu g/m^3$)	NO_2 Hourly mean ($\mu g/m^3$)	SO_2 15 minute mean ($\mu g/m^3$)	PM10 Particles, 24 hour mean ($\mu g/m^3$)	PM2.5 Particles, 24 hour mean ($\mu g/m^3$)
1 (Low)	0-33	0-66	0-88	0-11	0-16
2 (Low)	34-65	67-133	89-176	12-23	17-33
3 (Low)	66-99	134-199	177-265	24-34	34-49
4 (Moderate)	100-120	200-267	266-354	35-41	50-58
5 (Moderate)	121-140	268-334	355-442	42-46	59-66
6 (Moderate)	141-159	335-399	443-531	47-52	67-74
7 (High)	160-187	400-467	530-708	53-58	75-83
8 (High)	188-213	468-534	709-886	59-64	84-91
9 (High)	214-239	535-599	887-1063	65-69	92-99
10 (Very High)	≥240	≥600	≥1064	≥70	≥100

The reference levels and Health Descriptor used in the Table 2 are based on health-protection related limit, target or guideline values set by the EU, at national or local level or by the WHO.

Table 2. Air quality indices and their health impact (de Leeuw and Mol, 2005).

Banding	Value	Health Descriptor
Low	1-3	Effects are unlikely to be noticed even by individuals who know they are sensitive to air pollutants
Moderate	4-6	Mild effects, unlikely to require action, may be noticed amongst sensitive individuals.
High	7-9	Significant effects may be noticed by sensitive individuals and action to avoid or reduce these effects may be needed (e.g. reducing exposure by spending less time in polluted areas outdoors). Asthmatics will find that their 'reliever' inhaler is likely to reverse the effects on the lung.
Very High	10	The effects on sensitive individuals described for 'High' levels of pollution may worsen.

Results

Annual recurrence of AQI in "Low", "Moderate", "High" and "Very High" bands over territory of Sofia city for 2013 and 2014: Figures 2 and 3 demonstrate the spatial and diurnal variation of the annual recurrence of different AQI categories for the chosen hours 06:00 and 18:00GMT for 2013 and 2014. The picture shows the sum of recurrences of the AQI in each range - Low, Moderate and High range. What can be also noticed is: the recurrence in Low and Moderate range is different for both years, as in 2013 the recurrence in Low band is smaller than 2014, and reverse in Moderate range. In High range there is no any difference between both years.

In the Low range the air is most clean, so high recurrence values mean more cases with clean air and lower recurrence values mean, less cases with clean air (worse AQ status). In the other 2 plots (Moderate and High ranges) - high recurrence values means less favorable and respectively bad AQ status. It can be seen that most areas with high recurrence of cases with lower AQI status are in the city center and over the Vitosha Mountain early in the morning due to the weather conditions, higher NO_2 concentrations from the road transport and higher O_3 concentration in the mountain. This could be seen at Low and Moderate range maps in the morning hours. The major NO_2 sources in the city are the surface sources (road transport) and the surface NO_2 concentrations are higher early in the morning and much smaller at noon (the atmosphere is mostly unstable, and so the turbulence transports the NO_2 aloft more intensively). The maximal concentrations which are directly linked to the worse AQI status are formed in the city center and along the boulevard with most busy traffic.

In Moderate band at 18:00 GMT it can be also noticed about 20% recurrence with not so good AQI status over Vitosha mountain. Higher values over the Vitosha Mountain in the afternoon are due to the higher concentration of O_3 in mountain areas and intensive ozone transport from higher levels (intensive turbulence during midday). The behavior of the surface ozone is complex. The O_3 in Bulgaria is to a great extent due to transport from abroad (Gadzhev et al. 2013), (Kaleyna et al. 2013a, 2013b, 2014) and (Tcherkezova et al. 2013). This is the reason why the O_3 concentrations early in the morning are smaller (less intensive transport from higher levels), and higher at noon and afternoon (turbulence atmosphere and O_3 photochemistry)

High recurrence of cases with most polluted air (High band) appears again in the city center. In the city center can be observed about 20% "High" pollution in the morning and 10% in the afternoon. Bad AQI status from the High band never disappears.

Conclusions

The simulations for Sofia city show that the air quality status of Sofia is not so good (evaluated with a spatial resolution of 1km).

AQI status falls mostly in Low and Moderate bands, but the recurrence of cases with High pollution is close to 20% mostly at the city center.

The recurrence of Low band for 2013 is smaller than 2014, which means that in 2014 almost 90% the days have been with cleaner air.

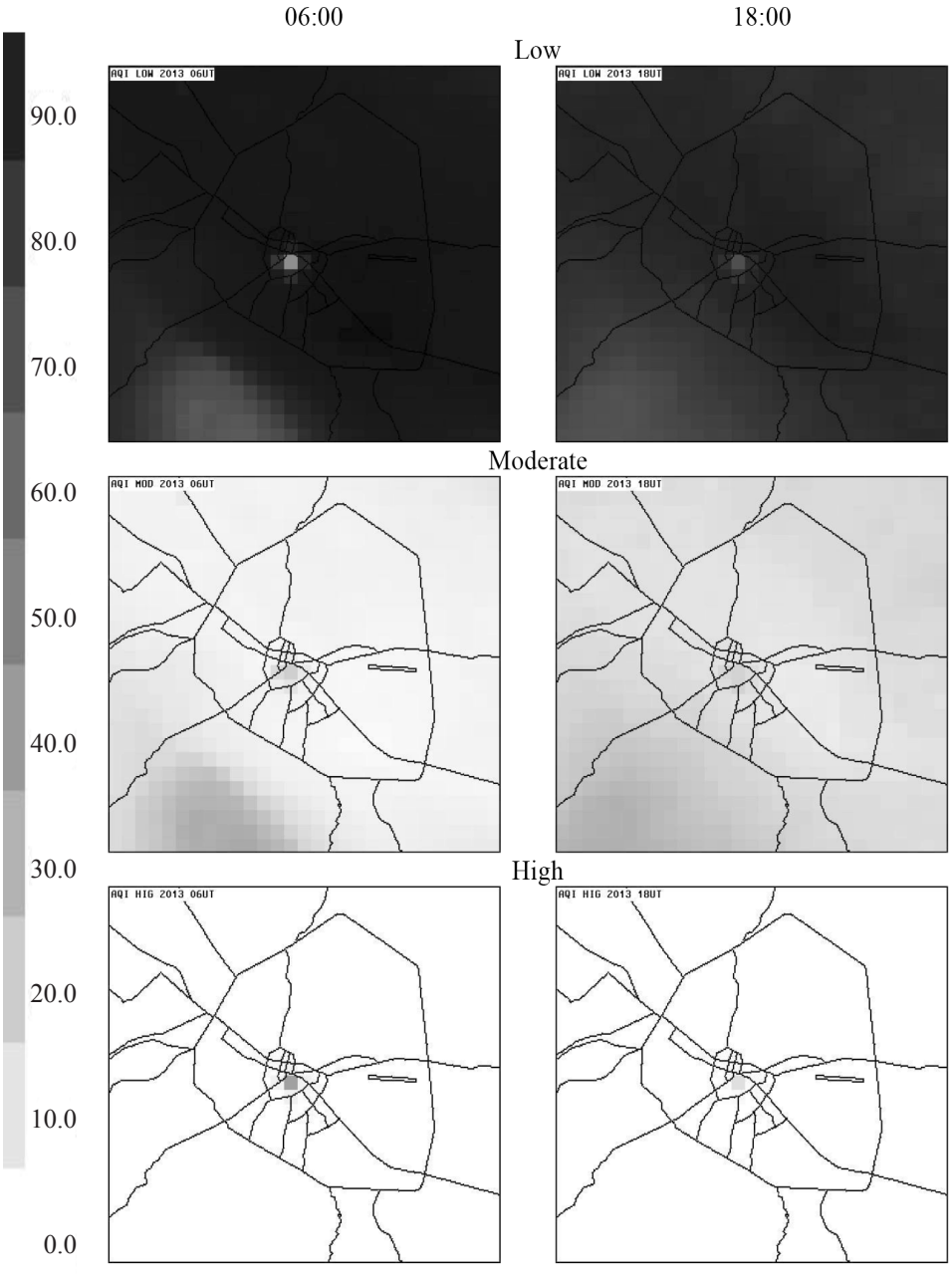

Fig. 2. Annual plots of the recurrence [%] of the AQI - Low, Moderate, and High bands in Sofia for 2013.

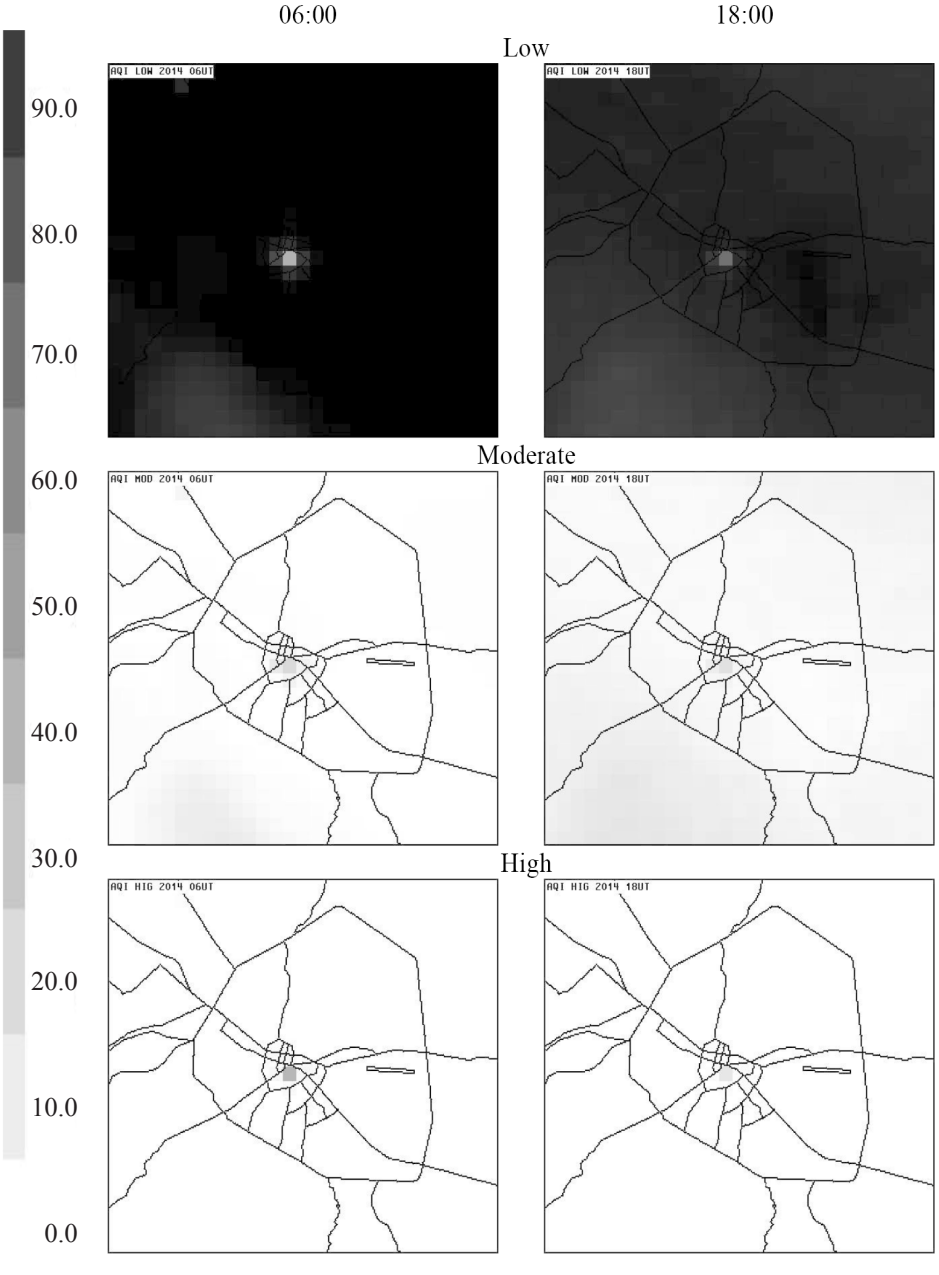

Fig. 3. Annual plots of the recurrence [%] of the AQI - Low, Moderate, and High bands in Sofia for 2014.

The pollution in the city is probably due to the surface sources like road transport and also the TPPs in the city.

Apart from these general features the climatic behavior of the AQI probabilities is rather complex with significant spatial, seasonal and diurnal variability. The areas with slightly worse AQ status are not necessarily linked to the big pollution sources. Wide rural and even mountain regions can also have significant probability for AQI from the Moderate range.

The hot spot in Sofia city, where index with higher impact (High band) is in the city center. The (High band) is relatively high - about 20 % in the morning and 10% in the afternoon.

Acknowledgments

This work was supported by Contract No D01-161/28.08.2018 (Project "National Geoinformation Center (NGIC)" financed by the National Roadmap for Scientific Infrastructure 2017-2023 and by Bulgarian National Science Fund (grant DN-04/2/13.12.2016).

Special thanks are due to US EPA and US NCEP for providing free-of-charge data and software and to the Netherlands Organization for Applied Scientific research (TNO) for providing the high-resolution European anthropogenic emission inventory.

References

Byun, D., Ching, J., (1999), Science Algorithms of the EPA Models-3 Community Multiscale Air Quality (CMAQ) Modeling System. EPA Report 600/R-99/030, Washington DC. http://www.epa.gov/asmdnerl/models3/doc/science/science.html.

Byun, D., Schere, K. L., (2006), Review of the governing equations, computational algorithms, and other components of the models-3 community multiscale air quality (CMAQ) modeling system. Appl. Mech. Rev. 59, 51–77

CEP, (2003), Sparse Matrix Operator Kernel Emission (SMOKE) Modeling System, University of North Carolina, Carolina Environmental Programs - CEP, Research Triangle Park, North Carolina.

Coats, C. J., Jr., and Houyoux, M. R., (1996), Fast Emissions Modeling With the Sparse Matrix Operator Kernel Emissions Modeling System, The Emissions Inventory: Key to Planning, Permits, Compliance, and Reporting, Air and Waste Management Association, New Orleans, September

Denier van der Gon, H., Visschedijk, A., van de Brugh, H., Droge, R., (2010), A high resolution European emission data base for the year 2005, TNO-report TNO-034-UT-2010-01895 RPT-ML, Apeldoorn, The Netherlands

Dennis, R. L., Byun, D. W., Novak, J. H., Galluppi, K. J., Coats, C. J., and Vouk, M. A., (1996), The Next Generation of Integrated Air Quality Modeling: EPA's Models-3, Atmospheric Environment 30:1925–1938.

EMEP/CORINAIR (2002), Atmospheric emission inventory guidebook, third edition, European Environmental Agency. http://reports.eea.europa.eu/EMEPCORINAIR3/en/page002.html

EPA (2009). Technical assistance document for the reporting of daily air quality - the Air Quality Index (AQI). EPA- 454/B-09-001, US Environmental Protection Agency, Research Triangle Park, North Carolina, Office of Air Quality Planning and Standards, Research Triangle Park, North Carolina 27711.EU (2007à). http://ec.europa.eu/environment/air/legis.htm

Etropolska, I., Prodanova, M., Syrakov, D., Ganev, K., Miloshev, N., Slavov, K., (2010), Lecture Notes in Computer Science (including subseries Lecture Notes in Artificial Intelligence and Lecture Notes in Bioinformatics), Volume 6046 LNCS, 2011, Pages 141-149

European Parliament (2002), DIRECTIVE 2002/3/EC of 12 February 2002 relating to ozone in ambient air, Official Journal of the European Communities (9.3.2002) L67: 14–30

Gadzhev, G., Ganev, K., Miloshev, N., Syrakov, D., Prodanova, M., (2013) Numerical Study of the Atmospheric Composition in Bulgaria, Computers and Mathematics with Applications 65, p. 402-422.

Georgieva, I., (2014) Study of the air quality index climate for Bulgaria, Proc. of the international conference on numerical methods for scientific computations and advanced applications, may 19-22, 2014, Bansko, ISBN978-954-91700-7-8, p. 39-42.

Georgieva I., G. Gadzhev, K. Ganev, M. Prodanova, D. Syrakov, N. Miloshev (2015) Numerical study of the air quality in the city of Sofia – some preliminary results, International Journal of Environment and pollution, Vol. 57, Nos. 3/4, 162-174,

Georgieva, I., Ivanov, I., (2017), IMPACT OF THE AIR POLLUTION ON THE QUALITY OF LIFE AND HEALTH RISKS IN BULGARIA,HARMO 18 - 18th International Conference on Harmonisation within Atmospheric Dispersion Modelling for Regulatory Purposes, Proceedings, (2017), pp. 647-652

Georgieva, I., Ivanov, I., (2018), Computer simulations of the impact of air pollution on the quality of life and health risks in Bulgaria, Int. J. Environment and Pollution, Vol. 64, Nos. 1/3, 2018, pp. 35-46

Houyoux, M. R., and Vukovich, J. M., (1999), Updates to the Sparse Matrix Operator Kernel Emission (SMOKE) Modeling System and Integration with Models-3, The Emission Inventory: Regional Strategies for the Future, Raleigh, NC, Air and Waste Management Association

Ivanov, V. and Georgieva, I., (2017) Air quality index evaluations for Sofia city, 17th IEEE International Conference on Smart Technologies, EUROCON 2017 - Conference Proceedings, Article number 8011246, Pages 920-925

Kaleyna P., Pl. Muhtarov, N. Miloshev, (2013a) Condition of The Stratospheric and Mesospheric Ozone Layer over Bulgaria for the Period 1996-2012: Part 1 – Total Ozone Content, Seasonal Variations, Bulgarian Geophysical Journal, Vol. 39, National Institute Of Geophysics, Geodesy And Geography, Bulgarian Academy Of Sciences

Kaleyna P., Pl. Muhtarov, N. Miloshev, (2013b) Condition of The Stratospheric and Mesospheric Ozone Layer over Bulgaria for the Period 1996-2012: Part 2 – Total Ozone Content, Short term variations, Bulgarian Geophysical Journal, Vol. 39, National Institute Of Geophysics, Geodesy And Geography, Bulgarian Academy Of Sciences

Kaleyna P., P. Mukhtarov, N. Miloshev, (2014) Seasonal Variations of the Total Column Ozone over Bulgaria in the Period 1996–2012, Comptes rendus de l'Acad´emie bulgare des Sciences, Tome 67, No 7.

Leeuw, F. de, Mol, W., (2005), Air Quality and Air Quality Indices: a world apart. ETC/ACC Technical Paper 2005/5 http://acm.eionet.europa.eu/docs/ETCACC_TechnPaper_2005_5_AQ_Indices.pdf

Monteiro, A., Lopes, M., Miranda, A. I., Borrego, C. and Vautard, R., (2005), Air pollution forecast in Portugal: a demand from the new air quality framework directive, Internat. J. Environment and Pollution 25: 4–15

Poupkou, A., I. Kioutsioukis, I. Lisaridis, K. Markakis, D. Melas, C. Zerefos and Giannaros, T., (2008b) Air quality forecasting for Europe, the Balkans and Athens, 3rd Environmental conference of Macedonia, 14-17 March 2008, Thessaloniki, Greece.

San Jose, R., J. Perez and R. Gonzalez, (2006), Air Quality Real-Time Operational Forecasting System for Europe: an application of MM5-CMAQ-EMIMO modeling system, in Brebia, C. (Ed.), "Air Pollution XIV", WIT Press, Southampton, Boston, 75

Skamarock et al., (2007), A description of the Advanced Research WRF Version 2, http://www.mmm.ucar.edu/wrf/users/docs/arw_v2.pdf

Sofiev, M., Siljamo, P., Valkama, I., (2006), A dispersion modeling system SILAM and its evaluation against ETEX data. Atmos. Environ. 40, 674–685

Syrakov, D., Etropolska, I., Prodanova, M., Ganev, K., Miloshev, N., Slavov, K., (2012), Operational Pollution Forecast for the Region of Bulgaria, American Institute of Physics, Conf. Proc. 1487, p. 88 - 94; DOI: 10.1063/1.4758945.

Syrakov, D., Etropolska, I., Prodanova, M., Slavov, K., Ganev, K., Miloshev, N., Ljubenov T., (2013), Downscaling of Bulgarian Chemical Weather Forecast from Bulgaria region to Sofia city, American Institute of Physics, Conf. Proc. 1561, p. 120-132, http://dx.doi.org/10.1063/1.4827221

Syrakov, D., Prodanova, M., Etropolska, I., Slavov, K., Ganev, K., Miloshev, N., Ljubenov T., (2014a), A multy-domain operational chemical weather forecast system, Lecture Notes in Computer Science (including subseries Lecture Notes in Artificial Intelligence and Lecture Notes in Bioinformatics), Volume 8353 LNCS, 2014, Pages 413-420

Syrakov, D., Prodanova, M., Georgieva, E., Etropolska, I., Slavov, K., (2014b), Impact of NOx emissions on air quality simulations with the Bulgarian WRF-CMAQ modelling system, HARMO 2014 - 16th International Conference on Harmonisation within Atmospheric Dispersion Modelling for Regulatory Purposes, Proceedings 2014, Pages 187-190

Syrakov, D., Prodanova, M., Georgieva, E., Etropolska, I., Slavov, K., (2015), Impact of NOx emissions on air quality simulations with the Bulgarian WRF-CMAQ modelling system, International Journal of Environment and Pollution, Volume 57, Issue 3-4, 2015, Pages 285-296

Tcherkezova E., P. Kaleyna, Pl. Mukhtarov, (2013) Modelling spatial distribution of global total column ozone in QGIS and GRASS GIS environment, Bulgarian Geophysical Journal, Vol. 39, National Institute Of Geophysics, Geodesy And Geography, Bulgarian Academy Of Sciences

Оценка на качеството на въздуха за град София за 2013 и 2014

Г. Гаджев

Резюме: В настоящето изследване са представени средногодишните Индекси за качеството на въздуха през 2013 и 2014 за територията на град София. Използвани са данни за приземните концентрации на някои замърсители, моделирани от Българската система за прогноза на химическото време за изчисление на индексите. Чрез използването на математически апарат са определени индексите за качеството на въздуха, а от там и съответните повторяемости в трите категории „Ниско“, „Средно“ и „Високо“за двете години 2013 и 2014. Установяват се т.н. горещи точки, в които категория „Високо“ достига до 20%. Изказано е предположение за високите концентрации в центъра на града, че най-вероятно се дължат на приземните източници и ТЕЦ-те в града.

THE OZONE LAYER OVER BULGARIA IN THE PERIOD 1997-2018

P. Muhtarov, N. Miloshev

National Institute of Geophysics, Geodesy and Geography, str. Acad. G. Bonchev, bl 3, Sofia1113, Bulgaria, e-mail:engpjm@abv.bg, miloshev@geophys.bas.bg

Abstract. A detailed analysis of the variations of the stratospheric and mesospheric ozone over Bulgaria, for the period 1997-2018, is presented in the article on the basis of ground and satellite measurements of the Total Ozone Content (TOC). The existing long-term trends of the move of the basic components of the seasonal course have been studied. In conclusion, it can be argued that the ozone layer over Bulgaria fully retains its protective functions.

Key words: total ozone content, seasonal course, long-term trends.

Introduction

The increased interest to the ozone layer condition of the Earth atmosphere over the last decades is due to the understanding that the protection of the whole biosphere from solar radiation UVB (280-315 nm) depends, to some extent, on this little atmospheric compound. Besides, the variations in its concentration have a substantial impact on the temperature regime and hence – on the whole dynamics of the middle atmosphere namely because of ozone's property to absorb solar energy (Georgieva et al. 2017). In relation to the task assigned to NIGGG by governmental organs to study the condition of the ozone layer over Bulgaria, a daily monitoring of the TOC was organized in 2008 with ground facilities working in Sofia also at present (Gadzhev and Ganev 2018a, 2018b). Since it is not possible to obtain a continuous data row (measurements with ground appliances are possible only by clear weather), the data was complemented with measurements from satellites (Kaleyna et al. 2013, Tcherkezova et al. 2013). The output row of daily values allowed tracking of the condition of the ozone layer in the atmosphere over Bulgaria for a sufficiently long period: from 1997 to 2018 and making some conclusions about the protective ability of the ozone layer.

Data of Total Ozone Content

The measurements of TOC in NIGGG were conducted with the sun photometer Microtops II, a product of Solar Light Company, USA, http://www.solarlight.com. The results were obtained completely automatically from the built-in microcomputer. The accuracy of the appliance, given by the manufacturer, was 1-2%. The error amounted to 6 DU by an average amount of the total content about 300 DU.

The measurements with Microtops II have been complemented with data from Ozone Monitoring Instrument (OMI) working on AURA Satellite which are available on http://toms.gsfc.nasa.gov/. The relation between the data obtained from Microtops II and OMI was for the period September 2009 to June 2009. There has been some systematic bias between the two types of measurements, about 11 DU, which has allowed recalculating the data from OMI and tying them to the data of Microtops II. The data row was extended to 1996 with the data from a Total Ozone Mapping Spectrometer (TOMS) aboard the Nimbus 7 polar-orbiting satellite. The simultaneous data from TOMS and OMI from October 2004 to December 2005 has allowed to calibrate the data of TOMS to OMI and then to the data of Microtops II. The resulting data row, notwithstanding that it has been obtained from different appliances, should be considered free of systematic bias (Kaleyna et al. 2013, Bojilova 2017).

Montly mean TOC

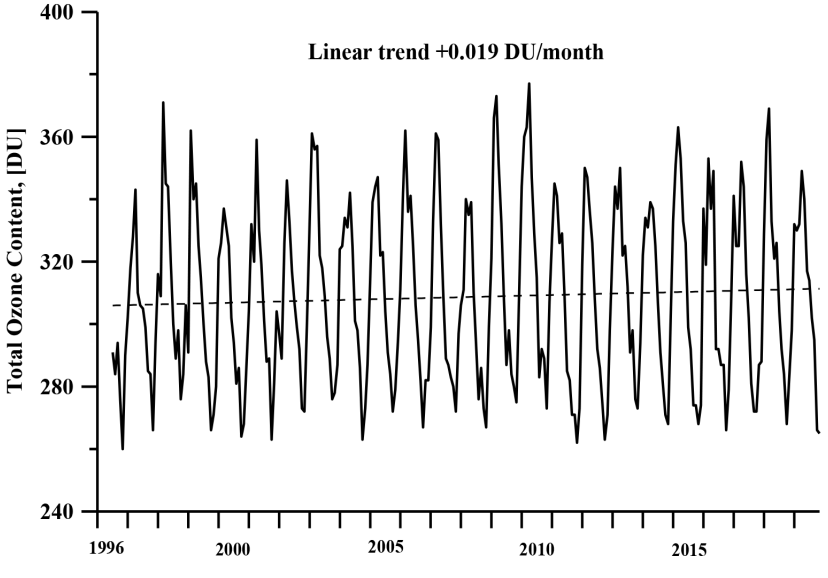

Fig. 1. Monthly averages of TOC over Bulgaria in the period 1996-2018.

The course of the annual monthly values of TOC over Bulgaria is displayed on Fig. 1. A certain seasonal cycle of the total ozone with a spring maximum and an autumn minimum may be readily seen. The linear approximation gives a positive trend of 0.019 DU/month, which allows making the conclusion that the ozone layer over Bulgaria was generally stable during the period.

Components of seasonal cycle.

A decomposition of the monthly mean values has been made with a sliding time segment of a year with a step of one month (Kaleyna et al. 2013). The course of yearly running mean values is displayed in Fig. 2. The value of the positive linear trend is 0.017 DU/month and practically coincides with the trend of monthly average values. Significant variations are observed over a period of about five years.

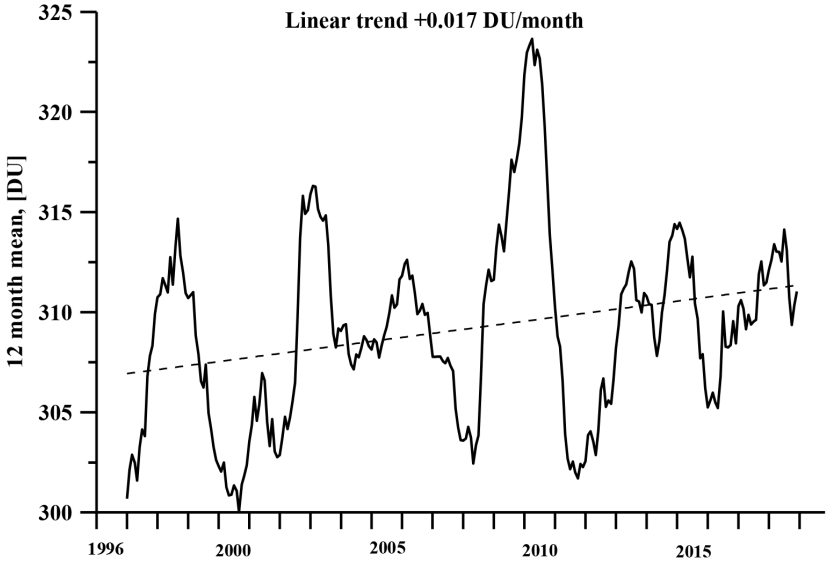

Fig. 2. Running yearly mean TOC.

The course of the annual amplitude shown in Figure 2 has a positive linear trend of 0.028 DU/month. This means that seasonal variation increases over time. The phase of the annual variation (the day of the year when TOC is maximal) is shown in Figure 4. Linear trend is negative- 0.055 days/month. At the beginning of the period the day of the maximum is at the end of March, at the end of the period it reaches the middle of the month.

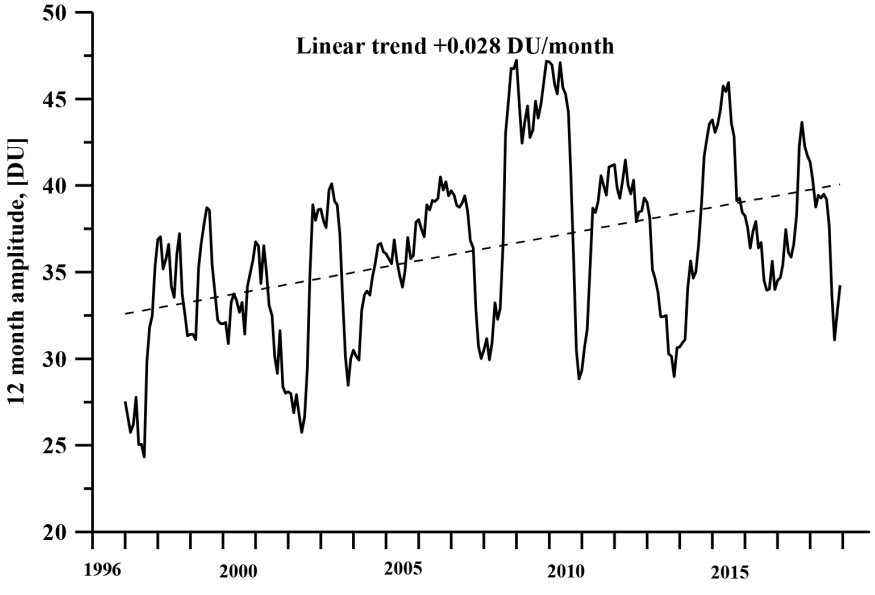

Fig. 3. 12-month amplitude.

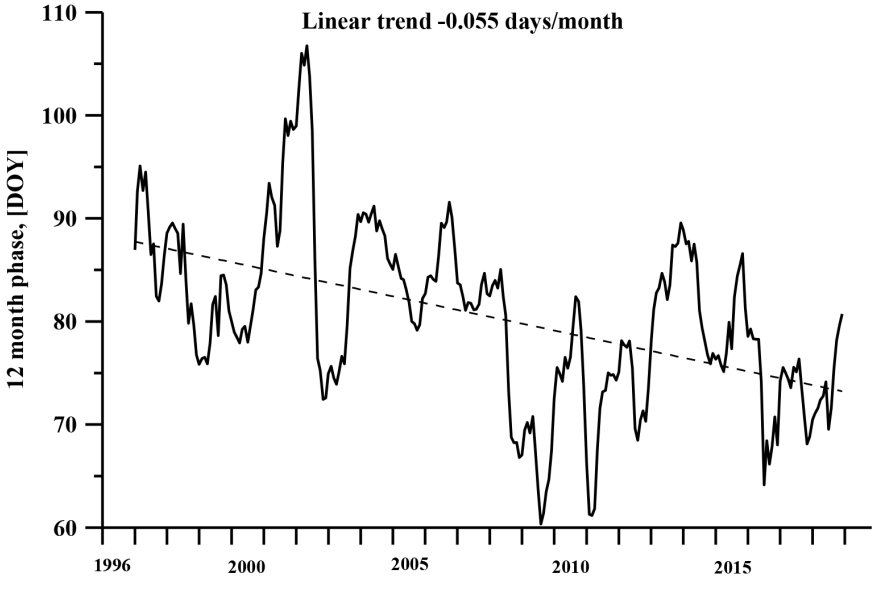

Fig. 4. 12-month phase.

Conclusions

The analysis of the seasonal cycle of the Total Ozone Content over Bulgaria made on the basis of assimilated dataset of daily values obtained by ground and satellite measurements and smoothed between each other with the use of regression fitting has shown that the condition of the stratospheric ozone which is the most important for the protection of the Earth's surface from the harmful impact of the ultraviolet solar radiation was stable during the studied period (1997-2018), and no trends towards its destruction have been observed. On the contrary, the total amount of ozone tends to increase slightly. Seasonal variations are also relatively persistent.

In conclusion, it can be argued that the ozone layer over Bulgaria fully retains its protective functions.

Acknowledgments. This work was supported by Contract No D01-161/28.08.2018 (Project "National Geoinformation Center (NGIC)" financed by the National Roadmap for Scientific Infrastructure 2017-2023 and by Bulgarian National Science Fund (grant DN-04/2/13.12.2016).

References

Bojilova R., 2017. Ionospheric anomalies over Bulgaria during geomagnetic storms and their impact on some communications, *Journal of Physics and Technology*, **Vol. 1**, Issue 1, 18–22.

Gadzhev G. and Ganev, K., (2018a), VERTICAL STRUCTURE OF SOME POLLUTANT OVER BULGARIA - OZONE AND NITROGEN DIOXIDE. SGEM 2018, 18, 4.3, ISBN:978-619-7408-70-6, ISSN:1314-2704, DOI:10.5593/sgem2018/4.3, pp. 449-454

Gadzhev G. and Ganev, K., (2018b), Vertical structure of atmospheric composition fields over Bulgaria, Int. Conf. (NMSCAA'18), Hisarya. Bulgaria, 27 – 31 May 2018, pp. 38-41

Georgieva, I., Gadzhev, G., Ganev, K., Melas, D., Wang, T., (2017), High Performance Computing Simulations of the Atmospheric Composition in Bulgaria and the City of Sofia. CYBERNETICS AND INFORMATION TECHNOLOGIES, Volume 17, No 5, pp. 37-48

Kaleyna P., Pl. Muhtarov, N. Miloshev, 2013. Condition of the Stratospheric and Mesospheric Ozone Layer over Bulgaria for the Period 1996-2012: Part 1 – Total Ozone Content, Seasonal Variations, *Bulgarian Geophysical Journal*, **Vol. 39**, 9-16.

Kaleyna P., Pl. Muhtarov, N. Miloshev, 2013. Condition of The Stratospheric and Mesospheric Ozone Layer over Bulgaria for the Period 1996-2012: Part 2 – Total Ozone Content, Short term variations, *Bulgarian Geophysical Journal*, **Vol. 39**, 17-25.

Kaleyna P., P. Mukhtarov , N. Miloshev, 2014. Seasonal Variations of the Total Column Ozone over Bulgaria in the Period 1996–2012, *Comptes rendus de l'Acad'emie bulgare des Sciences*, **Tome 67**, No 7, 979-986.

Tcherkezova E., P. Kaleyna, Pl. Mukhtarov, 2013. Modelling spatial distribution of global total column ozone in QGIS and GRASS GIS environment, *Bulgarian Geophysical Journal*, **Vol. 39**, 26-37.

Озоновият слой над България в периода 1997–2018 г.

П. Мухтаров, Н. Милошев

Резюме: Направен е детайлен анализ на вариациите на стратосферния и мезосферен озон над България за периода 1997–2018 г. на базата на наземни и спътникови измервания на тоталното озоново съдържание (ТОС). Изследвани са основните компоненти на сезонната изменчивост и съществуващите тенденции за изменението им. В заключение е направен извод, че озоновият слой над България напълно запазва своите защитни свойства.

ANNUAL REPORT OF THE OBSERVED GEOMAGNETIC ACTIVITY IN PANAGJURISHTE OBSERVATORY FOR 2013

M. Metodiev, P. Trifonova

Dept. of Geophysics, National Institute of Geophysics, Geodesy and Geography-BAS, Acad. G. Bonchev Str., Bl.3, 1113 Sofia, Bulgaria, p.trifonova@abv.bg

Abstract. Presently, in the era of Internet communication the preliminary time series (INTERMAGNET's reported data) acquired in geomagnetic observatories are available in near-real time, while the final absolute time series (definitive data) are disseminated with many months delay, being subject to many checks. This paper reports the definitive geomagnetic data obtained in Panagjurishte observatory in 2013, prepared in the form of local geomagnetic indices and absolute time-series of daily mean values plots. Verification of data quality is performed according to "IAGA guide for magnetic measurements and observatory practice".

Key words: PAG observatory, geomagnetic variations, geomagnetic activity, local geomagnetic indices, daily mean values.

Introduction

The Geomagnetic observatory in Panagjurishte (PAG) is established in 1937 – first on the Balkan Peninsula and unique in Bulgaria and during more than 80 years performs absolute measurements of the geomagnetic field elements and continuous registration of their variations. In 2007 PAG observatory was equipped with digital systems for the recording of geomagnetic field element's variations. Thus, the observatory implemented the technical requirements and was joined to the INTERMAGNET (International Real-time Magnetic Observatory Network), which establishes a global network of cooperating digital magnetic observatories, and facilitate data exchanges and geomagnetic products in close to real time. Preliminary recorded time series and local geomagnetic k-indices are published on the NIGGG web page (http://data.niggg.bas.bg/magn_data1/dailymag_bg.php) and automatically reported to INTERMAGNET. The present paper provides quasi-definitive geomagnetic data which are checked and processed to comply with the IAGA standards for observatory practices.

Local geomagnetic indices (K, A_K, ΣK) calculated at PAG observatory.

The K-index is often used as a quantitative measure of local magnetic activity. It is a 3-hour quasi-logarithmic scale developed to measure magnetic activity ranging from 0 to 9, with 0 indicating completely quiet conditions and 9, representing extreme magnetic activity. It is intended to measure geomagnetic disturbances outside the normal diurnal quiet time variations. In order to have a somewhat consistent scale of magnetic activity between observatories at high latitudes, where field variations can be quite large in amplitude, and those at low latitudes, each observatory is assigned its own set of amplitude ranges corresponding to the various K-index levels. Thus, for example, a K-index of 5 at College (TCO) observatory (212.4°E, 64.87°N) corresponds to a lower limit of magnetic activity range of 350 nT over the 3-hour interval, while at San Juan (SJG) observatory (293.85°E, 18.117°N) this same K-index level corresponds to a lower limit of magnetic activity of 40 nT. The idea is to have K-index compensation for the influence of latitude on magnetic activity, so that a K-index of 7 at College and San Juan would represent the same magnetic storm intensity despite the actual differences in the range of magnetic fluctuation amplitudes at the two latitudes.

The ranges of the individual *K* numbers in PAG observatory (24.177°EN, 42.515°N) are defined as follows:

Deviation from the normal *Sq variation* [nT]	<5	5-10	10-20	20-40	40-70	70-120	120-200	200-330	330-500	> 500
K	0	1	2	3	4	5	6	7	8	9

The eight three-hourly K numbers (after Bartels) are calculated by a computer code (FMI method, Sucksdorff et al., 1991) from the digital recordings of three component flux-gate variometer FGE.

Description of the geomagnetic storms and their possible effects on people and systems can be found at NOAA Space Weather Scale for Geomagnetic Storms (http://www.swpc.noaa.gov/NOAAscales/index.html#GeomagneticStorms).

A_K [nT] is the local equivalent daily amplitude index which is determined by converting K –indices into eight 3-hour equivalent linear amplitudes a_K, and calculating the mean value. The 3-hour equivalent amplitude a_K is assigned for each K value using the following table:

K	0	1	2	3	4	5	6	7	8	9
$a_{K\,[nT]}$	0	3	7	15	27	48	80	140	240	400

ΣK is the daily sum of the eight *K* numbers.

Table 1. Local geomagnetic indices (K, A_K, ΣK) calculated at PAG observatory in 2013.

Activity indices										
PAG Observatory									2013	
Day	**K**								**Ak[nT]**	**ΣK**
01-Jan-13	0	0	1	1	0	0	0	0	1	2
02-Jan-13	0	1	1	1	1	2	2	2	4	10
03-Jan-13	1	0	1	1	1	1	0	0	2	5
04-Jan-13	1	0	1	1	0	0	1	1	2	5
05-Jan-13	1	0	1	1	1	0	1	0	2	5
06-Jan-13	0	0	0	1	1	1	2	2	3	7
07-Jan-13	1	0	0	1	1	0	0	1	2	4
08-Jan-13	1	1	1	2	1	2	2	3	6	13
09-Jan-13	2	0	1	1	1	1	1	1	3	8
10-Jan-13	0	0	0	0	1	0	1	1	1	3
11-Jan-13	0	1	1	2	1	0	1	3	4	9
12-Jan-13	2	1	1	2	1	1	1	1	4	10
13-Jan-13	2	2	2	2	-	3	3	4	-	18
14-Jan-13	3	2	1	2	2	2	2	2	8	16
15-Jan-13	1	1	1	1	2	1	2	0	4	9
16-Jan-13	1	1	1	1	1	2	3	4	8	14
17-Jan-13	4	3	2	2	4	5	4	3	22	27
18-Jan-13	2	3	2	2	4	3	2	3	13	21
19-Jan-13	3	1	1	1	2	3	3	4	11	18
20-Jan-13	3	3	3	1	3	2	1	1	10	17
21-Jan-13	2	1	1	1	1	1	1	1	4	9
22-Jan-13	0	0	1	1	0	0	0	0	1	2
23-Jan-13	0	1	1	0	0	0	0	1	1	3
24-Jan-13	1	0	1	0	0	0	0	0	1	2
25-Jan-13	1	1	2	1	0	2	2	3	6	12
26-Jan-13	4	2	3	3	4	4	5	4	24	29

27-Jan-13	3	2	1	2	1	3	1	1	7	14
28-Jan-13	1	1	1	0	1	1	2	3	5	10
29-Jan-13	1	0	1	1	1	1	0	0	2	5
30-Jan-13	0	1	1	1	1	1	1	0	2	6
31-Jan-13	0	1	1	0	0	1	1	2	2	6
01-Feb-13	2	1	1	1	1	2	2	3	6	13
02-Feb-13	2	2	2	2	2	3	4	1	10	18
03-Feb-13	2	0	1	1	2	2	1	1	4	10
04-Feb-13	1	1	1	1	1	3	3	1	6	12
05-Feb-13	1	1	1	1	1	1	1	0	3	7
06-Feb-13	1	0	0	0	0	0	1	1	1	3
07-Feb-13	1	1	2	2	2	1	2	2	6	13
08-Feb-13	2	3	2	2	2	2	2	2	8	17
09-Feb-13	1	1	1	1	1	1	1	1	3	8
10-Feb-13	2	1	1	1	1	2	3	2	6	13
11-Feb-13	1	1	1	1	1	2	3	2	6	12
12-Feb-13	1	1	2	1	2	2	2	3	7	14
13-Feb-13	3	2	1	2	1	2	4	5	15	20
14-Feb-13	4	3	2	3	2	3	3	3	15	23
15-Feb-13	0	1	1	1	1	2	3	2	5	11
16-Feb-13	1	1	1	2	3	5	4	2	14	19
17-Feb-13	1	1	2	2	3	3	4	3	12	19
18-Feb-13	0	0	0	1	1	1	2	3	4	8
19-Feb-13	0	1	1	2	2	3	3	3	8	15
20-Feb-13	1	1	2	3	2	2	2	2	7	15
21-Feb-13	3	2	2	1	1	2	2	3	8	16
22-Feb-13	2	2	1	3	3	3	3	4	13	21
23-Feb-13	3	2	1	2	3	1	3	3	10	18
24-Feb-13	1	1	0	1	1	2	2	2	4	10
25-Feb-13	0	1	1	1	2	2	2	2	5	11

26-Feb-13	1	2	2	1	1	1	2	2	5	12
27-Feb-13	2	1	2	1	1	1	0	1	4	9
28-Feb-13	1	1	1	2	2	2	3	4	9	16
01-Mar-13	4	3	4	5	5	4	5	5	36	35
02-Mar-13	3	3	2	1	2	3	4	4	15	22
03-Mar-13	2	2	2	1	2	2	3	3	9	17
04-Mar-13	2	1	1	1	2	1	0	1	4	9
05-Mar-13	3	1	2	2	1	1	2	1	6	13
06-Mar-13	2	2	1	1	1	-	1	1	-	9
07-Mar-13	1	2	2	2	1	1	1	1	5	11
08-Mar-13	0	0	1	1	1	1	2	1	3	7
09-Mar-13	3	2	1	1	2	2	3	1	8	15
10-Mar-13	1	1	1	1	1	2	1	3	5	11
11-Mar-13	3	1	2	1	1	1	1	1	5	11
12-Mar-13	1	1	2	2	2	2	3	2	7	15
13-Mar-13	1	1	1	1	1	1	2	2	4	10
14-Mar-13	1	1	2	2	2	2	1	1	5	12
15-Mar-13	1	3	3	2	2	1	1	1	7	14
16-Mar-13	3	3	2	2	2	2	2	2	9	18
17-Mar-13	2	2	5	5	4	5	6	6	43	35
18-Mar-13	3	2	2	3	2	1	2	2	9	17
19-Mar-13	1	1	2	1	1	2	3	4	9	15
20-Mar-13	2	2	2	1	2	2	3	4	10	18
21-Mar-13	5	4	3	1	0	1	1	1	13	16
22-Mar-13	0	1	1	2	2	2	3	2	6	13
23-Mar-13	1	1	1	2	3	2	4	4	12	18
24-Mar-13	3	2	1	2	2	2	2	1	7	15
25-Mar-13	0	1	2	2	1	1	2	1	4	10
26-Mar-13	1	1	1	1	1	1	0	0	2	6
27-Mar-13	1	2	2	3	3	5	4	5	21	25
28-Mar-13	3	1	1	2	-	3	2	3	-	15

29-Mar-13	4	3	4	3	3	4	4	3	21	28
30-Mar-13	3	3	2	2	2	2	4	3	13	21
31-Mar-13	1	1	1	1	0	2	2	3	5	11
01-Apr-13	1	1	2	2	1	2	1	2	5	12
02-Apr-13	1	1	1	1	1	2	2	3	6	12
03-Apr-13	1	2	2	1	1	-	1	2	-	10
04-Apr-13	2	1	1	2	1	1	1	1	4	10
05-Apr-13	1	1	2	1	1	1	2	2	5	11
06-Apr-13	1	1	1	2	1	1	2	2	5	11
07-Apr-13	1	1	2	2	2	2	2	0	5	12
08-Apr-13	0	0	2	0	1	0	1	1	2	5
09-Apr-13	1	1	2	2	0	-	1	1	-	8
10-Apr-13	1	1	2	2	1	-	-	3	-	10
11-Apr-13	1	1	3	2	1	-	1	2	-	11
12-Apr-13	2	1	2	2	1	1	1	1	5	11
13-Apr-13	1	2	1	2	1	1	1	4	7	13
14-Apr-13	2	3	3	4	2	3	3	3	15	23
15-Apr-13	1	1	2	1	1	0	3	2	5	11
16-Apr-13	1	0	0	0	0	2	3	3	5	9
17-Apr-13	2	1	1	1	1	1	0	0	3	7
18-Apr-13	1	0	0	1	0	1	1	0	2	4
19-Apr-13	0	0	0	1	1	1	0	1	2	4
20-Apr-13	0	1	1	2	1	1	0	1	3	7
21-Apr-13	0	0	1	1	1	2	2	0	3	7
22-Apr-13	1	2	1	1	1	2	2	1	5	11
23-Apr-13	0	2	2	2	2	2	2	3	7	15
24-Apr-13	3	2	2	4	4	2	4	3	17	24
25-Apr-13	3	2	1	3	2	3	3	2	11	19
26-Apr-13	2	3	2	3	3	3	3	3	13	22
27-Apr-13	2	1	2	1	2	2	2	2	6	14
28-Apr-13	1	1	1	2	2	2	2	2	6	13

29-Apr-13	3	1	1	2	1	0	1	2	5	11
30-Apr-13	2	1	1	2	2	2	1	3	7	14
01-May-13	2	2	4	3	4	3	5	3	20	26
02-May-13	3	3	2	2	1	1	3	2	9	17
03-May-13	1	2	1	1	1	1	2	1	4	10
04-May-13	1	1	2	2	2	2	2	2	6	14
05-May-13	2	1	1	2	2	3	2	1	7	14
06-May-13	2	1	2	3	2	2	2	3	9	17
07-May-13	3	2	2	3	3	2	2	1	10	18
08-May-13	3	2	2	1	1	2	1	2	7	14
09-May-13	2	2	1	2	1	1	1	1	5	11
10-May-13	1	3	1	1	2	1	-	0	-	9
11-May-13	1	2	1	1	0	-	0	1	-	6
12-May-13	1	2	1	2	1	1	-	1	-	9
13-May-13	1	1	1	1	1	2	2	1	4	10
14-May-13	1	1	3	3	2	1	2	2	8	15
15-May-13	1	1	2	2	3	3	3	2	9	17
16-May-13	3	3	2	2	4	4	3	4	18	25
17-May-13	3	3	2	2	2	3	3	3	12	21
18-May-13	4	4	3	2	2	2	3	2	14	22
19-May-13	3	2	1	2	2	2	2	4	10	18
20-May-13	2	2	1	1	2	2	2	2	6	14
21-May-13	2	1	1	2	2	1	2	2	6	13
22-May-13	3	2	2	2	3	3	3	2	11	20
23-May-13	1	3	1	2	2	2	2	2	7	15
24-May-13	1	2	2	4	3	3	5	4	19	24
25-May-13	3	3	2	4	3	5	5	4	25	29
26-May-13	4	4	3	2	3	4	3	3	19	26
27-May-13	2	3	2	3	2	3	4	3	14	22
28-May-13	2	3	2	3	2	2	1	1	8	16
29-May-13	0	1	0	1	1	0	0	0	1	3

30-May-13	0	1	1	1	0	1	1	0	2	5
31-May-13	0	1	1	1	2	3	3	4	9	15
01-Jun-13	5	5	5	4	5	2	3	3	32	32
02-Jun-13	3	3	2	3	3	2	3	3	13	22
03-Jun-13	2	2	2	2	2	2	2	3	8	17
04-Jun-13	3	2	2	2	1	1	2	3	8	16
05-Jun-13	3	2	1	2	1	1	1	1	6	12
06-Jun-13	1	3	3	3	3	5	4	4	21	26
07-Jun-13	4	4	3	3	2	2	2	1	14	21
08-Jun-13	2	3	3	3	1	1	0	1	8	14
09-Jun-13	1	2	2	1	3	3	3	2	9	17
10-Jun-13	3	3	3	-	3	2	2	1	-	17
11-Jun-13	1	1	2	1	3	3	2	2	8	15
12-Jun-13	1	1	1	2	2	0	1	1	4	9
13-Jun-13	2	1	1	1	0	1	1	1	3	8
14-Jun-13	1	1	1	2	1	1	1	2	4	10
15-Jun-13	2	1	2	1	1	1	1	1	4	10
16-Jun-13	1	2	0	2	1	1	1	1	4	9
17-Jun-13	1	2	1	1	1	1	1	1	4	9
18-Jun-13	1	1	1	1	1	1	2	1	4	9
19-Jun-13	2	2	1	1	0	2	2	3	6	13
20-Jun-13	3	2	1	3	2	2	3	4	12	20
21-Jun-13	4	3	2	3	3	3	3	3	16	24
22-Jun-13	2	3	3	3	2	2	3	3	12	21
23-Jun-13	3	3	3	3	2	3	3	3	14	23
24-Jun-13	3	2	3	3	3	4	4	3	17	25
25-Jun-13	3	2	1	1	1	2	1	2	6	13
26-Jun-13	1	2	1	1	1	2	1	1	4	10
27-Jun-13	1	1	1	1	4	3	2	3	10	16
28-Jun-13	3	4	2	3	3	5	3	4	21	27
29-Jun-13	5	5	3	4	3	3	4	4	28	31

30-Jun-13	3	2	1	3	3	3	3	2	12	20
01-Jul-13	3	3	2	2	1	1	1	1	7	14
02-Jul-13	1	1	1	2	1	1	1	0	3	8
03-Jul-13	1	1	0	1	1	1	2	2	4	9
04-Jul-13	1	2	2	2	1	1	2	2	6	13
05-Jul-13	2	2	2	2	3	3	4	3	13	21
06-Jul-13	3	3	3	3	3	3	3	4	17	25
07-Jul-13	4	2	1	1	1	2	2	1	8	14
08-Jul-13	1	1	1	1	1	2	2	1	4	10
09-Jul-13	1	1	1	2	2	2	4	3	9	16
10-Jul-13	4	4	3	3	3	3	3	4	20	27
11-Jul-13	2	3	4	2	3	3	5	2	18	24
12-Jul-13	2	2	2	2	1	3	3	3	10	18
13-Jul-13	4	3	3	2	1	2	3	2	12	20
14-Jul-13	3	3	2	3	3	3	4	3	16	24
15-Jul-13	4	3	2	2	3	2	2	2	12	20
16-Jul-13	1	1	1	0	1	1	2	1	3	8
17-Jul-13	0	2	1	1	1	1	2	2	4	10
18-Jul-13	1	2	1	3	4	4	4	3	16	22
19-Jul-13	2	2	3	2	3	3	3	3	12	21
20-Jul-13	3	2	2	1	1	0	1	0	5	10
21-Jul-13	1	2	1	1	1	2	2	2	5	12
22-Jul-13	2	2	1	2	1	2	1	3	7	14
23-Jul-13	2	2	2	2	1	1	1	1	5	12
24-Jul-13	2	0	0	1	1	1	1	1	3	7
25-Jul-13	1	2	2	1	1	3	4	4	12	18
26-Jul-13	4	3	2	2	3	2	3	1	12	20
27-Jul-13	3	2	1	2	3	3	2	3	11	19
28-Jul-13	2	2	1	1	1	1	2	3	6	13
29-Jul-13	1	1	1	1	2	1	1	1	4	9
30-Jul-13	1	2	2	2	2	2	2	1	6	14

31-Jul-13	2	2	1	1	1	1	2	1	5	11
01-Aug-13	1	2	0	2	1	2	1	0	4	9
02-Aug-13	1	1	0	-	-	-	1	1	-	4
03-Aug-13	1	1	0	1	1	1	1	2	3	8
04-Aug-13	1	1	2	3	2	5	4	4	17	22
05-Aug-13	4	3	2	3	2	2	3	3	14	22
06-Aug-13	3	1	1	1	1	1	1	2	5	11
07-Aug-13	1	1	2	2	1	1	1	0	4	9
08-Aug-13	0	1	1	1	1	1	2	2	4	9
09-Aug-13	1	3	2	2	2	2	3	2	9	17
10-Aug-13	1	2	2	2	3	2	1	1	7	14
11-Aug-13	2	1	1	1	2	1	1	1	4	10
12-Aug-13	1	1	1	2	1	2	3	3	7	14
13-Aug-13	2	1	2	2	2	4	3	2	10	18
14-Aug-13	3	3	2	1	2	2	2	3	10	18
15-Aug-13	3	2	2	3	3	4	2	3	14	22
16-Aug-13	3	4	3	3	3	4	3	3	18	26
17-Aug-13	3	2	2	2	2	1	1	2	7	15
18-Aug-13	2	1	2	2	1	1	2	2	6	13
19-Aug-13	1	1	1	2	2	2	1	1	5	11
20-Aug-13	0	1	1	1	0	1	1	3	4	8
21-Aug-13	3	3	2	3	3	3	4	4	17	25
22-Aug-13	4	4	3	2	2	2	3	4	17	24
23-Aug-13	4	2	3	3	2	3	3	2	14	22
24-Aug-13	2	2	2	2	2	2	2	2	7	16
25-Aug-13	1	1	1	1	2	2	1	2	5	11
26-Aug-13	1	1	1	1	1	1	2	3	5	11
27-Aug-13	3	2	1	1	2	3	5	4	16	21
28-Aug-13	3	3	2	2	2	1	1	2	8	16
29-Aug-13	0	1	1	1	1	1	1	1	3	7
30-Aug-13	1	0	2	3	2	2	3	4	10	17

31-Aug-13	4	2	3	3	3	2	1	3	13	21
01-Sep-13	3	2	2	2	2	2	3	3	10	19
02-Sep-13	2	2	3	3	2	2	1	1	8	16
03-Sep-13	1	1	2	2	1	1	2	3	6	13
04-Sep-13	2	1	1	3	2	1	2	2	7	14
05-Sep-13	1	0	1	2	1	1	1	1	3	8
06-Sep-13	1	1	1	1	0	1	3	2	5	10
07-Sep-13	1	1	1	1	1	1	0	1	3	7
08-Sep-13	2	2	2	1	2	1	1	0	5	11
09-Sep-13	0	1	2	1	1	1	1	1	3	8
10-Sep-13	0	0	0	2	3	3	3	3	8	14
11-Sep-13	2	1	1	1	2	2	3	2	7	14
12-Sep-13	2	1	1	2	1	-	-	2	-	9
13-Sep-13	3	2	2	2	2	4	3	2	12	20
14-Sep-13	1	1	2	2	1	1	1	1	4	10
15-Sep-13	1	0	1	0	0	1	0	1	2	4
16-Sep-13	1	1	2	1	1	1	1	1	4	9
17-Sep-13	2	2	2	-	2	2	4	2	-	16
18-Sep-13	2	2	-	-	-	3	2	3	-	12
19-Sep-13	3	2	3	4	-	-	-	-	-	12
20-Sep-13	-	-	-	-	-	-	-	-	-	0
21-Sep-13	-	-	-	-	-	-	-	-	-	0
22-Sep-13	-	-	-	-	-	-	-	-	-	0
23-Sep-13	-	-	-	-	-	-	-	-	-	0
24-Sep-13	-	-	-	-	-	-	-	-	-	0
25-Sep-13	-	-	-	-	-	-	-	-	-	0
26-Sep-13	-	-	-	-	-	-	-	-	-	0
27-Sep-13	-	-	-	-	-	-	-	-	-	0
28-Sep-13	-	-	-	-	-	-	-	-	-	0
29-Sep-13	-	-	-	-	-	-	-	-	-	0
30-Sep-13	-	-	-	-	-	-	-	-	-	0

01-Oct-13	-	-	-	-	-	-	-	-	-	0
02-Oct-13	-	-	-	-	-	-	-	-	-	0
03-Oct-13	-	-	-	-	-	-	-	-	-	0
04-Oct-13	-	-	-	-	-	-	-	-	-	0
05-Oct-13	-	-	-	-	-	-	-	-	-	0
06-Oct-13	-	-	-	-	-	-	-	-	-	0
07-Oct-13	-	-	-	-	2	2	2	1	-	7
08-Oct-13	1	1	1	1	1	2	5	5	15	17
09-Oct-13	5	4	4	3	3	3	3	4	24	29
10-Oct-13	4	3	2	2	2	2	1	2	10	18
11-Oct-13	1	2	2	2	2	2	2	1	6	14
12-Oct-13	1	1	1	1	1	2	3	3	7	13
13-Oct-13	1	1	0	1	0	0	2	0	2	5
14-Oct-13	1	2	2	3	4	4	5	4	20	25
15-Oct-13	4	3	2	3	3	1	2	4	15	22
16-Oct-13	-	-	-	-	-	-	-	-	-	0
17-Oct-13	3	3	2	3	3	2	2	2	11	20
18-Oct-13	0	1	1	0	0	1	2	0	2	5
19-Oct-13	0	1	1	1	0	1	0	0	2	4
20-Oct-13	0	0	1	1	0	0	1	1	2	4
21-Oct-13	0	1	1	1	1	1	0	0	2	5
22-Oct-13	0	1	3	2	1	1	2	2	6	12
23-Oct-13	2	2	2	2	1	0	1	0	4	10
24-Oct-13	1	1	1	2	1	1	0	0	3	7
25-Oct-13	-	-	-	-	-	-	-	-	-	0
26-Oct-13	1	-	1	1	0	0	1	-	-	4
27-Oct-13	1	1	-	-	-	-	-	-	-	2
28-Oct-13	-	-	-	-	-	-	-	-	-	0
29-Oct-13	0	-	-	-	-	-	-	-	-	0
30-Oct-13	-	-	-	-	-	-	-	-	-	0
31-Oct-13	3	3	6	-	-	-	2	3	-	17

01-Nov-13	2	2	1	1	2	1	1	1	5	11
02-Nov-13	1	1	1	2	0	1	1	2	4	9
03-Nov-13	3	2	2	1	1	0	3	3	8	15
04-Nov-13	0	1	2	2	1	3	2	1	6	12
05-Nov-13	2	1	2	1	0	1	0	1	3	8
06-Nov-13	1	0	1	-	1	1	1	3	-	8
07-Nov-13	2	2	2	3	3	1	3	2	10	18
08-Nov-13	3	2	1	1	0	1	0	1	4	9
09-Nov-13	2	4	4	4	4	2	1	1	16	22
10-Nov-13	3	3	2	3	2	3	3	4	15	23
11-Nov-13	4	3	3	3	4	3	3	1	17	24
12-Nov-13	1	1	1	1	0	0	0	0	2	4
13-Nov-13	0	1	1	2	2	1	1	1	4	9
14-Nov-13	0	0	1	1	1	1	1	1	2	6
15-Nov-13	2	2	1	1	2	3	3	4	11	18
16-Nov-13	3	3	3	3	2	2	1	2	11	19
17-Nov-13	2	2	2	2	2	1	2	1	6	14
18-Nov-13	1	1	1	1	0	1	0	0	2	5
19-Nov-13	0	1	1	2	1	1	2	2	4	10
20-Nov-13	-	-	-	-	-	0	1	0	-	1
21-Nov-13	0	1	0	0	0	0	0	1	1	2
22-Nov-13	1	1	0	0	0	0	2	2	3	6
23-Nov-13	-	-	-	-	-	-	-	-	-	0
24-Nov-13	-	-	-	-	-	-	-	-	-	0
25-Nov-13	-	-	1	0	0	-	-	-	-	1
26-Nov-13	0	1	1	0	0	1	1	1	2	5
27-Nov-13	0	0	-	1	1	1	0	0	-	3
28-Nov-13	0	0	1	0	2	1	1	1	2	6
29-Nov-13	1	2	1	1	2	2	4	2	8	15
30-Nov-13	2	1	1	2	2	2	4	4	11	18
01-Dec-13	3	2	2	2	3	2	0	1	8	15

02-Dec-13	0	0	1	0	0	0	0	0	0	1
03-Dec-13	1	2	2	2	3	2	3	2	9	17
04-Dec-13	2	2	1	0	0	1	2	1	4	9
05-Dec-13	0	1	1	2	2	2	1	1	4	10
06-Dec-13	1	1	1	1	1	1	1	2	4	9
07-Dec-13	2	1	2	1	1	1	3	3	7	14
08-Dec-13	5	5	3	2	2	4	3	2	22	26
09-Dec-13	1	1	1	1	2	2	1	1	4	10
10-Dec-13	1	2	1	1	1	1	1	0	3	8
11-Dec-13	1	1	1	1	1	0	1	2	3	8
12-Dec-13	1	0	1	1	0	0	0	0	1	3
13-Dec-13	0	0	1	1	3	2	2	1	5	10
14-Dec-13	3	3	3	2	2	4	5	2	18	24
15-Dec-13	2	1	2	2	1	3	2	2	7	15
16-Dec-13	2	2	2	1	1	1	2	2	6	13
17-Dec-13	2	1	1	0	0	1	3	1	4	9
18-Dec-13	1	1	1	1	1	1	1	2	4	9
19-Dec-13	1	1	1	1	1	3	3	2	7	13
20-Dec-13	2	2	1	1	1	2	2	2	6	13
21-Dec-13	1	1	1	1	0	0	1	0	2	5
22-Dec-13	0	1	1	1	0	1	0	0	2	4
23-Dec-13	1	0	0	0	0	0	1	1	1	3
24-Dec-13	0	0	1	1	0	1	1	2	2	6
25-Dec-13	2	1	1	2	2	2	2	1	6	13
26-Dec-13	0	0	0	1	1	0	1	0	1	3
27-Dec-13	0	0	1	0	1	0	1	1	2	4
28-Dec-13	0	0	0	1	1	1	1	2	2	6
29-Dec-13	2	1	2	2	1	2	2	0	5	12
30-Dec-13	0	0	1	1	1	2	1	0	2	6
31-Dec-13	1	2	2	2	2	1	2	1	6	13

Definitive daily mean values of the Declination (D), Inclination (I), Horizontal (X and Y), and Vertical (Z) field components.

Presently, daily mean values are obtained from the hourly means (HMVs) which in turn comes from the minute mean values (MMVs), based on the digital recordings of the three-component fluxgate magnetometer FGE. The baseline of this magnetometer is determined from absolute measurements with a DI-flux theodolite and an Overhauser proton magnetometer.

Positions of the Variation house where the three-component fluxgate magnetometer FGE is installed and the Absolute house where absolute geomagnetic measurements are performed are given in the Fig. 1.

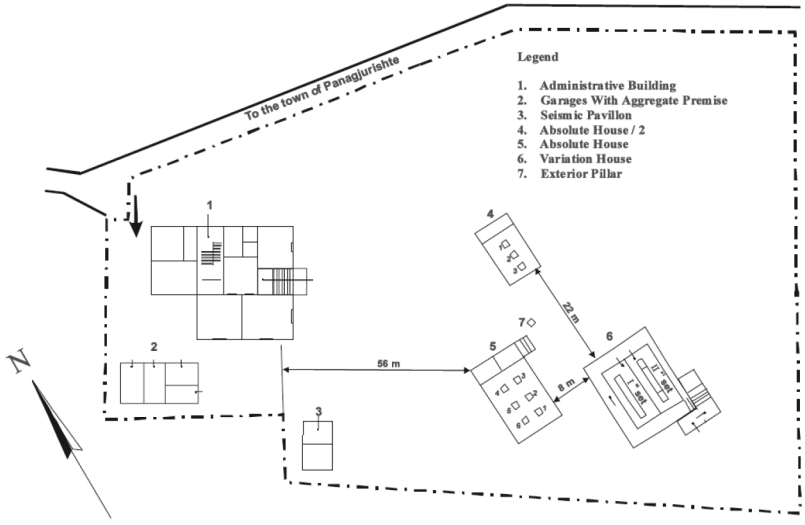

Fig. 1. Ground plan of the Panagjurishte observatory

Before calculating of MMVs, inspection and verification of the reported data is performed. The reported data (available in near real time) are usually used in applications where the reliable representation of higher-frequency magnetic field variations is more important rather than absolute levels or secular variation. This concerns, e.g. the forecast of magnetic activity, radio-wave propagation, or space weather. In the case of reported data it is not possible to verify them prior to dissemination. Careful monitoring of the automatically transmitted data and the present-day computer technologies enable us to improve the quality of data and reduce the number of gaps in the records. After the quality control procedures have been applied to the 2013 reported data, we obtained the definitive minute mean values and calculated the HMVs and DMVs. Due to technical problems there are gaps in the data records in September, October and November.

Daily mean values of the Declination (D), Inclination (I), Horizontal (X and Y), and Vertical (Z) field components for 2013 are plotted in the next figures:

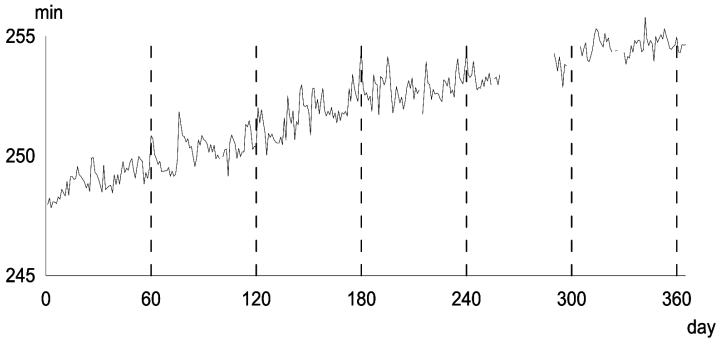

Fig. 2. Plot of the daily mean values of the **Declination (D)** registered in PAG observatory in 2013.

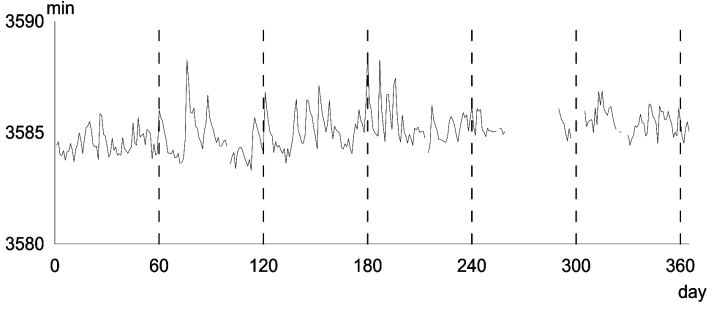

Fig. 3. Plot of the daily mean values of the **Inclination (I)** registered in PAG observatory in 2013.

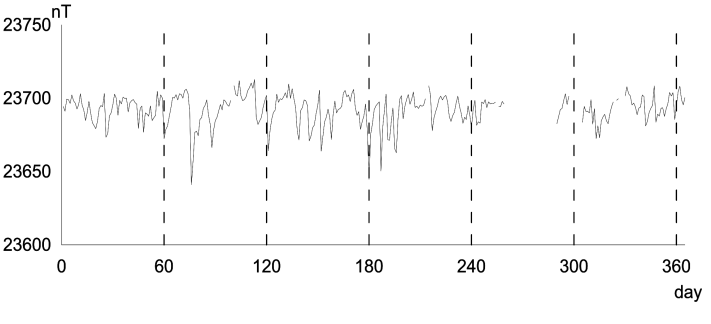

Fig. 4. Plot of the daily mean values of the **North geomagnetic field component (X)** registered in PAG observatory in 2013.

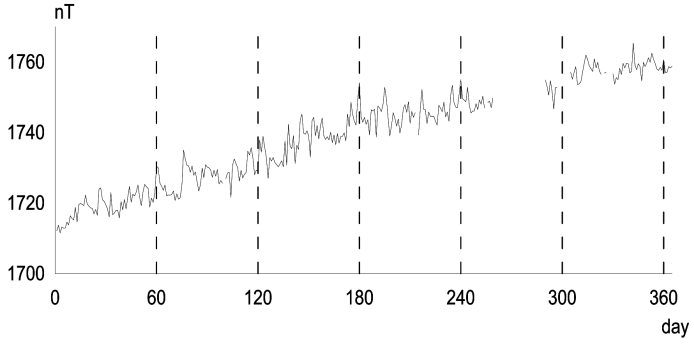

Fig. 5. Plot of the daily mean values of the **East geomagnetic field component (Y)** registered in PAG observatory in 2013.

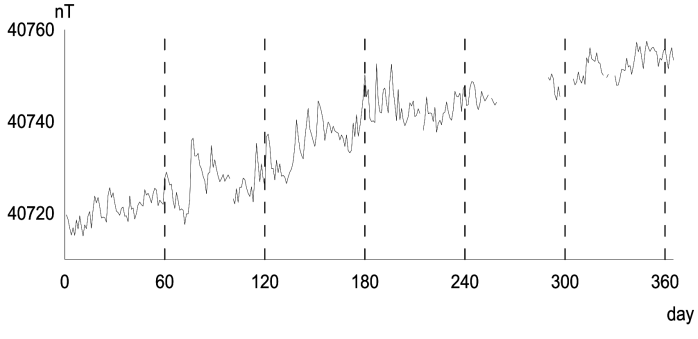

Fig. 6. Plot of the daily mean values of the **Vertical geomagnetic field component (Z)** registered in PAG observatory in 2013

Conclusions

Continuous registration of the geomagnetic field components gives the sum of all field contributions from the internal and external to the Earth sources. A straightforward separation of the individual contributions is impossible and many scientific studies deal with different aspects of this problem (Mandea nad Korte, 2010). Approximate description of the strength of different external variations however, are provided by geomagnetic indices. A quantitative measure of the 2013 local geomagnetic activity in the form of 3 hour *K*-index is published here, based upon the range of fluctuations in the PAG observatory records over 3 h. intervals. Tables show that 2013 has relatively quiet geomagnetic field with only 15 disturbed days having K-index = 5. Annual variations of the geomagnetic field components are plotted by means of daily mean values. Data are checked and verified according to IAGA requirements (Jankowski and Sucksdorff, 1996).

References

Buchvarov I., 2006. Field and observatory geomagnetic measurements in Bulgaria. in Rasson and Delipetrov (*eds*.) Geomagnetics for Aeronautical Safety, *Springer, p.61-62*

Jankowski J., Sucksdorff C., 1996. *Guide for magnetic measurements and observatory practic.*, International Association of Geomagnetism and Aeronomy, Warsaw, Poland.

Mandea M., Korte M. (*eds)*, 2010 *Geomagnetic observation and models*, IAGA Special Sopron Book Series 5, Springer.

Sucksdorff, C., Pirjola, R. and Häkkinen, L., 1991. Computer production of K-values based on linear elimination, Geophysical Transactions, 36, 333-345

Годишен доклад за наблюдаваната геомагнитна активност в Обсерватория Панагюрище през 2013

М. Методиев, П. Трифонова

Резюме: Понастоящем, в ерата на интернет комуникациите, записите от геомагнитните обсерватории се предоставят на заинтересованите потребители почти в реално време, докато обработените времеви серии (окончателни данни) са обект на много проверки и се разпространяват с месеци закъснение. Настоящият доклад представя дефинитивните геомагнитни данни, получени в Обсерватория Панагюрище през 2013 г., дадени под формата на локални геомагнитни индекси и графики на среднодневните стойности на компонентите на магнитното поле. Верификацията на данните е извършена в съответствие с изискванията на IAGA.

DATA AND ANALYSIS OF THE EVENTS RECORDED BY NOTSSI IN 2015

E. Botev, V. Protopopova, I. Aleksandrova, B. Babachkova, S. Velichkova, I. Popova, P. Raykova, M. Popova, T. Iliev

National Institute of Geophysics, Geodesy and Geography, BAS, Akad. G. Bonchev, Str., bl.3, Sofia, Bulgaria, e-mail: ebotev@geophys.bas.bg

Abstract. A map of epicenters of 1426 earthquakes that occurred during 2015 in the Balkan Peninsula (sector outlined by latitude j =37^0- 47^0N and longitude l=19^0-30^0E) is presented. Expert generalized analysis of the seismicity over the territory of Bulgaria and its very adjacent lands (with more than 1042 localized events) is proposed. Catalog of earthquakes with magnitude M>2.5 is applied.

Key words: Balkan Peninsula, Bulgaria, seismicity

The present scientific communication contains generalized information on the results of collection, processing and analysis of the data about the seismic events recorded by the National Operative Telemetric System for Seismological Information (NOTSSI) in 2015. The expanded information about the realized seismicity is suggested as a natural generalization and supplementation of the monthly compilations of the preliminary seismological bulletin of NOTSSI. The analysis and evaluation of the space, time and energy distribution of the seismicity, periodically been made, open up possibilities for searching for time correlations with the parameters of different geophysical fields aiming to find out eventual precursor anomalies.

The recording and space localization of the seismic events in NOTSSI during 2015 is realized by means of the digital network (Solakov et al., 2006). The routine processing and acquisition of the initial data is organized in a real time duty regime. The operations are fulfilled by the authors of this communication. In such a way the main goal of NOTSSI, namely the seismicity monitoring in order to help the authorities' and social reaction in case of earthquakes felt on the territory of the country, is realized. The computing procedure for determining the parameters of the seismic events is an adaptation of the widespread product HYPO'71 (Solakov, 1993). The energy parameters of the events are

presented mainly by the magnitude M calculated according to the records duration by the formula (Christoskov and Samardjieva, 1983).

$$M = 1.92 + 2.72\log\tau - 0.026\Delta$$

After bringing into use the digital broadband seismometers of NOTSSI network, the magnitude determination for local and regional events is calculated by P wave amplitude ratio (Christoskov at all., 2011 a, b).

The focal mechanism parameters are obtained by means of a program FOCMEC (Snoke, 2009). The high sensitivity of the seismographs allows recording and processing of a great number of long distance earthquakes. As a result of the achieved experience in the authors interpretation work, different magnitude's lower threshold for successful determination of local, regional and long distance earthquakes is established: M=1.5 for the territory of Bulgaria, M=3.0 for the central part of the Balkans, M=5.0 for long distance events. The precision of the epicenter's determination is different; except on the distance it depends also on the specific position of the epicenter in relation to the recording network. The parameters of seismic events occurring at a distance more than 100-150 km outside the territory of Bulgaria should be accepted only informatively and cannot be used for responsible seismotectonic investigation.

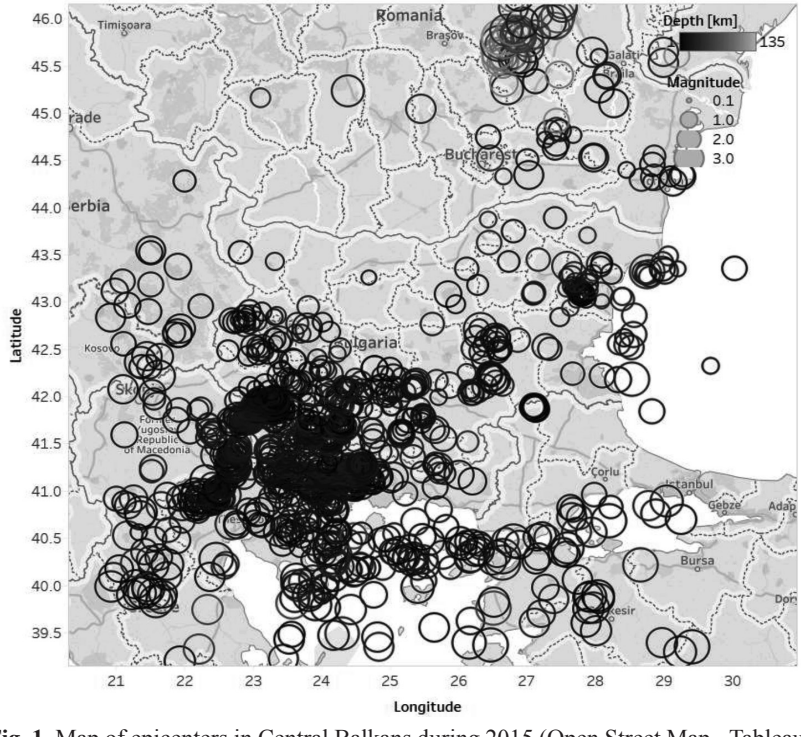

Fig. 1. Map of epicenters in Central Balkans during 2015 (Open Street Map - Tableau Desktop 10.4.)

For the period of observations presented in this communication, the primary data about 2000 local, regional, distant earthquakes and industrial explosions on the territory of Bulgaria are recorded, classified and processed (as a work bulletin) in NOTSSI. After comprehensive analysis of the records and application of the above mentioned calculation procedures it is established that 1426 of all registered earthquakes are in the Balkan Peninsula region outlined by geographic latitude 37^0 - 47^0 N and longitude 19^0 - 30^0 E. The epicenters of the earthquakes differentiated by magnitude levels are plotted on Fig.1. The number of the events in the magnitude interval M≤1.9 is 670, in M=2.0-2.9 - 576, in M=3.0-3.9 - 155, in M=4-4.9 – 25 earthquakes. During this not so active period there is only 1 events with magnitude M>4.0 on Bulgarian territory and one in Black sea, which is close to the Bulgarian coast line. All other earthquakes with magnitude more than 4 are out of Bulgarian borders.

As a whole, the seismic situation in the studied part of the Balkans during 2015 is characterized as not very activity - 1426 events, which is less than previous years 1622 events in 2014, 1602 in 2013, 1508 in 2012, 1829 in 2011, 2401 in 2010, 2744 in 2009, 1775 in 2008, and around 1100-1400 for most of the previous years. The maximum realized earthquake is with magnitude Ml=4.9 in Vranchea seismic zone, Romania, while this value for the previous year is Ms=6.6 in North Aegean sea. The observed tendency of decrease of the activity compared with the former years is not only due to the low level of earthquake activation in North Aegean sea, Central Greece, Serbia and West Turkey, but also due to decrease of number of microearthquekes in the territory of Bulgaria.

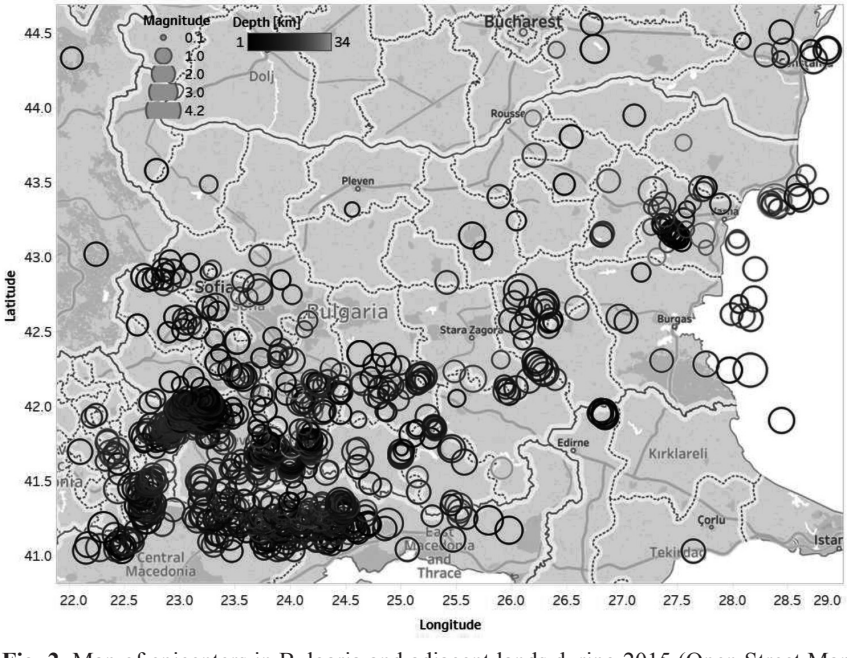

Fig. 2. Map of epicenters in Bulgaria and adjacent lands during 2015 (Open Street Map - Tableau Desktop 10.4.)

The strongest event outside Bulgaria during the study period occurred in the region situated around the Vranchea seismic zone (Romania) with magnitude M=4.9. Shakable effects because of Vranchea source zone in Romania during the study period occurred 2 times in north-eastern Bulgaria- with intensity II-III in towns of Ruse and Silistra.

As a whole, events with M<3.0 which occur outside Bulgaria are difficult to be localized by the national seismological system; consequently, not all of them have been marked on the scheme in Fig.1.

Fig. 2 illustrates the seismicity just in the territory of Bulgaria and nearby lands ($j = 41^0 - 44.5^0$N, $l = 22^0 - 29^0$E). The earthquakes are differentiated by magnitude intervals. The parameters of relatively stronger earthquakes are presented in Table 1.

Table 1. List of earthquakes with M³2.5 in Bulgaria and adjacent lands during 2015

Date	Time	Latitude [N]	Longitude [E]	Magnitude	Depth [km]
2 January 2015	5:50:53.7	41.21	23.98	3.3	9
	15:20:51.6	42.64	23.33	2.6	10
6 January 2015	7:48:57.2	41.00	22.17	2.6	7
10 January 2015	22:37: 3.6	41.69	23.89	2.6	15
14 January 2015	3:10:54.0	41.21	25.79	3.1	2
20 January 2015	17:21:47.1	42.65	26.31	2.6	9
4 February 2015	19:18: 9.3	42.57	26.97	2.5	15
5 February 2015	6:16:45.2	42.75	26.08	4.1	12
12 February 2015	6:21:50.6	41.74	23.83	2.9	14
13 February 2015	13:13:41.9	41.38	22.73	2.6	10
18 February 2015	18:58:40.9	41.67	24.59	2.5	17
3 March 2015	18:33:27.3	41.95	24.29	2.8	13
17 March 2015	20:59:38.4	41.20	22.70	2.5	8
18 March 2015	22:53:55.7	41.21	22.72	2.7	5
19 March 2015	16:56:28.4	42.17	23.58	2.7	7
24 March 2015	3: 7:37.6	42.09	24.83	2.7	15
	20:37:50.3	41.97	23.26	3.1	14
27 March 2015	22: 3: 2.6	41.84	22.85	2.8	15
28 March 2015	17:29: 1.6	41.30	22.69	3.8	10
	18:50:52.4	41.29	22.71	2.8	14
	19: 0:29.7	41.30	22.74	3.5	15
31 March 2015	2:12:35.6	41.46	23.57	2.5	12
2 April 2015	2:24:10.4	42.25	26.23	3.2	11
	2:27: 7.7	42.22	26.27	3.4	14
	2:28:45.0	42.21	26.29	3.2	14
	2:29:35.6	42.24	26.24	3.1	8
3 April 2015	22: 1: 8.6	41.05	22.46	2.5	2

6 April 2015	9: 7:12.0	41.46	22.74	2.5	11
	18:28:20.2	41.26	22.67	2.8	5
8 April 2015	4:23:37.0	42.00	23.29	2.5	10
12 April 2015	12:41:51.4	41.10	23.46	2.8	6
16 April 2015	13:42: 5.2	41.11	24.11	3.0	9
19 April 2015	3:10:31.4	41.17	24.68	2.6	12
22 April 2015	9:30: 2.7	44.31	28.46	2.6	20
24 April 2015	14:18: 3.2	41.91	26.84	2.6	2
27 April 2015	21:26:14.6	41.02	22.29	2.8	15
5 May 2015	0:17:13.5	41.06	22.52	2.7	11
	1:24:21.9	41.07	22.53	2.8	15
	20:34: 8.1	42.01	24.10	2.9	13
7 May 2015	12:48:37.0	41.11	23.79	3.0	7
9 May 2015	18:52:50.5	42.27	23.36	2.6	2
10 May 2015	12:57:39.4	41.25	23.23	2.9	11
15 May 2015	20:36:46.2	41.99	23.16	2.5	7
20 May 2015	12:24:35.1	42.22	27.96	2.5	2
21 May 2015	5:13:39.4	41.07	23.97	2.7	7
28 May 2015	14:16:37.9	41.17	24.58	2.5	7
5 June 2015	1:29:33.5	41.26	22.73	2.5	8
7 June 2015	1:37:46.8	42.18	25.20	3.2	15
8 June 2015	4:28:24.9	41.84	22.76	2.7	9
10 June 2015	23:48:39.3	41.14	25.98	2.8	2
11 June 2015	11:11:50.8	41.97	23.22	2.5	7
12 June 2015	18:25: 2.2	42.16	25.65	2.6	20
13 June 2015	17:17:33.5	41.64	25.00	2.5	13
16 June 2015	14:15:53.7	41.92	26.83	2.5	5
17 June 2015	10:53:41.0	42.69	28.18	2.5	14
1 July 2015	20:24: 3.7	41.24	23.21	2.5	10
4 July 2015	23:23:17.6	41.29	24.48	2.7	12
5 July 2015	4:20:25.9	41.19	24.89	3.3	12
7 July 2015	12:15: 6.0	41.73	24.26	2.7	12
9 July 2015	0: 6:18.9	41.49	23.21	2.9	20
10 July 2015	0: 6:19.3	41.47	23.19	3.0	13
	2:39:37.8	41.48	23.21	2.6	16
15 July 2015	8:30:37.3	43.34	28.37	4.2	28
16 July 2015	3:33:42.5	41.96	23.27	3.3	10
	10:13: 4.4	42.66	26.29	3.3	10
24 July 2015	15:42:34.3	41.33	24.46	3.3	10
	21:30:25.2	41.29	24.48	2.8	12
28 July 2015	1: 3:46.8	41.27	24.47	3.5	13

31 July 2015	8:33: 4.7	43.35	28.60	2.5	13
2 August 2015	8:24:36.5	41.31	24.46	2.8	13
4 August 2015	22:42: 4.5	41.43	22.58	2.9	6
5 August 2015	13:53:42.5	41.77	22.71	3.1	6
15 August 2015	10:32: 8.6	41.96	23.01	2.7	17
16 August 2015	9:39: 5.0	41.42	22.46	3.1	16
	21:36:57.8	41.62	23.71	2.7	11
20 August 2015	2:18: 5.7	41.28	23.24	2.7	14
	13:45:23.5	41.89	23.28	2.5	2
23 August 2015	1:28: 0.1	44.33	26.75	3.3	2
27 August 2015	22:41:56.1	41.79	22.79	2.5	5
6 September 2015	12:15:29.9	41.19	23.55	2.5	10
8 September 2015	3:13:13.3	41.93	23.14	2.5	16
11 September 2015	21:44:16.0	41.51	23.76	2.7	18
12 September 2015	7: 8:19.7	41.90	23.26	2.8	13
19 September 2015	13:23:52.7	43.11	25.64	2.6	3
21 September 2015	21:33:57.7	41.60	25.57	2.5	10
25 September 2015	2:55:33.4	41.31	22.63	2.5	2
5 October 2015	0:40:12.8	42.76	23.71	3.2	15
	9:52:36.2	42.28	24.02	2.5	13
8 October 2015	21:35:16.8	41.28	24.48	2.5	13
9 October 2015	7:56:55.7	41.30	25.52	2.8	18
10 October 2015	0:49:47.9	41.68	23.82	2.5	9
	17: 6:50.5	41.63	23.80	3.1	18
	19: 4:26.5	41.61	24.02	2.8	5
	20:13:17.5	41.55	24.02	2.5	17
12 October 2015	21:31:58.1	41.91	23.25	2.8	5
15 October 2015	16:49:15.1	41.64	23.81	2.5	15
16 October 2015	17:54:33.9	42.01	23.24	2.8	5
18 October 2015	19:33:17.5	41.60	24.00	2.5	17
20 October 2015	22:40:27.5	41.60	24.01	3.2	12
21 October 2015	4:20:33.8	41.61	23.99	2.5	10
22 October 2015	4:34:33.0	41.68	23.82	2.8	8
6 November 2015	0:54:46.5	42.33	24.63	2.5	2
6 November 2015 11 November 2015	1: 4:43.1	41.31	22.73	2.8	12
	23:54:46.5	42.33	24.63	2.5	2
	9: 1:33.3	41.27	24.47	2.5	5
11 November 2015 13 November 2015	13: 6: 0.8	41.91	26.83	2.5	8
	7:14:56.9	41.43	22.62	2.8	5
14 November 2015	20:44:10.9	43.40	27.27	3.2	21
20 November 2015	22: 1: 4.3	41.08	24.24	2.5	11

21 November 2015	0:42:34.9	41.16	22.32	3.5	2
21 November 2015 1 December 2015	6:13:52.4	41.69	25.46	2.8	12
	9:28:20.5	41.65	25.00	2.5	14
4 December 2015	7: 1:10.7	41.91	23.27	2.8	2
4 December 2015 5 December 2015	23: 4:15.5	41.29	24.48	3.1	10
	6:34:48.5	41.97	23.28	2.6	2
11 December 2015	21:52:41.7	42.41	23.52	2.5	10
13 December 2015	14: 4:34.8	41.70	24.17	2.6	13
21 December 2015	8:56:13.0	41.79	22.67	2.5	11
23 December 2015	12:35:49.2	41.93	26.80	2.5	7

On the territory of Bulgaria relatively normal activity of earthquakes is observed during 2015 – 1042 events are observed, against 947 in 2014, 1124 in 2013, 932 in 2012, 1205 in 2011 and 1607 in 2010. The earthquakes of a magnitude higher than 3.0 are in normal amount – 30 events compared with an averaged number of about 20-35 for most of the all previous years.

The maximum realized magnitude is Ms=4.9 in the region of Vranchea seismic zone which is the lowest maximal magnitude of earthquakes, in comparison with the maximum magnitude in the course of previous years. The strongest event during 2015, close to Bulgarian border (on Romanian territory) occurs on 23th of August and caused very weak macroseismic effects with intensity of II-III degree of MSC scale in the town of Tutrakan – not so far from the town of Ruse.

As usual, the largest concentration of the epicenters in the other regions of Bulgarian territory during 2015 is marked in the southwestern part of the investigated region (presented in Fig. 2). The Kroupnik seismic source is known with the strongest crustal earthquakes in Europe (M=7.8, 7.1) for the last 160 years. In 2015 only 3 events of M≥3.0 occurred in this region. The strongest felt earthquake for this part of Bulgarian territory is with magnitude M=3.3, it is felt on 16th of July in Blagoevgrad region by intensity of III of MSC scale – in the village of Dolno Osenovo (south-western slopes of Rila mountain).

The other Bulgarian seismic sources in 2015 are relatively not so active than during the previous years. They produced not more than 10 earthquakes affecting different localities in this country by intensity of up to IV-V degrees of MSC scale. Several earthquakes with magnitude more than 3.0 have occurred in the Monastery uplift and are felt by III degree of MSC scale on 2th of April. The maximum number of felt earthquakes is occurred around North-eastern Bulgaria. Three cases of magnitudes about 3.0 aroused shocks of intensity three or a bit more are felt in Provadia region – the strongest event is with magnitude M=3.2 on 14th of November . The maximum event for whole Bulgarian territory with M=4.2 in Black sea caused V degree of MSC scale on 03 December in Shabla region (Kaliakra cape in the north-eastern Black sea cost). A strong event M=4.1 in the neighbor region of Sliven town caused effects of IV-V degree of MSC on 5 th of February.

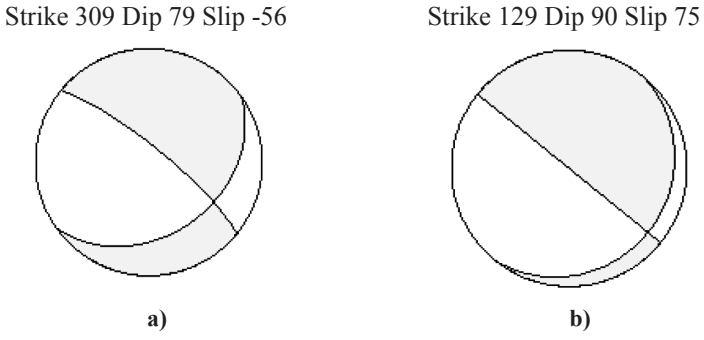

Fig. 3. Focal plane solutions of two earthquakes: **a)** 15 km north-western of Sliven (05.02.2015, 6:16 GMT, Ml=4.1, H=12 km) and **b)** in Black sea, 5 km south-eastern of Kaliakra cape (15.07.2015, 8:30 GMT, Ml=4.2, H=28 km)

For the determination of the earthquake mechanism the program FOCMEC is used. Input data are the polarities of the P wave. Forty-six first motion polarities data are used for defining the focal mechanism of the earthquake near Sliven city (Fig. 3.a) and only twelve for the earthquake near the Kaliakra cape (Fig 3.b). Data from seismological stations in Bulgaria and surrounding area, taken from NOTSSI and GFZ Seismological Data Archive database (Bianchi et al., 2015) are included in the double - couple focal mechanism - Fig. 3. The solutions are displayed on lower hemisphere. All polarities are check as waveform. The strike, dip and rake are determined in accuracy up to 5 degrees for first earthquake and up to 10 degrees for second. Both earthquakes are characterized as a dip-slip faulting, with very small strike-slip component.

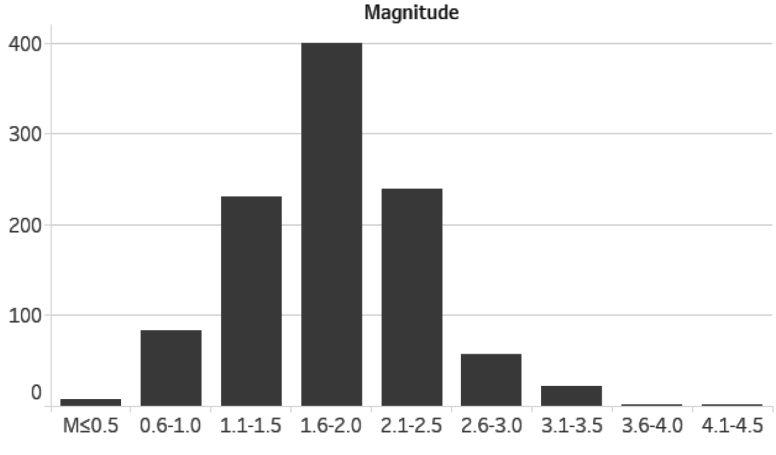

Fig. 4. Magnitude - frequency distribution of the earthquakes

A detailed analysis of seismicity in the individual seismic zones is hard to be fulfilled because of the insufficient quantity of events and the narrow magnitude range of the earthquakes. The joint statistics of all the events in Fig. 2 characterize predominantly the seismicity parameters of the southwestern part of the territory under investigation.

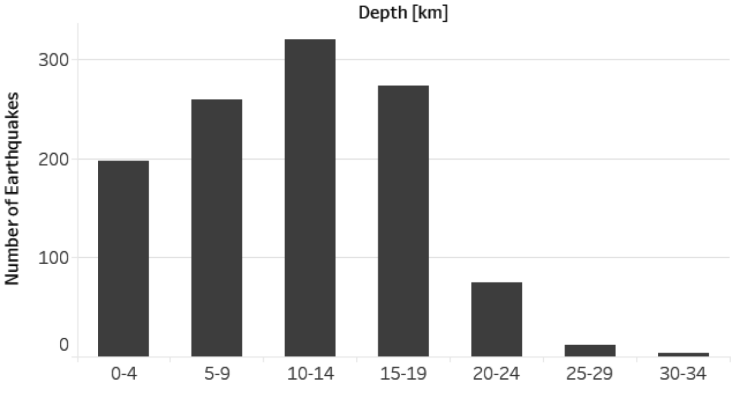

Fig. 5. Depth - frequency distribution of the earthquakes

The magnitude-frequency distribution for the entire data set is presented in Fig. 4. The number of localized events increases with the magnitude decreasing: for M> 4.0 is 3 events, M=3.6-4.0 is 1 event, for M=3.1-3.5 is 22 events, for M=2.6-3.0 - 57, for M=2.1-2.5 – 239, 1.6-2.0 - 400 and so on. The abrupt diminishing of the number of earthquakes in the first three intervals (M<1.5) in Fig. 4 determines also the registration power of the seismic stations network. Taking the latter into account, it can be supposed that the magnitude sample for levels with M > 1.5 is comparatively closer to the reality for the bigger part of the Bulgarian territory.

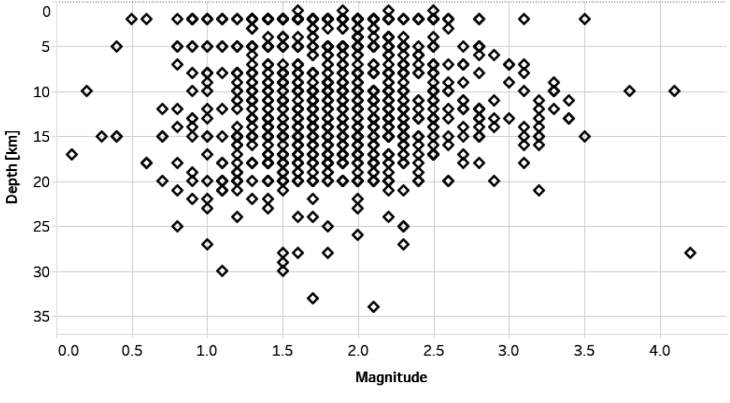

Fig. 6. Depth - magnitude distribution of the earthquakes

The picture of the depth distribution in Fig.5 shows that the majority of events occur in range 10-14 km depth. The number of events does not decrease smoothly with increase of the depth. It is possible the established predominating depth (from 5 to 20 km) to be also due to the presence of small number of unidentified industrial explosions. In the same time the number of events in the central interval is bigger.

The magnitude distribution of the events in depth (Fig. 6) permits to note some differentiation of depth "floors" with the increase of magnitude - the maximums can be traced out for the depth interval from 5 to 15 km. It is remarkable that the strongest events are not deep situated and the maximal event is associated with 10 km depth.

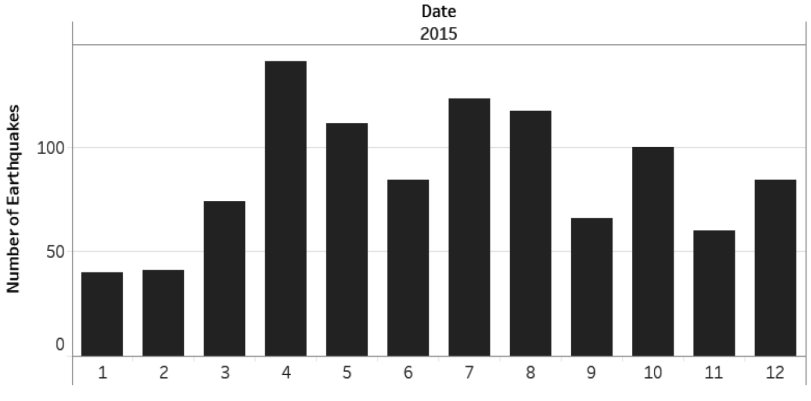

Fig. 7. Time - frequency distribution of the earthquakes

Fig. 7 illustrates the distribution of seismicity in time according to the number of events per months. The biggest earthquake's amount is displayed in April, when more then 140 earthquakes occurred, and it is associated with swarm activity in the beginning of April. The lowest earthquake quantity is in January - February, around 40 events. The energy release suggests that the period July - August, when the relatively high activity in Kaliakra cape region occurred, is one of the time with maximum of energy release. Local maximum of events is observed in October, when about 100 earthquakes occurred.

Additionally, about 800 distant earthquakes have been recorded in the period under study, as well as more than 700 industrial explosions, processed and classified in the preliminary monthly bulletins. In order to identify the artificial seismic sources the methodical approach described by Deneva et al. (1988) and some information about the quarry sites in Bulgaria have been used.

Acknowledgements: The authors owe their gratitude to the engineering staff for the perfect software and hardware ensuring of NOTSSI and to Team VISION Bulgaria Ltd. for the kind grant of the Tableau Desktop software.

References

Bianchi, Marcelo; Evans, Peter L.; Heinloo, Andres; Quinteros, Javier, 2015: WebDC3 Web Interface. GFZ Data Services. doi:10.5880/GFZ.2.4/2016.001

Christoskov L. and E. Grigorova, 1968. Energetic and space characteristics of the destructive earthquakes in Bulgaria since 1900. Izv.BAS, vol XII .

Christoskov L. and E. Samardjieva, 1983. Investigation on the duration of the seismic signals like a energetic characteristic of the earthquakes. BGJ, vol.IX, N1.

Christoskov L. et al., 1987. Real time and background data processing in the Bulgarian seismological network. Proc. Xx gen. Assembly 1986, Kiel., Zurich.

Christoskov L., L. Dimitrova, D. Solakov, 2011a. Magnitude determinations of P wave by digital broadband seismometers of NOTSSI network for local and regional events. Compres rendus de l'Acade'mie bulgare des Sciences, Vol 65, No5, pp.653-660

Christoskov L., L. Dimitrova, D. Solakov, 2011b. Digital broadband seismometers of NOTSSI for practical magnitude determinations of P waves. BGS. v.XXXVII, N1-4/2011, ISSN 1311-753X, 62-72.

Deneva D. et al., 1988. On the discrimination between industrial explosions and weak earthquakes using records of local seismics networks. Proc. of conference in Liblice, 1988, Praha.

Snoke J.A, 2009. FOCMEC: FOCal MECanism Determinations. VirginiaTech, Blacksburg, VA, USA, 2009, Manual.

Solakov, D., 1993. An algorithm for hypocenter determination of near earthquakes. Bulg. Geophys. J. 19 (1), 56-69

Solakov, D. et all., 2006. National Seismological Network – state and development. Proceedings of Scientific-practical conference on management in extraordinary situations and people protection, BAS, Sofia, 2005, 265-272.

Данни и анализ на сеизмичните събития регистрирани от НОТССИ през 2015

Е. Ботев, В. Протопопова, И. Попова, Бл. Бабачкова, С. Величкова, И. Александрова, Пл. Райкова, М. Попова, Т. Илиев

Резюме. Предлаганото научно съобщение съдържа обобщена информация за резултатите от събирането, обработката и анализа на първичните данни за сеизмичните събития, регистрирани от Националната Оперативна Телеметрична Система за Сеизмологична Информация (НОТССИ) през 2015 г. Представена е карта на епицентрите на общо 1426 земетресения в частта от Балканския полуостров, ограничена от географска ширина 37^0 - 47^0 N и дължина 19^0 - 30^0 E. По-подробно се анализира сеизмичността за територията на България и прилежащите й земи (повече от 1042 сеизмични събития в район с координати l= 22^0 - 29^0E и j =41^0 - 44.5^0N). Предлага се и каталог на земетресенията с магнитуд M>2,5. Сеизмогенните прояви се обсъждат по зони, сравнени със съседни периоди време.

Bulgarian Geophysical Journal, 2018, Vol. 41
National Institute of Geophysics, Geodesy and Geography, Bulgarian Academy of Sciences

DATA AND ANALYSIS OF THE EVENTS RECORDED BY NOTSSI IN 2016

E. Botev, V. Protopopova, I. Aleksandrova, B. Babachkova, S. Velichkova, I. Popova, P. Raykova, M. Popova, T. Iliev

National Institute of Geophysics, Geodesy and Geography, BAS, Akad. G. Bonchev, Str., bl.3, Sofia, Bulgaria, e-mail: ebotev@geophys.bas.bg

Abstract. A map of epicenters of 1399 earthquakes that occurred during 2016 in the Balkan Peninsula (sector outlined by latitude j =37^0- 47^{0}N and longitude l=19^0-30^{0}E) is presented. Expert generalized analysis of the seismicity over the territory of Bulgaria and its very adjacent lands (with more than 1038 localized events) is proposed. Catalog of earthquakes with magnitude M>2.5 is applied.

Key words: Balkan Peninsula, Bulgaria, seismicity

The present scientific communication contains generalized information on the results of collection, processing and analysis of the data about the seismic events recorded by the National Operative Telemetric System for Seismological Information (NOTSSI) in 2016. The expanded information about the realized seismicity is suggested as a natural generalization and supplementation of the monthly compilations of the preliminary seismological bulletin of NOTSSI. The analysis and evaluation of the space, time and energy distribution of the seismicity, periodically been made, open up possibilities for searching for time correlations with the parameters of different geophysical fields aiming to find out eventual precursor anomalies.

The recording and space localization of the seismic events in NOTSSI during 2016 is realized by means of the new digital network (Solakov et al., 2006). The routine processing and acquisition of the initial data is organized in a real time duty regime. The operations are fulfilled by the authors of this communication. In such a way the main goal of NOTSSI, namely the seismicity monitoring in order to help the authorities' and social reaction in case of earthquakes felt on the territory of the country, is realized. The computing procedure for determining the parameters of the seismic events is an adaptation of the widespread product HYPO'71 (Solakov , 1993). The energy parameters

of the events are presented mainly by the magnitude M calculated according to the records duration by the formula (Christoskov and Samardjieva, 1983).

$$M = 1.92 + 2.72\log\tau - 0.026\Delta$$

After bringing into use the new digital broadband seismometers of NOTSSI network, the magnitude determination for local and regional events is calculated by P wave amplitude ratio (Christoskov at all, 2011a, b).

The focal mechanism parameters are obtained by means of a program FOCMEC (Snoke,2009). The high sensitivity of the seismographs allows recording and processing of a great number of long distance earthquakes. As a result of the achieved experience in the authors interpretation work, different magnitude's lower threshold for successful determination of local, regional and long distance earthquakes is established: M=1.5 for the territory of Bulgaria, M=3.0 for the central part of the Balkans, M=5.0 for long distance events. The precision of the epicenter's determination is different; except on the distance it depends also on the specific position of the epicenter in relation to the recording network. The parameters of seismic events occurring at a distance more than 100-150 km outside the territory of Bulgaria should be accepted only informatively and cannot be used for responsible seismotectonic investigation.

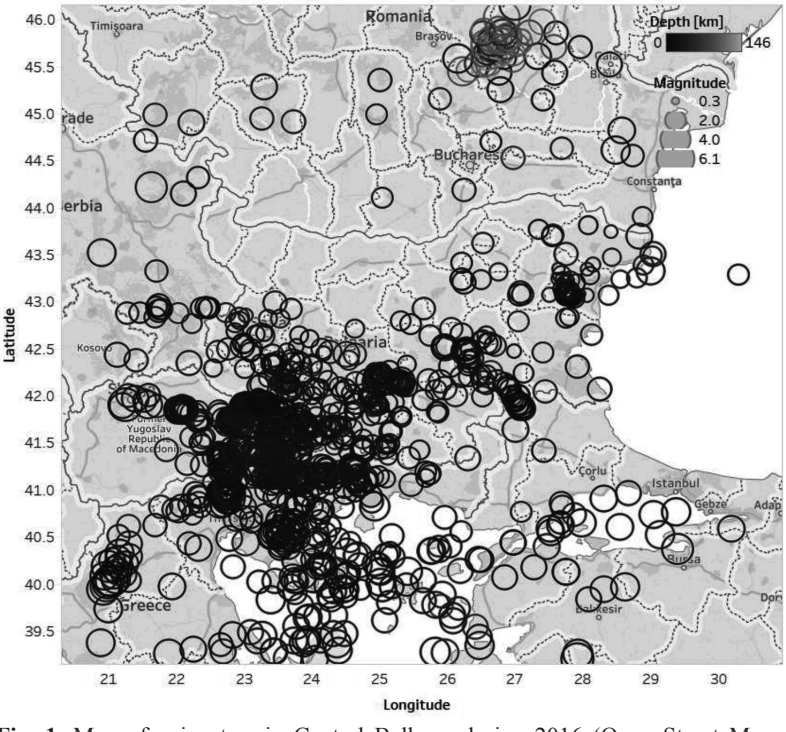

Fig. 1. Map of epicenters in Central Balkans during 2016 (Open Street Map - Tableau Desktop10.5.)

For the period of observations presented in this communication, the primary data about 2000 local, regional, distant earthquakes and industrial explosions on the territory of Bulgaria are recorded, classified and processed (as a work bulletin) in NOTSSI. After comprehensive analysis of the records and application of the above mentioned calculation procedures it is established that 1399 of all registered earthquakes are in the Balkan Peninsula region outlined by geographic latitude 37^0 - 47^0 N and longitude 19^0 - 30^0 E. The epicenters of the earthquakes differentiated by magnitude levels are plotted on Fig. 1. The number of the events in the magnitude interval M=0.5-1.9 is 594, in M=2-2.9 - 615, in M=3-3.9 - 157, in M=4-4.9 – 29, in M=5-5.9 – 2 earthquakes. During this not so active period there are 2 events with magnitude M>6.0. All earthquakes with magnitude more than 4.3 are out of Bulgarian borders.

As a whole, the seismic situation in the studied part of the Balkans during 2016 is characterized as not so high activity - 1399 events, compared with previous years: 1426 events in 2015, 1602 in 2014, 1622 in 2013, 1508 in 2012. The maximum realized earthquake is with magnitude Ms=6.1 in Vranchea, Romania, while this value for the previous years is M=6.6 in North Aegean sea (Greece, in 2014). It can be noted that the observed tendency of decrease of the activity compared with the former years is partly due to the lower level of earthquake activation out of Bulgaria, despite of relative increase of number of microearthquekes in the territory of our country.

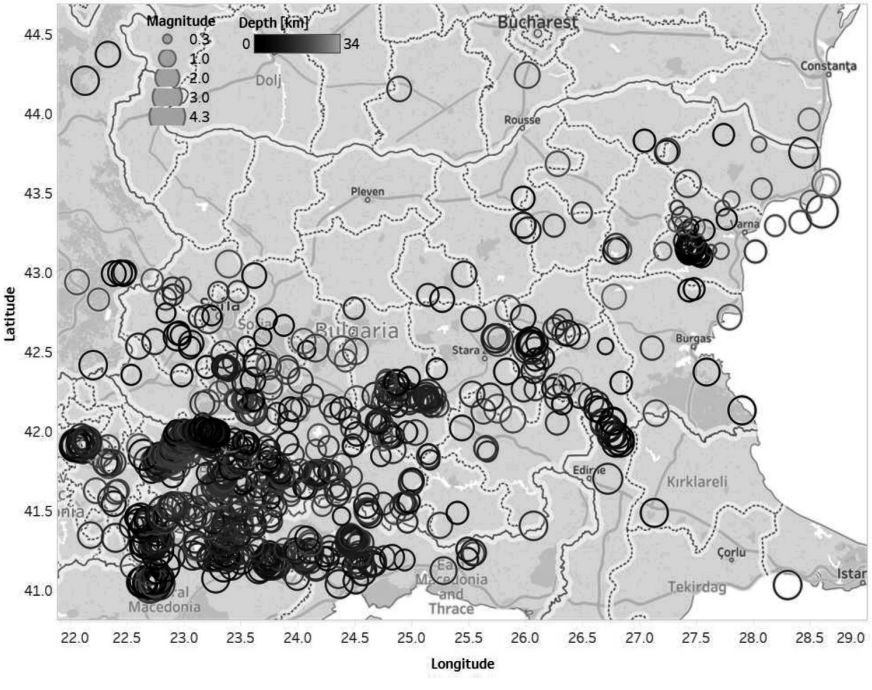

Fig. 2. Map of epicenters in Bulgaria and adjacent lands during 2016 (Open Street Map - Tableau Desktop 10.5.)

The strongest event outside Bulgaria during the study period occurred in the region situated in the Vranchea source zone in Romania with magnitude M=6.1. Shakable effects because of attacks from this side during September and December 2016 occurred 3 times in north-eastern Bulgaria (maximal intensity V-VI in towns of Ruse, Tutrakan and Silistra).

As a whole, events with M<3.0 which occur outside Bulgaria are difficult to be localized by the national seismological system; consequently, not all of them have been marked on the scheme in Fig.1.

Fig. 2 illustrates the seismicity just in the territory of Bulgaria and nearby lands ($j = 41^0 - 44.5^0$N, $l = 22^0 - 29^0$E). The earthquakes are differentiated by magnitude intervals. The parameters of relatively stronger earthquakes are presented in Table 1.

Table 1. List of earthquakes with M ³ 2.5 in Bulgaria and adjacent lands during 2016

Date	Time	Latitude [N°]	Longitude [E°]	Local magnitude	Depth [km]
3 January	14:42: 4.8	41.01	24.37	2.7	7
24 January	21:19:52.4	41.12	23.43	2.5	7
27 January	21:31: 0.3	43.35	28.59	3.5	13
31 January	23:45:41.1	41.24	22.66	2.8	8
1 February	19: 7:26.6	42.19	25.69	2.5	9
	22:16:40.9	41.26	22.67	2.7	3
2 February	12:10:45.1	41.38	22.68	3.4	8
	18:49:43.3	41.43	22.63	2.7	5
5 February	14:44:25.1	41.86	24.83	2.5	14
6 February	3:49:17.5	41.42	23.06	2.5	14
12 February	16:58:18.1	41.26	24.48	2.5	13
15 February	6:59: 6.8	44.15	22.14	2.8	8
16 February	11:17:16.9	41.46	22.84	4.1	12
18 February	2:21:25.1	41.30	24.46	2.7	11
19 February	11:55:32.0	41.76	22.79	2.6	13
28 February	11:17:16.9	41.46	22.84	4.1	12
29 February	20:28:10.5	41.97	23.26	2.7	4
2 March	23:44:49.8	41.28	24.47	3.3	13
3 March	3: 5:55.3	41.29	24.47	2.5	9
	8:48:49.4	41.29	24.47	2.8	9
	14: 3:59.9	41.29	24.47	2.7	13
	18:55:17.9	41.28	24.47	2.6	10

4 March	0:12:45.9	43.71	28.43	3.0	9
5 March	8: 2: 4.4	41.17	24.07	2.6	10
8 March	21: 4:48.9	42.39	22.21	2.8	5
9 March	7:55:12.4	41.78	22.70	3.0	10
13 March	13: 5:46.4	42.46	23.36	2.5	13
17 March	6:13:51.0	41.25	23.12	2.7	20
19 March	11:55:32.9	41.78	22.86	2.5	17
20 March	23:55: 3.6	41.82	22.80	2.5	4
21 March	3:36:53.6	41.82	22.84	2.9	12
	5: 7:20.2	41.80	22.78	2.8	9
	21:19:47.6	43.52	28.63	2.8	22
22 March	13:12:37.9	41.16	23.51	2.5	4
	15:42:10.3	41.78	22.33	2.5	16
27 March	7: 1:10.4	41.04	23.29	2.6	5
	17: 6: 7.0	42.11	23.61	3.0	12
30 March	13:24:48.5	41.26	22.74	2.5	4
	16:15:23.6	42.50	24.16	2.5	16
31 March	8: 2: 4.4	41.17	24.07	2.6	10
1 April	19:29:53.6	42.56	25.73	2.6	15
	19:46: 5.0	42.56	25.74	2.8	11
	19:51:11.6	42.55	25.75	3.3	17
13 April	0:48:42.8	41.12	24.16	2.5	14
	0:59: 6.1	41.12	24.16	2.9	15
	18: 4: 6.6	41.96	23.25	2.5	5
16 April	14:57:52.1	41.30	22.78	2.6	11
17 April	13:12:31.2	41.29	24.04	2.7	20
18 April	6:46:14.4	42.51	26.03	3.9	12
	6:48:18.7	42.48	26.08	2.5	17
	10:38:44.4	42.51	26.04	3.0	11
2 May	17:13:52.2	41.33	23.47	2.5	9
	20:16:25.8	42.53	26.03	2.5	6
4 May	11: 6:28.6	42.68	23.22	2.9	15
6 May	2:46:49.6	41.78	22.78	3.3	12
	12:17:21.8	41.12	22.84	3.0	2
	13:45:11.7	41.04	22.80	2.7	6

9 May	12:52: 3.2	41.69	23.79	2.9	17
	17:20: 4.1	42.21	25.14	3.0	11
19 May	18:52:32.3	42.57	22.95	2.7	3
22 May	8:58: 8.6	41.67	23.35	4.3	20
23 May	6:22: 1.8	41.62	23.29	2.7	16
	7: 3:50.1	41.63	23.28	2.7	15
30 May	21:52:11.8	41.15	24.65	3.1	10
11 June	6: 6:30.8	41.09	25.28	2.5	12
14 June	16:34:12.8	43.12	27.43	2.7	2
	16:46:26.3	43.11	27.44	2.6	2
15 June	5:21:14.0	41.46	27.12	2.7	2
17 June	17:55:58.7	42.54	26.04	2.7	6
18 June	17:24:18.5	41.95	26.74	2.5	11
19 June	5:54:18.3	41.39	23.22	3.1	20
23 June	13:59:34.5	41.28	24.50	2.8	13
	15:34:11.5	41.26	24.50	2.5	10
	16:40:21.0	41.28	24.50	2.8	10
24 June	18:48:40.4	41.94	23.03	3.0	19
6 July	18: 5:34.5	41.76	22.94	2.7	17
11 July	22:18:51.0	41.15	23.76	4.1	9
12 July	0: 1:47.0	41.14	23.76	3.8	9
	3:18:47.4	41.16	23.76	2.8	9
	13: 8: 8.2	41.15	23.73	2.5	8
15 July	9:14:36.4	42.35	27.58	2.5	2
16 July	19:16:56.8	41.58	23.32	2.6	20
21 July	14: 6:37.4	41.95	23.12	2.7	18
27 July	5:10: 7.1	42.04	23.74	2.5	16
29 July	13:24: 0.5	41.43	22.82	2.6	15
1 August	18:39:25.0	41.50	22.91	2.9	13
4 August	8:21:39.0	42.12	25.75	2.7	20
5 August	17: 2:29.6	41.10	23.66	2.6	8
7 August	1:44:45.6	41.88	22.05	2.7	1
8 August	0:39:42.3	41.87	22.12	2.9	10
12 August	21: 8:55.7	41.89	22.11	2.5	10
17 August	15:21:20.8	41.18	24.07	2.5	17

18 August	9:10:36.7	41.95	23.18	3.3	11
	22:55:15.2	41.88	22.11	2.7	10
19 August	9:10:37.0	41.96	23.19	3.0	6
	9:13:14.1	41.96	23.19	2.5	7
20 August	5:26:39.1	41.97	23.23	2.5	5
27 August	15:18:54.9	41.50	24.93	2.6	17
30 August	9:26: 5.7	42.11	27.89	2.7	2
12 September	13:49:39.1	41.57	23.65	2.9	18
14 September	2:42:34.8	42.41	23.65	2.7	3
18 September	8:28:13.5	41.34	23.36	3.5	15
	9:19:47.6	41.96	23.22	2.5	20
	10:26:45.2	41.30	23.33	4.0	13
	15: 9: 8.3	41.39	23.38	2.6	15
	15:39:40.6	41.38	23.37	2.8	13
19 September	1:32:43.2	41.24	23.32	2.8	8
20 September	12:35: 8.9	43.52	27.42	2.5	16
	17:37:24.9	41.88	22.05	3.0	2
21 September	11: 6:32.7	41.89	22.11	2.5	11
22 September	10:13:44.5	41.09	24.57	2.8	10
24 September	22: 4:22.5	41.83	22.65	3.1	2
26 September	2:38:23.4	41.19	23.08	2.8	9
29 September	8:41:32.2	41.12	23.36	3.1	2
5 October	17:27: 7.2	41.38	26.07	2.8	13
9 October	21: 0:40.9	41.89	22.10	2.7	21
12 October	17:58:55.5	41.87	22.93	2.6	15
13 October	5:58:16.7	41.78	22.81	2.6	6
14 October	13: 5:55.2	41.97	23.19	2.5	8
17 October	0:49:16.7	41.68	26.72	3.0	10
	13: 2:33.3	41.29	22.70	3.8	8
	14:19:31.8	41.96	23.02	2.6	19
18 October	13:51: 7.3	41.90	22.16	2.8	10
21 October	7:24: 0.7	42.48	24.39	3.0	20
25 October	8:11:39.5	41.90	22.05	2.9	7
26 October	8:59:26.6	42.19	24.98	2.9	14
	12: 6:24.3	41.18	23.25	2.6	12

27 October	13:51:30.9	42.04	26.76	2.5	0
10 November	4:40:27.5	41.47	23.17	3.5	16
	12:44:45.9	41.02	22.69	3.0	1
16 November	7:38:50.5	41.01	22.79	3.6	14
19 November	1:44:20.2	41.01	22.76	3.4	3
	17: 5:48.3	41.03	22.65	2.7	2
	17: 5:49.3	41.01	22.75	2.6	3
21 November	8:42:33.4	41.02	22.64	3.1	6
22 November	3:47:31.3	41.02	22.65	3.2	2
24 November	1:25:38.1	41.03	22.75	3.7	22
	1:56:47.3	41.91	22.16	3.1	13
29 November	18:45:18.4	41.00	22.69	2.5	12
30 November	6:19: 7.0	41.01	22.69	2.7	2
	14:50: 7.4	41.02	22.75	2.6	20
	17:36:41.1	41.00	22.71	4.2	16
5 December	15: 1:30.9	41.90	26.78	2.5	1
6 December	9: 4:51.4	41.00	22.68	2.8	1
11 December	1:29: 5.6	41.02	22.73	2.8	2
12 December	13:15:35.5	41.90	26.83	2.5	3
15 December	4: 4:39.5	41.61	23.51	3.2	18
18 December	13:10:59.1	41.30	22.41	2.7	10
20 December	12: 6:16.1	41.00	28.29	2.9	10
23 December	10:33: 0.7	41.19	22.76	2.7	2
	11:48: 3.8	41.22	22.79	2.8	2
24 December	23:27: 5.1	43.02	23.40	2.5	20
29 December	3:32:26.9	41.94	22.96	2.5	13
31 December	14:33: 1.0	41.84	22.27	2.8	20

On the territory of Bulgaria relatively normal activity of earthquakes is observed during 2016 – 1038 events are observed, against 1042 in 2015, 947 in 2014, 1124 in 2013 and 932 in 2012. The earthquakes of a magnitude higher than 3.0 are in normal amount – 41 events compared with an averaged number of about 20-35 for most of the all previous years.

The maximum realized magnitude during 2016 is Ms=6.1 in close to Bulgarian border (on Romanian territory) occurs on 27th of December and caused macroseismic effects with intensity of V-VI degree of MSC.

As usual, the largest concentration of the epicenters in the other regions of Bulgarian territory during 2016 is marked in the southwestern part of the investigated region (presented in Fig.2). The Kroupnik seismic source is known with the strongest crustal earthquakes in Europe (M=7.8, 7.1) for the last 160 years. 27 of the events of M≥3.0 occurred in this region during 2016. The strongest felt earthquake for the south-western part of Bulgarian territory is with magnitude M=4.3, it is felt on 22nd of May in Sandanski region (western slopes of Pirin mountain) by intensity of VI degree of MSC scale.

The other Bulgarian seismic sources in 2016 are relatively not so active than during the previous years. They produced not more than 15 earthquakes affecting different localities in this country by intensity of up to IV-V degrees of MSC scale. The maximum number of felt earthquakes is occurred in the region around the town of Petrich. About four cases of magnitudes more than 3.0 aroused shocks of intensity three or more are felt in this region of the south-west territory of Bulgaria. The maximum event with magnitude M=4.0 south of town of Petrich caused IV-V degree of MSC scale on 18 September in the town. A stronger event M=4.2 in the neighbor region of Doiran lake (Greek territory) caused effects of III-IV degree of MSC in the boundary regions located west of town of Petrich on the 30 November 2016. In the rest part of the Bulgarian territory the felt events caused excitation of lesser intensity during 2016.

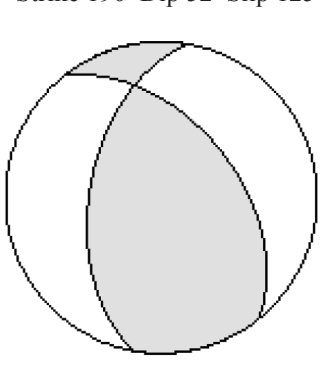

Fig. 3. Focal plane solution of earthquake near to Sandanski city (22.05.2016, 8:58 GMT, Ml=4.3, H=20 km)

For the determination of the earthquake mechanism the program FOCMEC is used. Input data are the polarities of the P wave. Forty-five first motion polarities data from seismological stations in Bulgaria and surrounding area are used (Fig.3), taken from NOTSSI and GFZ Seismological Data Archive database (Bianchi et al., 2015) are included in the double - couple focal mechanism The solution is displayed on lower hemisphere. The polarities are check as waveform. The strike, dip and rake are determined in accuracy up to 5 degrees. The earthquake is characterized as a reverse faulting, with very small dip-slip component.

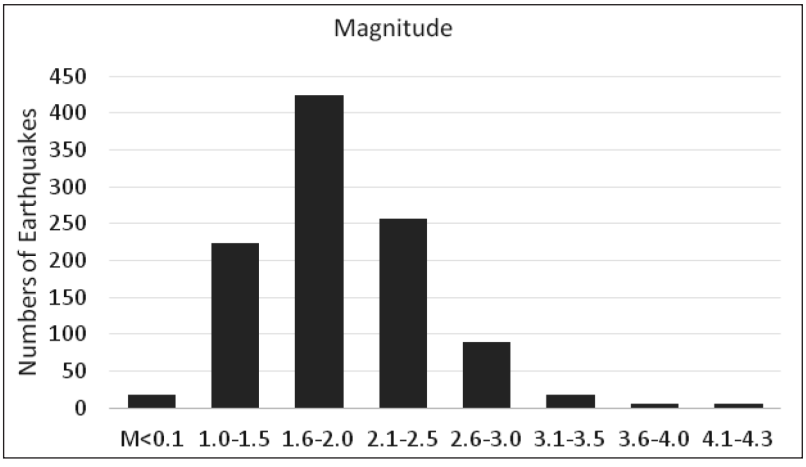

Fig. 4. Magnitude - frequency distribution of the earthquakes

A detailed analysis of seismicity in the individual seismic zones is hard to be fulfilled because of the insufficient quantity of events and the narrow magnitude range of the earthquakes. The joint statistics of all the events in Fig. 2 characterize predominantly the seismicity parameters of the southwestern part of the territory under investigation.

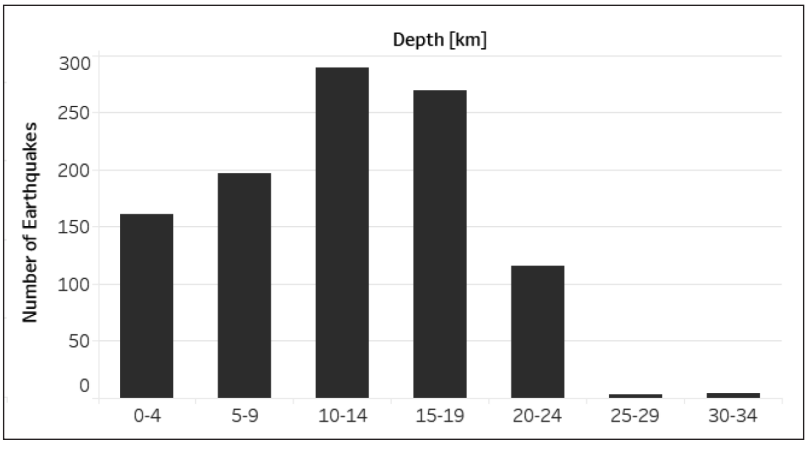

Fig. 5. Depth - frequency distribution of the earthquakes

The magnitude-frequency distribution for the entire data set is presented in Fig.4. The number of localized events increases with the magnitude decreasing: for M= 4.1-4.3 are 6 events, M=3.6-4.0 are 6 events, for M=3.1-3.5 are 17 events, for M=2.6-3.0 - 89, for M=2.1-2.5 - 256 and so on. The abrupt diminishing of the number of earthquakes in the first two intervals (M<1.5) in Fig. 4 determines also the registration power of the seismic

stations network. Taking the latter into account, it can be supposed that the magnitude sample for levels with M > 1.5 is comparatively closer to the reality for the bigger part of the Bulgarian territory.

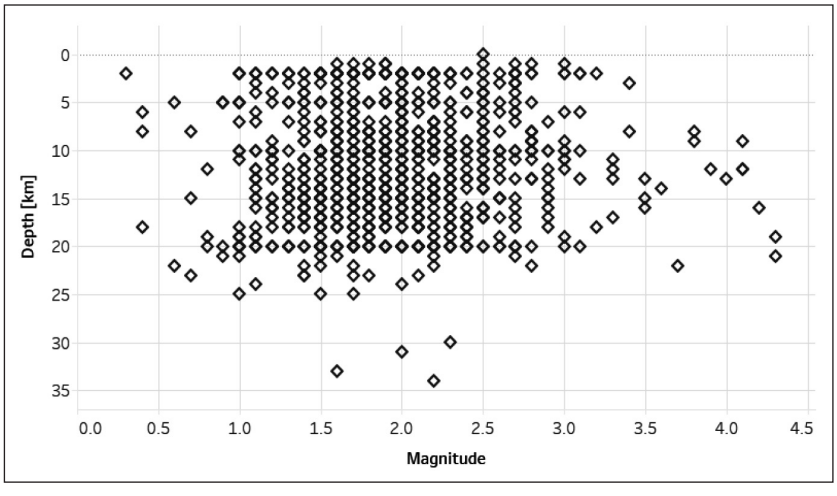

Fig. 6. Magnitude - depth dependence

The picture of the depth distribution in Fig. 5 shows that the majority of events occur in range 10-14 km depth. The number of events does not decrease smoothly with increase of the depth. It is possible the established predominating depth (from 10 to 20 km) to be also due to the presence of small number of unidentified industrial explosions on the surface. In the same time the number of events in the interval 10-14 km is biggest.

The magnitude distribution of the events in depth (Fig. 6) permits to note some differentiation of depth "floors" with the increase of magnitude - the maximums can be traced out for the depth interval from 8 to 22 km. It is remarkable that the strongest events are relatively deep situated and the maximal events are associated with 20 km depths.

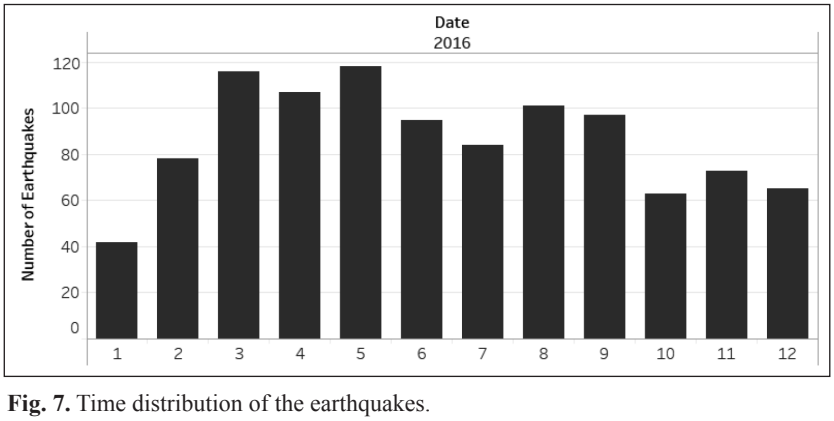

Fig. 7. Time distribution of the earthquakes.

Fig. 7 illustrates the distribution of seismicity in time according to the number of events per months. The biggest earthquake's amount is in the months from April to May, when about one third of all earthquakes occurred. The maximal months amount (about 120 events) during the May is associated with aftershock activity of 22May maximal earthquake. The lowest earthquake quantity is in January - around 40 events. The energy release suggests that the period April - September, when the relatively all biggest earthquakes occurred, is the time with maximum of energy release.

Additionally, about 900 distant earthquakes have been recorded in the period under study, as well as more than 800 industrial explosions, processed and classified in the preliminary monthly bulletins. In order to identify the artificial seismic sources the methodical approach described by Deneva et al. (1988) and some information about the quarry sites in Bulgaria have been used.

Acknowledgements: The authors owe their gratitude to the engineering staff for the perfect software and hardware ensuring of NOTSSI and to Team Vision Bulgaria Ltd. for the kind grant of the Tableau Desktop software.

References

Barrier, E., N.Chamot-Rooke, G.Giordano, 2004. Geodynamic map of the Mediterranean, Sheet 1- Tectonics and Kinematics, CGMW, France.

Christoskov L. and E. Grigorova, 1968. Energetic and space characteristics of the destructive earthquakes in Bulgaria since 1900. Izv.BAS, vol XII .

Christoskov L. and E. Samardjieva, 1983. Investigation on the duration of the seismic signals like a energetic characteristic of the earthquakes. BGJ, vol.IX, N1.

Christoskov L. et al., 1987. Real time and background data processing in the Bulgarian seismological network. Proc. Xx gen. Assembly 1986, Kiel. , Zurich.

Christoskov L., L. Dimitrova, D. Solakov, 2011a. Magnitude determinations of P wave by digital broadband seismometers of NOTSSI network for local and regional events. Compres rendus de l'Acade'mie bulgare des Sciences, Vol 65, No5, pp.653-660

Christoskov L., L. Dimitrova, D. Solakov, 2011b. Digital broadband seismometers of NOTSSI for practical magnitude determinations of P waves. BGS. v.XXXVII, N1-4/2011, ISSN 1311-753X, 62-72.

Deneva D. et al., 1988. On the discrimination between industrial explosions and weak earthquakes using records of local seismics networks. Proc. of conference in Liblice, 1988, Praha.

Georgiev, I. D.Dimitrov, T.Belijashki, L.Pashova, S.Shanov, G.Nikolov, 2007. Geodetic constraints on kinematics of southwestern Bulgaria from GPS and leveling data, Geological Society, London, Special Publications, 2007; 291: 143-157.

Snoke J.A, 2009. FOCMEC: FOCal MECanism Determinations. VirginiaTech, Blacksburg, VA, USA, 2009, Manual.

Solakov, D., 1993. An algorithm for hypocenter determination of near earthquakes. Bulg. Geophys. J. 19 (1), 56-69

Solakov, D. et all., 2006. National Seismological Network – state and development. Proceedings of Scientific-practical conference on management in extraordinary situations and people protection, BAS, Sofia, 2005, 265-272.

Данни и анализ на сеизмичните събития регистрирани от НОТССИ през 2016

Е. Ботев, В. Протопопова, И. Попова, Бл. Бабачкова, С. Величкова,
И. Александрова, Пл. Райкова, М. Попова, Т. Илиевс

Резюме. Предлаганото научно съобщение съдържа обобщена информация за резултатите от събирането, обработката и анализа на първичните данни за сеизмичните събития, регистрирани от Националната Оперативна Телеметрична Система за Сеизмологична Информация (НОТССИ) през 2016 г. Представена е карта на епицентрите на общо 1399 земетресения в частта от Балканския полуостров, ограничена от географска ширина 37^0 - 47^0 N и дължина 19^0 - 30^0 E. По-подробно се анализира сеизмичността за територията на България и прилежащите й земи (повече от 1038 сеизмични събития в район с координати l= 22^0 - 29^0E и j =41^0 - 44.5^0N). Предлага се и каталог на земетресенията с магнитуд M>2,5. Сеизмогенните прояви се обсъждат по зони, сравнени със съседни периоди време.